Vlaanderen
is omgeving

Seismicity in Flanders

Eindrapport

DEPARTEMENT
OMGEVING

omgevingvlaanderen.be

SEISMICITY IN FLANDERS

Deze studie beoogde een revisie van de seismiciteit in Vlaanderen. Hoewel algemeen beschreven als een regio met lage seismiciteit, werd Vlaanderen de voorbije jaren geconfronteerd met seismische activiteit gerelateerd aan een diepeaardwarmteproject. Voorafgaand aan dit project werd niet specifiek seismisch gemonitord op activiteiten in de diepe ondergrond van Vlaanderen en liet de detecteerbaarheid van het nationale meetnet niet overal toe om kleine bevingen te registreren. De natuurlijke microseismiciteit en het risico op geïnduceerde (micro)seismiciteit bij ondergrondtoepassingen in Vlaanderen is onvoldoende gekend. De Vlaamse Overheid wordt geconfronteerd met een reeks open vragen en onzekerheden binnen deze thematiek. Om adequate meetplannen te kunnen opleggen aan exploitaties en om een beter beeld te krijgen van de natuurlijke (micro)seismiciteit en de rol van breuken met het oog op een onderbouwde vergunningverlening, wenste Vlaanderen een gericht onderzoek aan te besteden. Deze studie diende daarom te focussen op i) de (gedeeltelijke) reconstructie van een natuurlijke aardbevingsbaseline voor zover gegevens bewaard zijn die dit kunnen reflecteren, ii) een beter begrip van de rol van breuken in de context van de (potentiële) toepassingen in de diepe ondergrond van Vlaanderen, iii) het opzetten van adequate seismische monitoring van zulke activiteiten en van de natuurlijke baseline en iv) een evaluatie van de geïnduceerde aardbevingen bij het diepeaardwarmteproject. Naast het rapporteren van de onderzoeksresultaten moesten ook beleidsaanbevelingen geformuleerd worden. Daarbij werd gevraagd om lessen die in het buitenland reeds geleerd zijn toe te passen op de situatie in Vlaanderen.

De uitgevoerde studie omvat drie delen. In het eerste deel wordt een zo volledig mogelijke aardbevingscatalogus samengesteld voor Vlaanderen en omringend gebied. Daarnaast wordt het huidige regionale breukenmodel vergeleken met de Vlaamse catalogus en worden breukmechanismen onderzocht. In het tweede deel wordt een revisie gemaakt van de geïnduceerde seismiciteit bij het diepeaardwarmteproject. In het derde deel worden aanbevelingen gedaan voor het beheer van risico's op geïnduceerde seismiciteit bij activiteiten in de diepe ondergrond van Vlaanderen.

DEPARTEMENT
OMGEVING

omgevingvlaanderen.be

COLOFON

Verantwoordelijke uitgever
Peter Cabus
Departement Omgeving
Vlaams Planbureau voor Omgeving
Koning Albert II-laan 20 bus 8, 1000 Brussel
vpo.omgeving@vlaanderen.be
www.omgevingvlaanderen.be

Auteurs
Dr. Stefan Baisch – Q-con GmbH
Christopher Koch – Q-con GmbH
Dr. Elmar Rothert – Q-con GmbH
Meike Seidemann, PhD – Q-con GmbH
Dr. Robert Vörös – Q-con GmbH

Wijze van citeren
Q-con (2021). *Seismicity in Flanders*. Vlaams Planbureau voor Omgeving.
[www.omgevingvlaanderen.be]

PARTNERS

MANAGEMENTSAMENVATTING

Het Vlaamse grondgebied wordt gekenmerkt door een lage aardbevingsactiviteit. Het merendeel van de recente aardbevingen zijn gesitueerd in de Roerdalslenk, terwijl paleoseismische activiteit zich verder uitstrekt tot in het Bekken van de Kempen. De stabiliteit van de tektonische breuken in het Bekken van de Kempen is onvoldoende gekend. Tegelijk vinden menselijke activiteiten plaats in het Bekken van de Kempen die het spanningsveld in de ondergrond kunnen wijzigen en mogelijks aardbevingen veroorzaken.

In deze studie wordt de natuurlijke en geïnduceerde aardbevingsactiviteit binnen Vlaanderen onderzocht om seismogene processen en de rol van natuurlijke breuken in het Bekken van de Kempen beter te begrijpen. Op basis van de bevindingen worden richtlijnen ontwikkeld voor het beheersen van de risico's met betrekking tot geïnduceerde seismiciteit. Deze studie is opgesplitst in drie delen.

In het eerste deel werd een inventaris van aardbevingsactiviteit in Vlaanderen samengesteld op basis van bestaande data van de nationale aardbevingsdiensten van België (ROB, Royal Observatory of Belgium / KSB, Koninklijke Sterrenwacht van België) en van de omringende landen. Naast het samenvoegen van verschillende aardbevingscatalogi werden ongeveer 32 Terabytes aan seismogramgegevens verwerkt om aanvullend aardbevingen met kleinere magnitudes op te sporen. Terwijl enkele honderden bijkomende geïnduceerde bevingen werden gedetecteerd, werd geen enkele bijkomende natuurlijke aardbeving gevonden binnen Vlaanderen. De meest volledige catalogi van aardbevingen tot nu toe in Vlaanderen ('Flanders Catalogue') en omringend gebied ('Extended Catalogue') werden in deze studie gecompileerd.

Door de locatie van de aardbevingen te vergelijken met gekarteerde tektonische breuken kunnen de meeste natuurlijke aardbevingen in het Bekken van de Kempen verbonden worden met gekende breuken. De aardbevingsmechanismen die in de huidige studie bepaald werden, zijn over het algemeen onvoldoende afgelijnd en laten niet toe om de vervorming van individuele breuken verder te onderzoeken. Gemiddeld gezien vertonen de breuksegmenten waarop de aardbevingen zich kunnen hebben voorgedaan relatief hoge tektonische spanningen. Dit houdt in dat het bestaande regionale breukenmodel (G3Dv3) kan helpen bij het identificeren van regionale breuken die een beperkte stabiliteit vertonen. De geïnduceerde bevingen op twee geothermische sites in het Bekken van de Kempen kunnen echter met geen enkele gekarteerde breuk uit het model gecorreleerd worden. Het is bijgevolg mogelijk dat zelfs schaderelevante seismische activiteit kan optreden op breuken die niet in het bestaande regionale model vervat zijn.

In het tweede gedeelte van deze studie werd de seismische gevarenanalyse uitgevoerd door INERIS voor het geothermisch project op de Balmattsite gereviseerd. De processen die tot de geïnduceerde seismiciteit geleid hebben in het Balmattproject zijn nog niet volledig begrepen, voornamelijk wegens onvoldoende observatiegegevens. Waar de INERIS-studies aannemen dat aseismische vervorming een sleutelrol speelt, geven wij de voorkeur aan een meer gebruikelijke verklaring waarbij de evolutie van de seismiciteit gecontroleerd wordt door hydraulische overdruk in combinatie met spanningswijzigingen ten gevolge van eerdere aardbevingen. In ons begrip zijn de voorspellingen van grondtrillingen en daaraan gekoppelde gevolgen in de INERIS-studie onvoldoende gekalibreerd. Dit wordt ook gereflecteerd in het responsprotocol ("verkeerslichtsysteem") dat INERIS voorstelt voor toekomstige geothermische activiteiten. We

menen dat dit protocol mogelijks niet voldoende restrictief is om met een hoge mate van betrouwbaarheid schaderelevante seismiciteit te vermijden.
In deel III van deze studie werden aanbevelingen gegeven voor het beheer van risico's op geïnduceerde seismiciteit bij activiteiten in de diepe ondergrond van Vlaanderen. Deze aanbevelingen zijn gebaseerd op algemene ervaring, op een conceptuele geomechanische benadering van processen die seismiciteit uitlokken en op bestaande praktijken in buurlanden. De aanbevelingen beslaan een breed scala aan ondergrondtechnologieën, i.e., geothermische installaties, ondergrondse gasopslag, warmteopslag in aquifers (ATES, aquifer-thermal-energy-storage), steenkoolgaswinning (CBM, coal bed methane), mijnbouw en geologische koolstofdioxideopslag.

Onze aanbevolen aanpak voor het beheer van geïnduceerde seismische risico's start met een pre-operationele gevarenscreening (de zogenaamde 'Quick-Scan') en / of een pre-operationele gevaren/risico-analyse. Deze analyses bepalen de mate van detail dat vereist is voor de monitoring van geïnduceerde seismiciteit (al dan niet opgelegd via een Meetplan) en de te nemen beperkende maatregelen ('response protocol/ verkeerslichtsysteem').

Voor een laag-risico scenario, gekenmerkt door de bevinding dat gelijkaardige ondergrondactiviteiten elders niet tot seismiciteit hebben geleid, wordt basismonitoring als voldoende beschouwd. In dit geval volstaat de standaardmonitoring via het nationale seismologische netwerk dat door de KSB (ROB) beheerd wordt. Onder specifieke omstandigheden kan geadviseerd worden om het bestaande KSB/ROB netwerk uit te breiden met een bijkomend individueel meetstation in de onmiddellijke nabijheid van de ondergrondse activiteiten.

Voor een scenario waarin geïnduceerde seismiciteit niet met hoge zekerheid uitgesloten kan worden, wordt een lokaal monitoringnetwerk toegespitst op de specifieke ondergrondactiviteit aanbevolen. Voorgestelde richtlijnen voor projectspecifieke responsprotocollen stellen dat ondergrondse activiteiten opgeschort kunnen worden na het optreden van seismiciteit (van een bepaalde grootteorde). Het heropstarten van de activiteiten zou een gedetailleerde analyse vereisen van de oorzaak van de beving(en), het vastleggen van beperkende maatregelen en een herziening van de seismische risicoanalyse. Voor de communicatie en het beheer van geïnduceerde seismiciteitsaspecten wordt aanbevolen om een expertgroep samen te stellen.

MASTER SUMMARY

The region of Flanders is characterized by low earthquake activity. Most of the recent earthquakes occur in the Roer Valley Graben, while paleoseismic activity extended into the Campine Basin. However, the stability of tectonic faults in the Campine Basin is not well-understood. Concurrently, anthropogenic activities in the Campine Basin may alter stresses in the subsurface and possibly induce earthquakes.

In this study, we investigate the natural and induced earthquake activity in Flanders to promote a better understanding of seismogenic processes and the role of natural faults in the Campine Basin. Based on our findings, we develop guidelines for managing the risks related to induced seismicity. The study is subdivided into three parts.

In the first part, we build an inventory of the earthquake activity in Flanders based on existing data of the national earthquake services of Belgium (ROB) and neighboring countries. Besides merging different earthquake catalogues, approx. 32 Terabytes of seismogram data were re-processed to detect additional earthquakes of small magnitude. While several hundred additional induced earthquakes were detected, no additional natural earthquakes were found in Flanders. The currently most complete catalogues of earthquakes in Flanders ('Flanders Catalogue') and surrounding regions ('Extended Catalogue') are compiled in this study.

By comparing the location of earthquakes to the mapped tectonic faults, we find that most natural earthquakes in the Campine Basin can be associated with known faults. Earthquake mechanisms determined in the current study are generally not well-constrained and do not allow to further investigate how individual faults deform. On average, the fault segments on which the earthquakes may have occurred exhibit relatively high levels of tectonic stresses. This implies that the existing model of fault trajectories may help identify regional faults exhibiting little stability. Nevertheless, seismic events induced by activities at two geothermal sites in the Campine Basin do not correlate with any mapped fault. Therefore, even damage relevant seismicity may occur on faults, which are not resolved in the existing fault model.

In the second part of this study, we review the seismic hazard assessment for the geothermal project at Balmatt performed by INERIS. The processes leading to the induced seismicity at Balmatt are not fully understood yet, which is mostly due to insufficient observation data. While the studies by INERIS consider aseismic deformations to play a key role, we favor a more common explanation, where the evolution of seismicity is controlled by hydraulic overpressure in combination with stress changes resulting from previous earthquakes. In our view, predictions of ground vibrations and associated consequences are not sufficiently calibrated in the INERIS study, leading to an underestimation of the associated risks. This is also reflected in the response protocol ('traffic light system') that INERIS suggests for future geothermal activities. We feel that the protocol may not be restrictive enough to prevent damage-relevant seismicity at a high confidence level.

In Part III of this study, we provide recommendations for managing induced seismicity risks associated with deep subsurface operations in Flanders. These recommendations are based on global experience, a conceptual geomechanical understanding of the processes causing seismicity and existing practices in neighboring countries. Our recommendations cover a broad range of subsurface technologies, i.e., geothermal exploitation, gas storage, aquifer-thermal-energy-storage, coal bed methane, mining, carbon capture and storage.

Our recommended approach for managing induced seismicity risks starts with a pre-operational hazard screening (so called 'Quick-Scan') and/or a pre-operational hazard/risk assessment. These analyses define the degree of detail required for monitoring ('measurement plan') and mitigating ('response protocol/ traffic light system') induced seismicity.

For a low-risk scenario, characterized by the observation that similar subsurface activities conducted elsewhere have not caused any seismicity, we consider basic monitoring to be sufficient. In this case, the monitoring is sufficiently performed by the routine processing within the seismological network operated by the ROB. Under specific circumstances, complementing the existing ROB network with a single seismometer station deployed in the immediate vicinity of the subsurface operations may be advised.

For a scenario, in which induced seismicity cannot be ruled out at a high confidence level, a dedicated local monitoring network is recommended. Proposed guidelines for project-specific response protocols state that subsurface activities may need to be suspended after seismicity (of a certain strength) has occurred. Resuming operations would require a detailed assessment of the cause of the earthquake(s), the definition of mitigation measures and an update of the seismic risk assessment. For communicating and managing induced seismicity aspects, we recommend establishing an Expert Panel.

CONTENTS

1 PART I: EVALUATION OF INSTRUMENTALLY RECORDED SEISMICITY AND THE ROLE OF FAULTS

1.1 INTRODUCTION

1.1.1 Scope

An inventory of the earthquake activity in Flanders ("earthquake catalogue") should be built based on existing data of the national earthquake services in Belgium (ROB) and neighboring countries. By merging and re-inspecting existing data it should be attempted to compile the most complete earthquake catalogue. Even the smallest magnitude earthquakes should be included, and the catalogue does not need to fulfil any criterion on a lower magnitude of completeness.

The potential of applying template matching techniques to the existing data should be analyzed and recommendations should be made on how this could be implemented in the national earthquake monitoring.

Fault plane solutions should be determined for the different regions of earthquake activity in Flanders.

Earthquake activity and mechanisms should be interpreted in combination with an existing fault model to better understand the role of faults in the Campine Basin regarding natural and induced earthquakes.

1.1.2 Structure of Part I

Part I of the study is divided into three technical work packages (Figure 1).

In chapter 1.2 earthquake catalogues from the ROB and neighboring countries are merged. The combined catalogue is subsequently screened for spatial-temporal correlations of earthquakes to identify redundant entries. This provides the baseline catalogues (Flanders Catalogue and Extended Catalogue) for the following work package.

In chapter 1.3 waveform analysis is performed for detecting additional earthquakes which are not included in the baseline catalogue. This is the most laborious procedure of the current study. Up to 15 years of time-continuous seismogram recordings of seismometer stations operated in and around Flanders were processed for compiling the final catalogue. Additionally, an assessment is made regarding the (spatially and temporarily varying) earthquake detection threshold. A template matching approach is tested to further increase the detection capabilities.

In chapter 1.6 earthquake locations and mechanisms are interpreted in combination with an existing model of faults in the Campine Basin. A slip tendency analysis is performed to investigate whether observed earthquakes can be associated with critically stressed faults. It is investigated to what extent the potential for future natural and induced seismicity can be assessed with the current model.

Part I concludes with recommendations for future earthquake monitoring and updating of the catalogues (chapter 1.7).

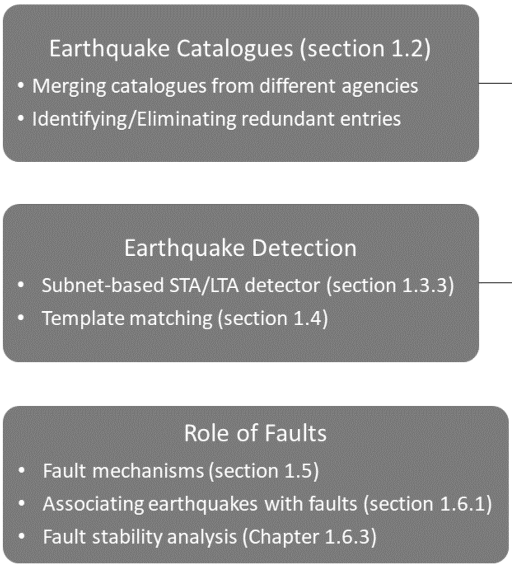

Figure 1: Structure of Part I of the study.

1.1.3 Terminology

We adopt the following description by Bohnhoff et al. (2009):

Earthquakes are the vibratory motion of the earth created by the sudden release of energy within the solid rock mass of the planet. Most earthquakes are caused by slip on faults, and as a consequence the term "earthquake" is commonly used to refer to the earthquake source process rather than the seismic waves it causes.

In the scientific literature, different terminologies were proposed for characterizing the size (magnitude) of an earthquake. Below the level of human perceptibility, small earthquakes are frequently referred to as “micro-earthquakes” or “nano-earthquakes” (e.g., Bohnhoff et al., 2009). We note several shortcomings when using these terminologies:

(i) In the scientific literature, there is no generally accepted definition of these terminologies and the associated magnitude ranges.

(ii) The magnitude of an earthquake is subject to measurement uncertainty. The same earthquake may fall into two different classification categories when accounting for its magnitude uncertainty.

(iii) In public perception, earthquake strength is frequently equated with damage potential. For example, “micro-earthquakes” are not suspected to cause damage. This perception is not necessarily correct. Even small magnitude earthquakes (M<3) can cause damage to buildings if occurring at a shallow depth.

Throughout this report, we therefore use the term “earthquake” without further distinguishing between earthquakes of different sizes. We also employ the term “earthquake” for seismic events of very small magnitude (including negative magnitudes), which can only be measured with very sensitive instruments. These earthquakes may be referred to as “micro-“ or “nano-earthquakes” elsewhere.
It is important to notice that seismometers continuously measure ground vibrations. This ‘’background noise” originates from different anthropogenic and natural vibration sources, such as e.g. traffic, industry, and wind. Background noise is not associated with earthquakes and the term “earthquake” does not apply.

1.1.4 Reference Coordinates

In the current study, data is displayed and provided either in Belgian Lambert 72 coordinates or in spherical WGS84 coordinates.

1.1.5 Abbreviations and Glossary

ε	Threshold value for declaring an event detection (i.e., if STA/LTA > ε).
GMPE	**G**round **M**otion **P**rediction **E**quation. Empirical relation to estimate the ground vibration amplitude for an earthquake.
KNMI	**K**oninklijk **N**ederlands **M**eteorologisch **I**nstituut.
LTA	**L**ong **T**ime **A**verage, absolute seismogram amplitudes averaged over a long time window.
M_c	Magnitude of completeness. The lowest magnitude level above which an earthquake catalogue is considered to be complete.
M_L	Local magnitude.
M_w	Moment magnitude.
n_c	Number of coincident signal detections.
PGV	**P**eak **G**round **V**elocity. Maximum ground velocity that occurred during earthquake shaking at a location. Peak ground velocity is measured in units of m/s.
RENASS	**Ré**seau **Na**tional de **S**urveillance **S**ismique, national earthquake agency of France.
ROB	**R**oyal **O**bservatory of **B**elgium, national earthquake agency of Belgium.
ST	**S**lip **T**endency
STA	**S**hort **T**ime **A**verage. Absolute seismogram amplitudes averaged over a short time window.
STA/LTA	**S**hort **T**ime **A**verage over **L**ong **T**ime **A**verage. Criterion to identify seismic signals.
TB	Terabyte
UGS	**U**nderground **G**as **S**torage
VITO	Independent Flemish research organization operating the Balmatt geothermal project.

1.2 MERGING EARTHQUAKE CATALOGUES

The study focusses on earthquake activity within Flanders. Most earthquake activity, however, is located near the borders of Flanders. For allowing geological interpretations across the borders, we have compiled two earthquake catalogues:

- The “Flanders Catalogue” containing only those earthquakes located strictly within Flanders (chapter 1.2.3).

- The “Extended Catalogue” containing earthquakes located within Flanders and up to 50 km from the Flanders boundaries (chapter 1.2.4).

1.2.1 Data Sources

For the current study, earthquake catalogues from different agencies were requested according to Table 1. Figure 2 to Figure 5 show earthquake locations listed in the different catalogues.

Additionally, the induced events observed at the Beerse location were included in the final catalogues. Five of these events could not be located due to a small signal-to-noise ratio (Broothaers, 2020). These were assigned the hypocenter location of the strongest M_L=-0.7 earthquake and a generic (large) location error of 2.5 km (1 σ) into all three directions.

Table 1: Earthquake catalogues considered in the current study.

Seismic catalogue	Time	Accessed/ received on	Source
ROB, Belgium	01.01.1350 – 01.01.2021	15.01.2021	provided by Michel van Camp (ROB)
Balmatt (VITO), Belgium	05.12.2018 – 08.11.2019	17.03.2021	provided by Ben Laenen (VITO)
KNMI, Netherlands	30.05.1911 – 10.01.2021 (tectonic) 26.12.1986 – 10.01.2021 (induced)	12.01.2021	https://www.knmi.nl/kennis-en-datacentrum/dataset /aardbevingscatalogus
Bensberg (University of Cologne), Germany	27.11.1975 – 01.01.2021	12.01.2021	http://www.seismo.uni-koeln.de/catalog/index.htm
RéNaSS, France	02.02.1962 – 31.12.2009 (SIHexv2) 09.09.2000 – 13.01.2021 (RéNaSS)	13.01.2021	http://www.franceseisme.fr/SIHex/catalogue-SI-Hex.zip (SIHexv2) https://renass.unistra.fr/recherche (RéNaSS)
Beerse (Janssen Pharmaceutica), Belgium	14.12.2019 01:22:43 01.08.2020 20:15:13 - 01.08.2020 21:03:15	08.12.2021	Broothaers (2020) provided by VPO

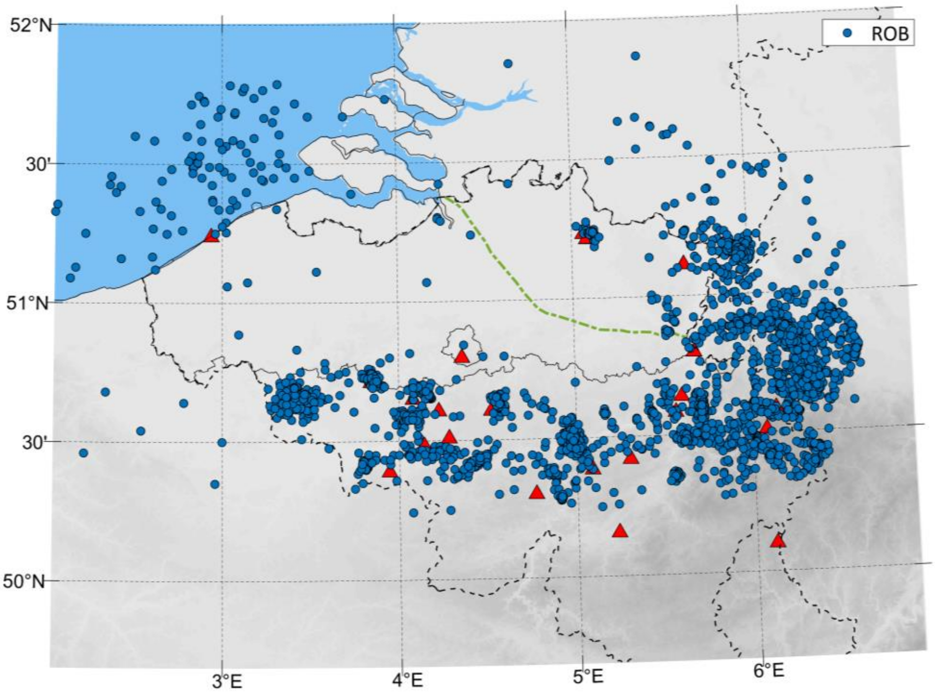

Figure 2: Distribution of the epicenters of the events of the ROB within Flanders and up to 50 km distance from the border. The red triangles show the ROB stations for which data is available. Green dash-dotted line indicates the western boundary of the "geological" Campine Basin after Vandenberghe et al. (2014).

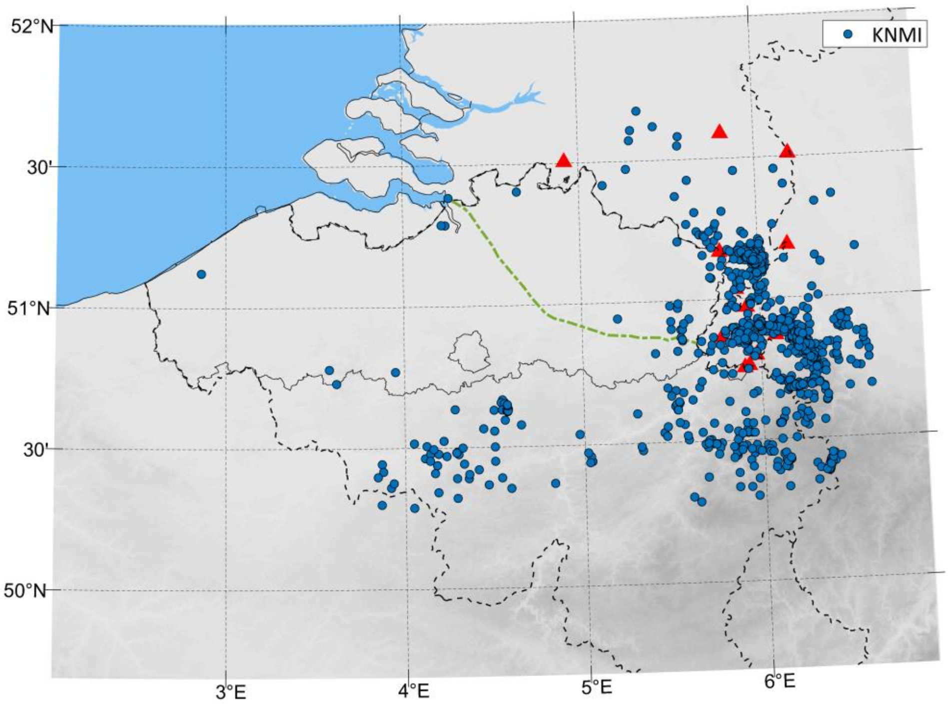

Figure 3: Distribution of the epicenters of the events of the KNMI (The Netherlands) within Flanders and up to 50 km distance from the border. The red triangles show the KNMI stations for which data is available. Green dash-dotted line indicates the western boundary of the "geological" Campine Basin after Vandenberghe et al. (2014).

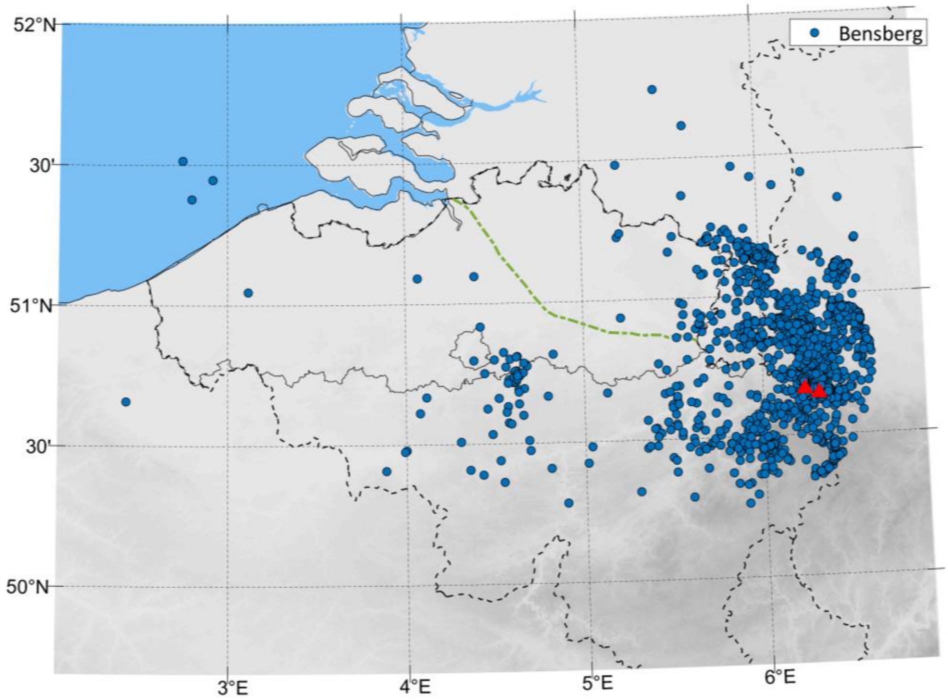

Figure 4: Distribution of the epicenters of the events of Bensberg (University of Cologne) within Flanders and up to 50 km distance from the border. The red triangles show the Bensberg stations for which data is available. Green dash-dotted line indicates the western boundary of the “geological” Campine Basin after Vandenberghe et al. (2014).

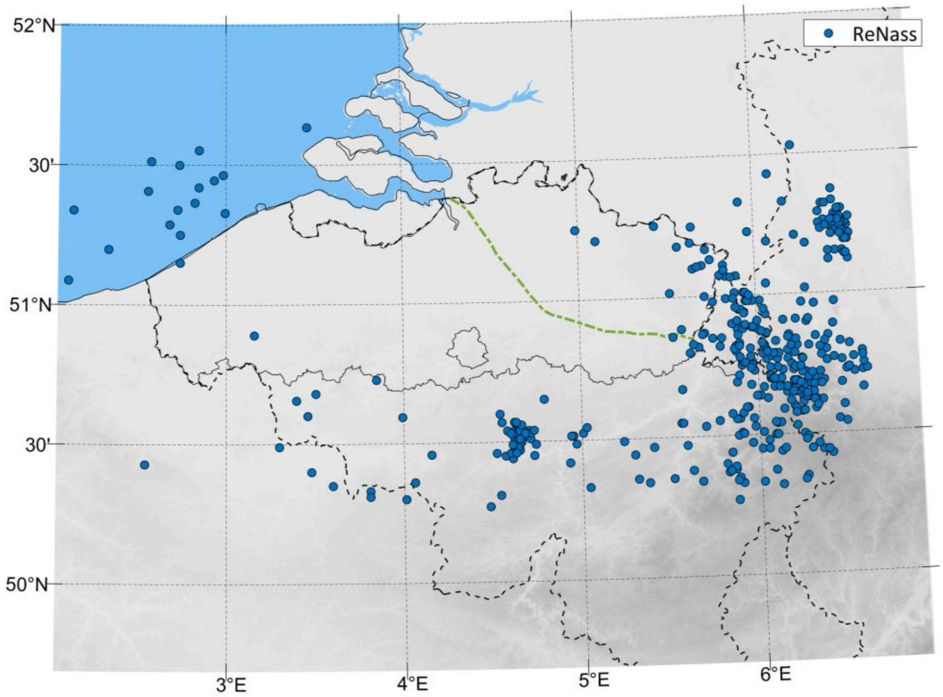

Figure 5: Distribution of the epicenters of the events of RéNaSS (France) within Flanders and up to 50 km distance from the border. Green dash-dotted line indicates the western boundary of the “geological” Campine Basin after Vandenberghe et al. (2014).

1.2.2 Merging Catalogues

Earthquakes from all data sources (section 1.2.1) were combined into a single catalogue. Different data sources may provide different solutions for the location and magnitude of the same earthquake. This can result from using a different set of recording stations and from differences in data processing and seismogram interpretation. Ideally, different solutions are consistent within their confidence bounds.

A redundant entry in the merged catalogue results if the same earthquake is listed by different data sources. Redundant earthquakes were identified and flagged based on temporal and spatial correlations. Keeping only a single entry for each earthquake requires a choice of the authoritative data source (Bossu & Mazet-Roux, 2012).

In general, we consider a national earthquake agency the most reliable data source for an earthquake occurring in its own country.

We acknowledge, however, that a neighboring agency might have better data for locating an earthquake occurring e.g., close to the borders of a country. This aspect is less relevant for the more recent earthquakes, for which seismogram data is generally shared between different national agencies. But data sharing was less common for locating earthquakes that occurred before routine data exchange has been established (say before 2006-2008). Given that national earthquake services have the mandate to monitor earthquakes in their own country, however, we recommend considering them the authoritative data source. This recommendation is motivated by political aspects rather than scientific considerations.

In detail, we applied the following rules:

- If the ROB locates an earthquake inside Flanders or Belgium, then the ROB catalogue is considered the most reliable data source.
- If a foreign agency locates an earthquake inside Flanders and the earthquake is not listed in the ROB catalogue or located outside Flanders by the ROB, a more detailed analysis is performed by a seismologist, possibly using seismogram data.
- If an earthquake occurs within 5 km of the Balmatt geothermal site, the VITO catalogue is considered the most reliable data source. Note that this is an exception to our general approach. However, the ROB is currently integrating the induced earthquakes near Balmatt into their catalogue. Once completed, the ROB catalogue should be considered the primary data source.

Additional rules for the “Extended Catalogue”:

- If the KNMI locates an earthquake inside The Netherlands, then the KNMI catalogue is considered the most reliable data source.
- If RéNaSS locates an earthquake inside France, then the RéNaSS catalogue is considered the most reliable data source.
- If Bensberg locates an earthquake inside Germany, then the Bensberg catalogue is considered the most reliable data source.
- If two or more different national agencies locate the same earthquake each in their own country, then this event is marked as redundant for all agencies. Consequently, the same earthquake is listed several times in the catalogue.
- If two or more different national agencies locate the same earthquake each in the neighboring country, then this event is marked as redundant for all agencies. Consequently, the same earthquake is listed several times in the catalogue.

A sensitivity analysis was performed for estimating the differences between occurrence time and location of the same seismic event reported by different agencies. Figure 6 shows the number of coinciding events in Flanders as a function of the difference between occurrence times (ΔT). The time difference is calculated with respect to the occurrence time listed in the ROB catalogue and only those event pairs were considered where epicenter locations differ by 100 km or less. The number of coinciding events mostly saturates for all data sources for $\Delta T \geq 5$ seconds and we have chosen $\Delta T=5$ seconds as the tolerance level for identifying redundant events.

Similarly, Figure 7 shows the number of coinciding events in Flanders as a function of the difference between epicenter locations. The location difference is calculated with respect to the epicenter listed in the ROB catalogue and only those event pairs with $\Delta T \leq 5$ seconds were considered. The number of coinciding seismic events saturates for all data sources for $\Delta d \geq 100$ km and we have chosen $\Delta d=100$ km as the tolerance level for identifying redundant events.

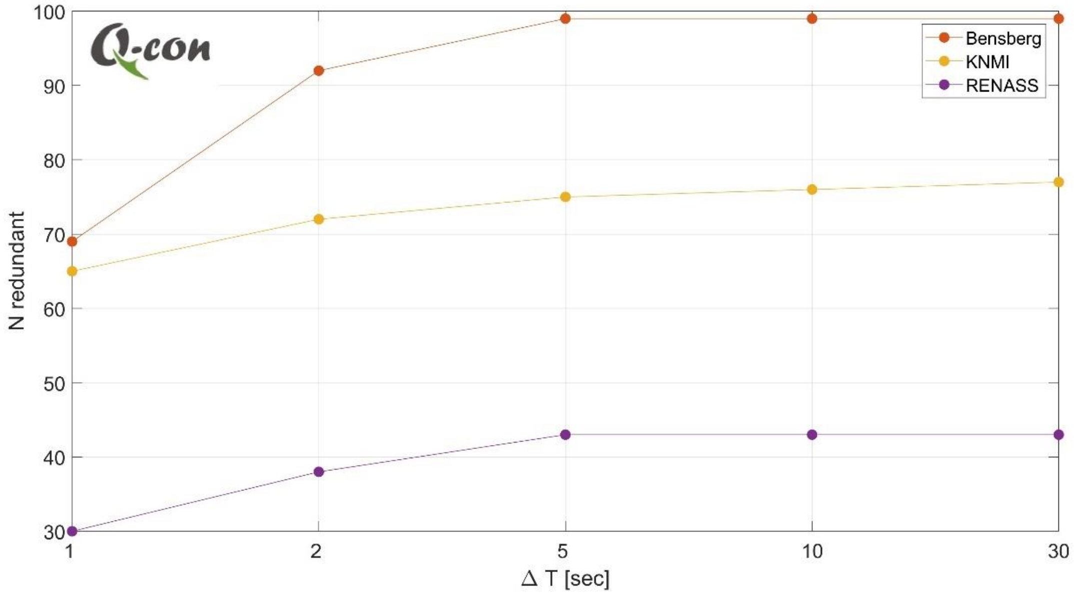

Figure 6: Number of coinciding seismic events listed in different earthquake catalogues for Flanders as a function of the difference between occurrence times (ΔT). Time difference is calculated with respect to the occurrence time listed in the ROB catalogue and only those event pairs were selected, where epicenter locations reported differ by 100 km or less compared to the location reported by the ROB.

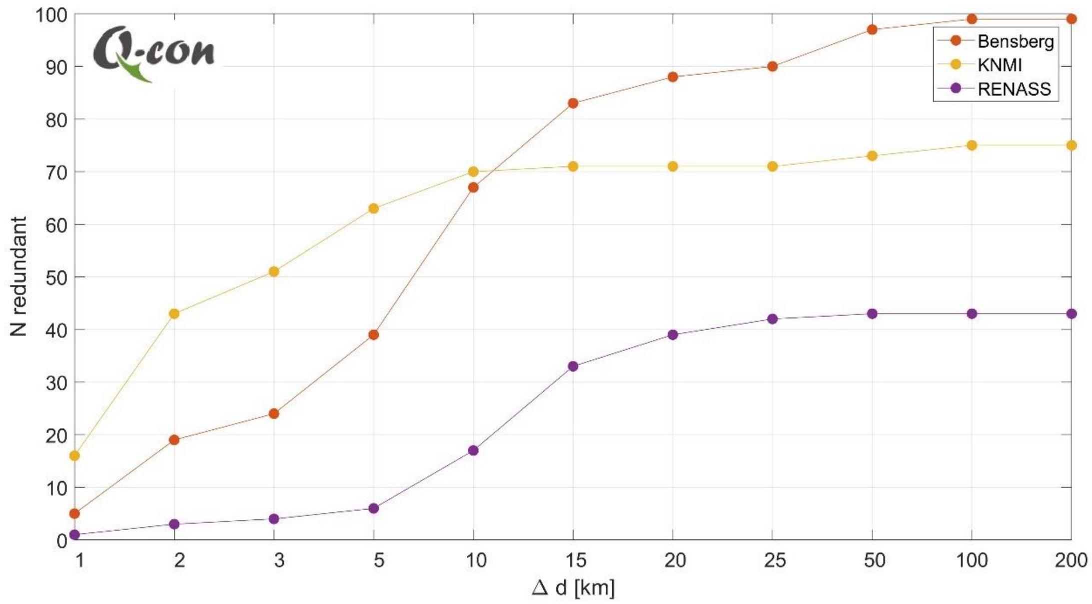

Figure 7: Number of coinciding seismic events listed in different earthquake catalogues for Flanders as a function of the difference between epicenter locations (Δ d). The location difference is calculated with respect to the epicenter listed in the ROB catalogue and only those combinations were considered where the time difference compared to the ROB catalogue is Δ T≤5 seconds.

1.2.3 Flanders Catalogue

Merging the catalogues from the different data sources (compare previous sections) results in 451 seismic events. Of these, 119 seismic events were identified as redundant entries using the criteria established in the previous section. From the remaining 332 seismic events, 23 events were classified as mining-induced events (quarry blasts) leading to a total number of 66 natural and 243 induced earthquakes (Figure 8).

The Flanders catalogue contains 7 earthquakes, which are not listed in the ROB catalogue but listed in the catalogue of one or more foreign agencies (Figure 9 and Table 2).

Table 2: Earthquakes, which are not listed in the ROB catalogue but listed in the catalogue of one or more foreign agencies.

Data source	Occurrence time	Magnitude M_L	Comment
Bensberg	21-Mar-1977 06:04:01	2.6	waveform data not available
Bensberg	11-Jan-1985 20:39:09	1.7	waveform data not available
KNMI, Bensberg	05-Dec-1985 15:48:44	1.7, 1.5	waveform data not available; higher confidence since reported by different agencies
RéNaSS	02-Jul-2001 16:06:29	3.1	waveform data not available
KNMI, Bensberg, RéNaSS	22-Feb-2003 05:56:09	1.4, 1.4, 1.6	waveform data not available; event is located within Flanders by Bensberg, but south of Flanders by KNMI and RéNaSS → most likely mislocated by Bensberg
KNMI, Bensberg	17-Sep-2004 12:35:28	1.5, 1.5	waveform data not available; higher confidence since reported by different agencies
Bensberg	28-Jan-2007 05:18:35	2.2	waveform data only partly available, most likely mislocated

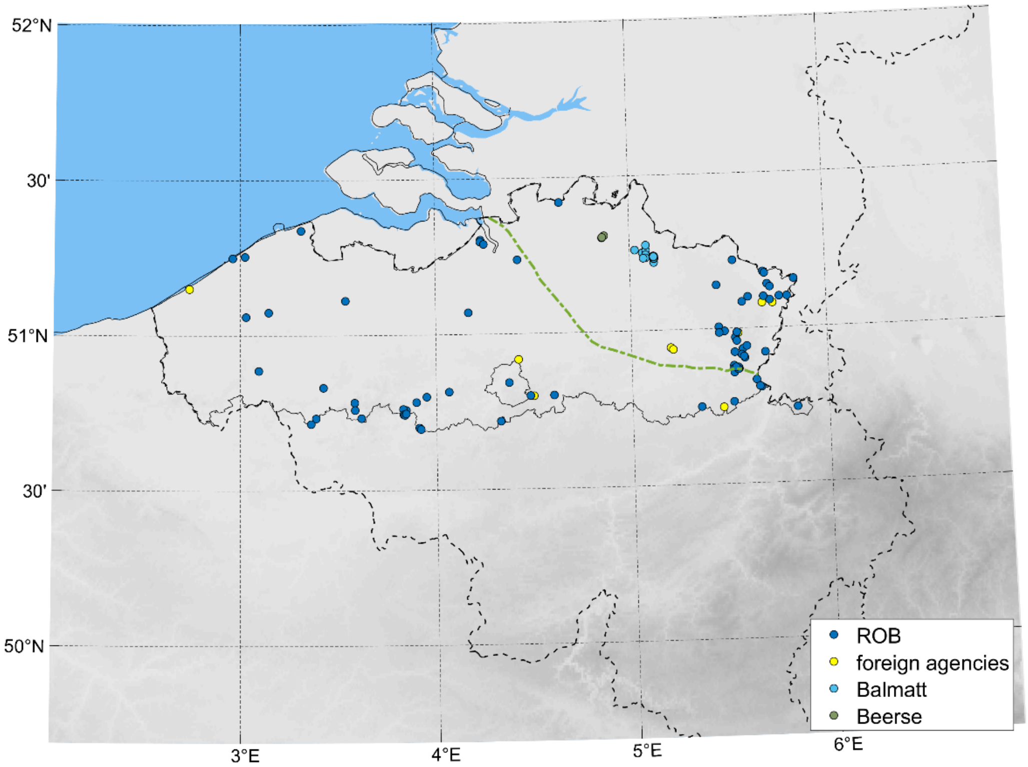

Figure 8: Natural and induced earthquakes within Flanders ("Flanders Catalogue"). Blue dots mark earthquakes located by the ROB. Earthquakes located by foreign agencies but not by the ROB are marked as yellow dots. The earthquake sequence induced by the Balmatt geothermal project in Mol is highlighted in light blue. Earthquakes induced by the geothermal project at Beerse are highlighted in dark green. Green dash-dotted line indicates the western boundary of the "geological" Campine Basin after Vandenberghe et al. (2014).

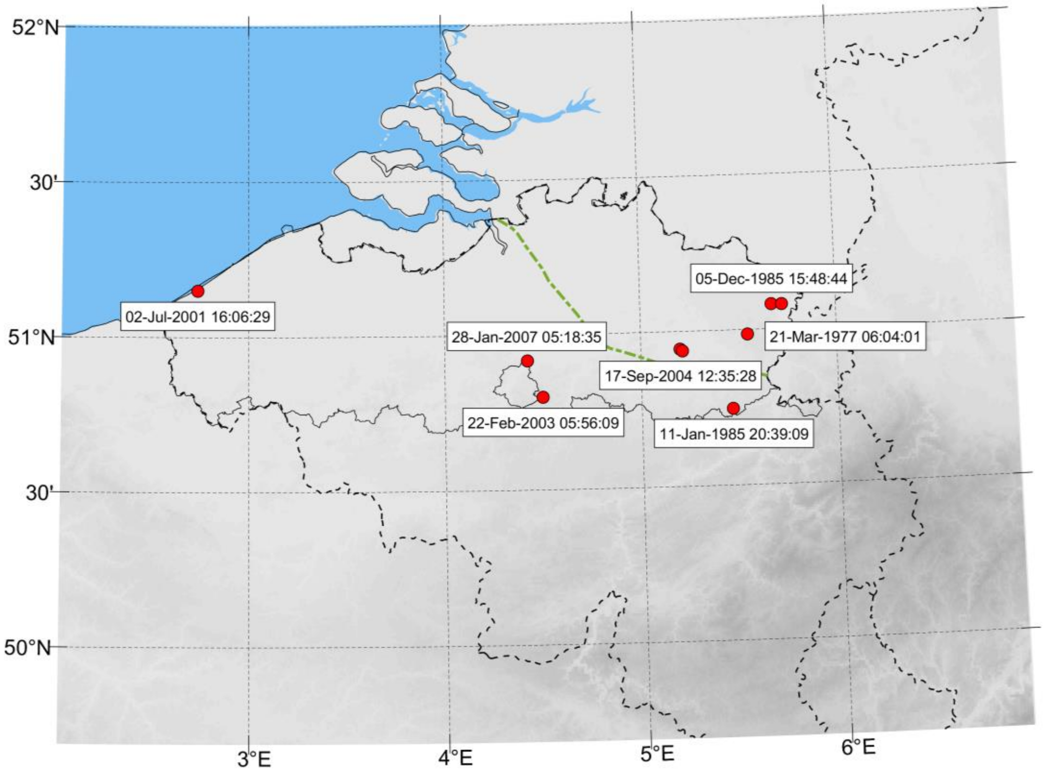

Figure 9: Location of earthquakes in Flanders which are not included in the ROB catalogue but listed by foreign agencies. Green dash-dotted line indicates the western boundary of the "geological" Campine Basin after Vandenberghe et al. (2014).

1.2.4 Extended Catalogue

The extended catalogue contains earthquakes within Flanders and up to 50 km from the Flanders boundaries. The aspects of catalogue homogeneity and data redundancy are less relevant for the extended catalogue as the extended catalogue primarily serves as basis for interpreting geological structures across the boundaries of Flanders.

The same criteria for merging data sources (section 1.2.2) were applied to the extended data catalogue, while no seismogram-based re-interpretation was made if an earthquake is missing in a national catalogue.

A total number of 65 redundant earthquake combinations exist, where the primary data source is unclear. These constellations occur predominantly in the Graben system towards the East (Figure 11). According to the rules defined in section 1.2.2, the event combinations are flagged as redundant in the Extended Catalogue.

The extended catalogue consists of 6787 seismic events. Of these, 2382 seismic events were identified as redundant. The remaining 4405 unique seismic events include 2911 natural earthquakes, 263 induced earthquakes and 1231 quarry blasts (Figure 10).

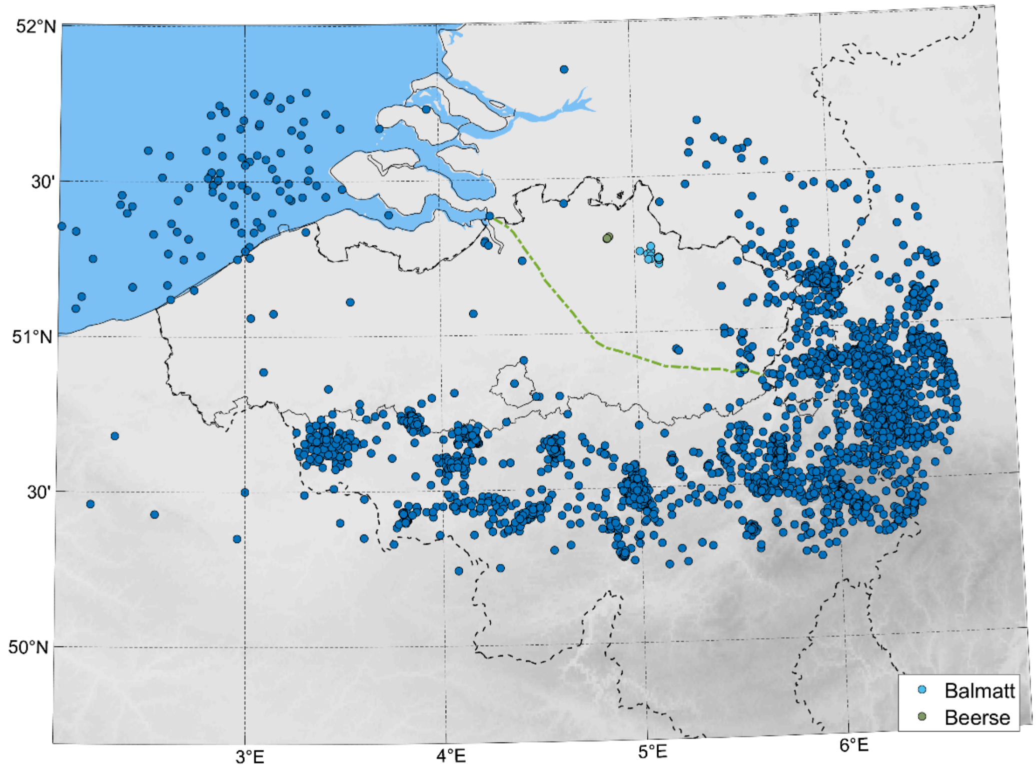

Figure 10: Extended earthquake catalogue including seismic events located within Flanders and up to 50 km from the boundaries of Flanders. The earthquake sequence induced by the Balmatt geothermal project in Mol is highlighted in light blue. Earthquakes induced by the geothermal project at Beerse are highlighted in dark green. Green dash-dotted line indicates the western boundary of the "geological" Campine Basin after Vandenberghe et al. (2014).

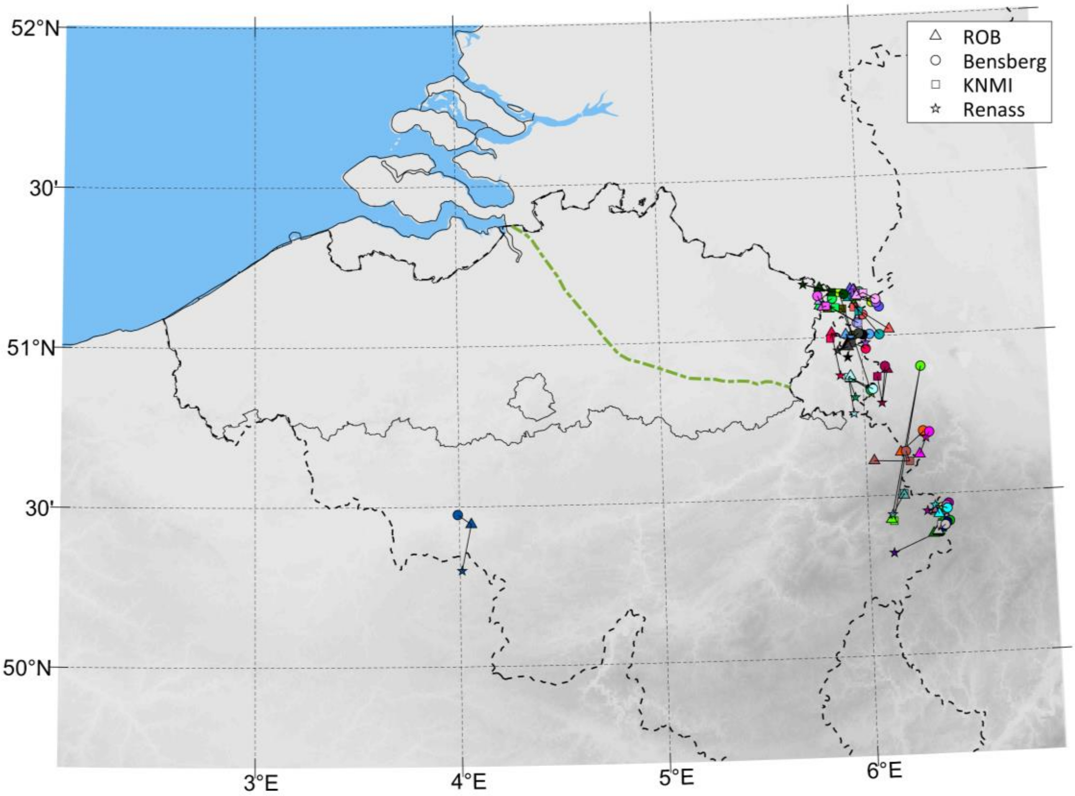

Figure 11: Earthquakes which are located by two or more foreign agencies inside another country, while the national agency of the respective country locates the earthquake outside their own country, or which are located by two or more different national agencies in their own country. Different locations of the same earthquake are connected by a line and the associated agencies are indicated by different symbols according to the legend. Green dash-dotted line indicates the western boundary of the "geological" Campine Basin after Vandenberghe et al. (2014).

1.3 EARTHQUAKE DETECTION

In this chapter time-continuous seismogram data is analyzed for detecting additional earthquakes which are not included in the Flanders Catalogue.

1.3.1 Approach

The magnitude of completeness of the ROB catalogue is reported as M_c=1.7 to M_c=1.8 for the time after 1996 (Van Camp et al., 2020). The current study focusses on detecting earthquakes below this completeness level.

It is important to notice that the ROB had access to the same waveform data used in the current study. To increase the sensitivity for earthquake detections in our study, we have chosen an approach, where the network of seismological monitoring stations is divided into local subnets. Subnet configurations are designed to improve the detection sensitivity for earthquakes occurring within approximately 50 km of the center of a subnet. Sensitivity improvements compared to the routine processing of the ROB were achieved by operating more sensitive trigger settings. This approach comes at the cost of getting many false triggers, which had to be inspected by a seismologist.

Data coverage and availability changed with time (compare section 1.3.2). Therefore, trigger settings had to be adapted according to the actual data situation. While several trigger parameters were kept constant for the entire data set, the number of coincident signal detections and the triggering threshold were varied (Table 3). These variations reflect a compromise between detection sensitivity and the rate of false triggers. With the parameter settings chosen in this study, a total number of approx. 94,000 false triggers had to be processed. An assessment of the detection sensitivity is provided in section 1.3.4.

Table 3: Parameter settings for STA/LTA detector. Note that the epicenter of an earthquake can only be determined if the earthquake is recorded by at least 3 independent monitoring stations. Therefore, we have chosen $n_c \geq 3$.

Parameter	Settings
band pass filter	0.5 Hz to 10 Hz, 4th order Butterworth
STA	0.4 s
LTA	4 s
triggering channels	vertical
ε „triggering threshold“	variable, see subnet descriptions
n_c „number of coincident signal detections”	$n_c \geq 3$, variable, see subnet descriptions

1.3.2 Waveform Data

Existing time-continuous waveform data was requested from the ROB and national agencies operating seismological stations within 50 km of Flanders boundaries. Waveform data was transferred using Arclink, webtransfer, and hard drives. Figure 12 shows the seismometer stations considered for the current study. For most stations, time-continuous data exist only after 2008 (Figure 13 - Figure 15). In total, 32 TB of waveform data were collected and integrated into a local data base. For this, data was converted into a homogeneous data format and resampled to 100 Hz.

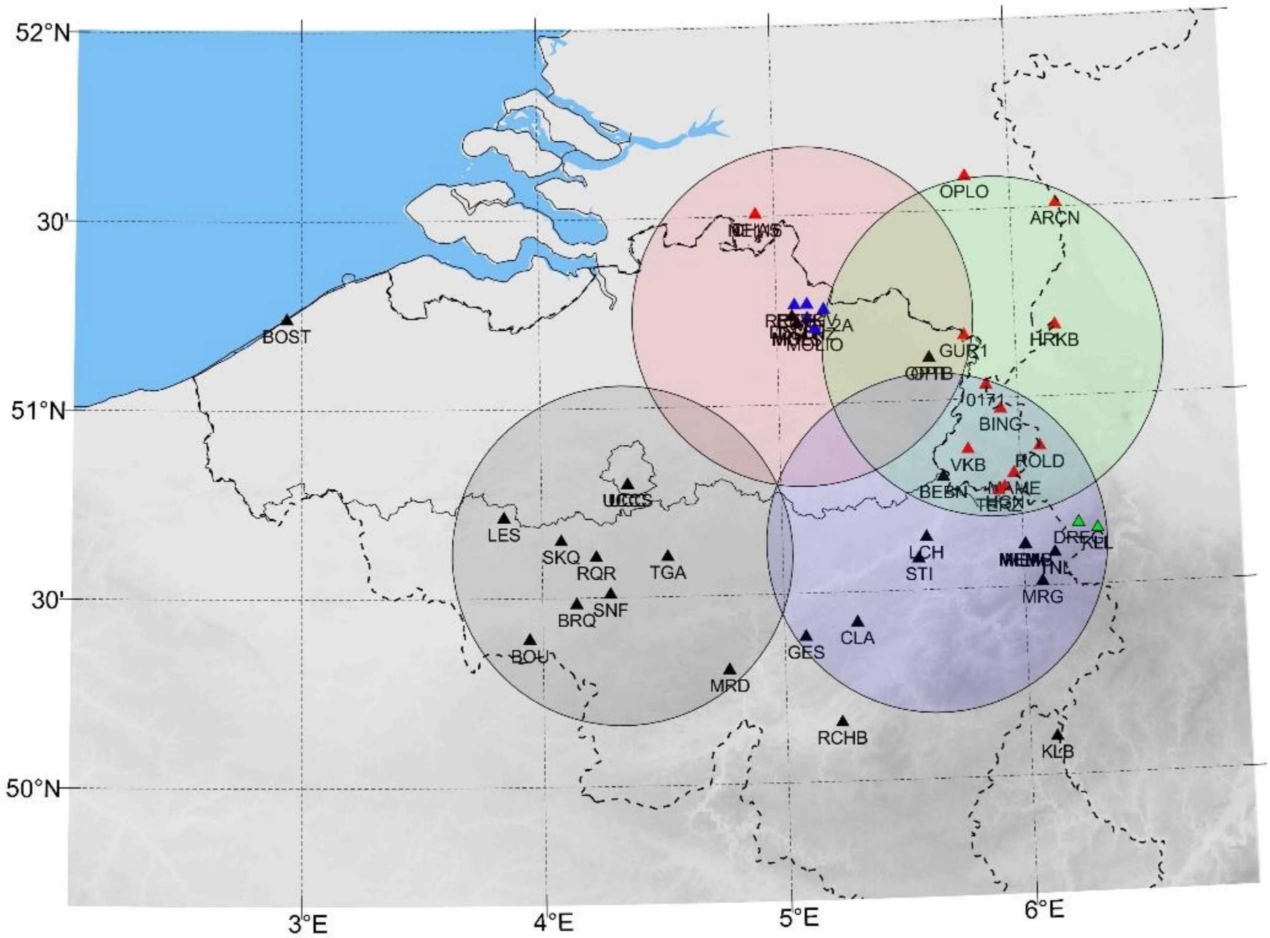

Figure 12: Delimitation of the four local subnetworks (1=red, 2=green, 3=blue, 4=gray). The triangles denote the location of seismic stations, for which data is available.

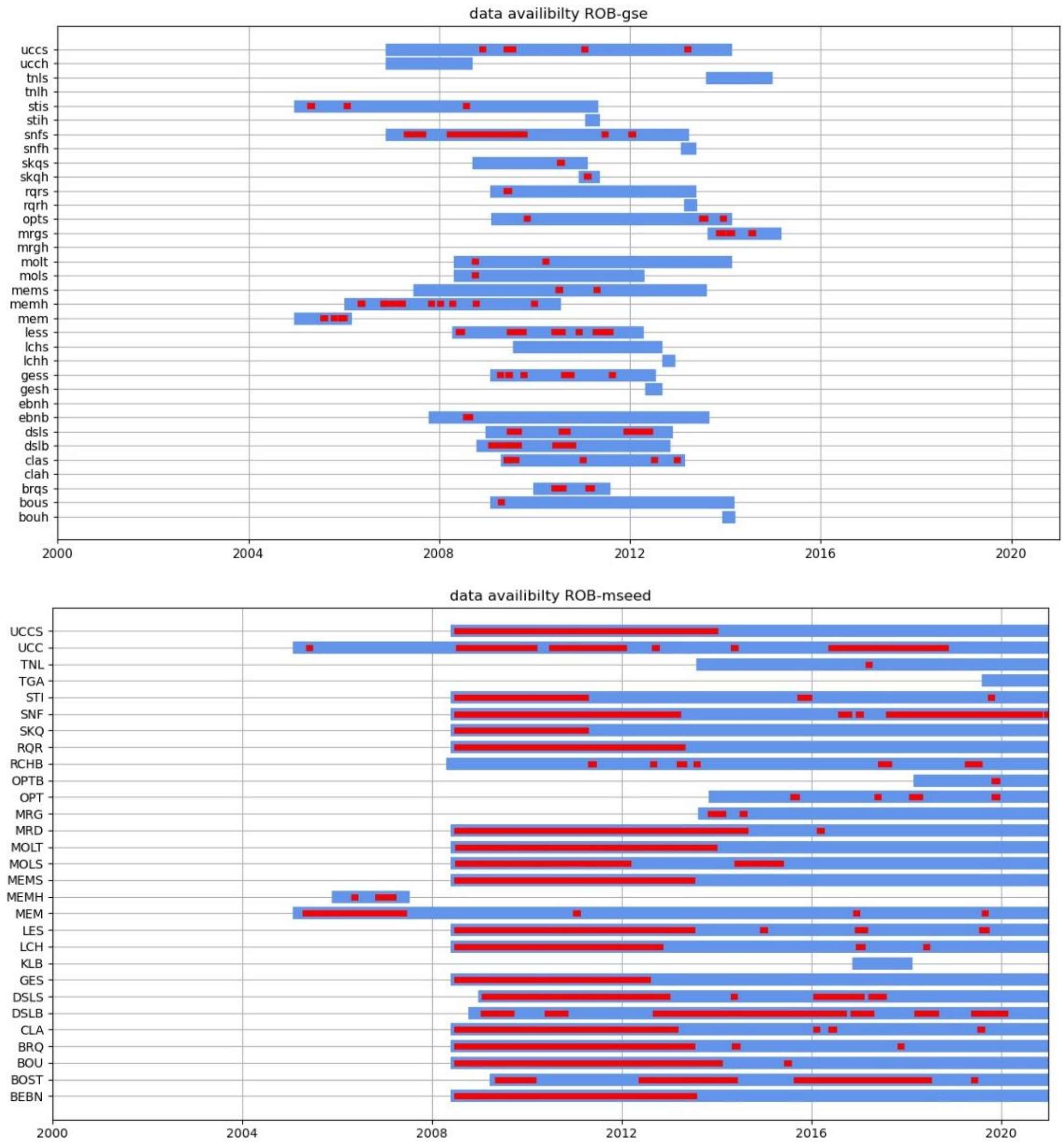

Figure 13: Data availability as a function of time for stations operated by the ROB. Time-continuous seismogram data was provided in two different data formats, GSE (top) and miniSeed (bottom).

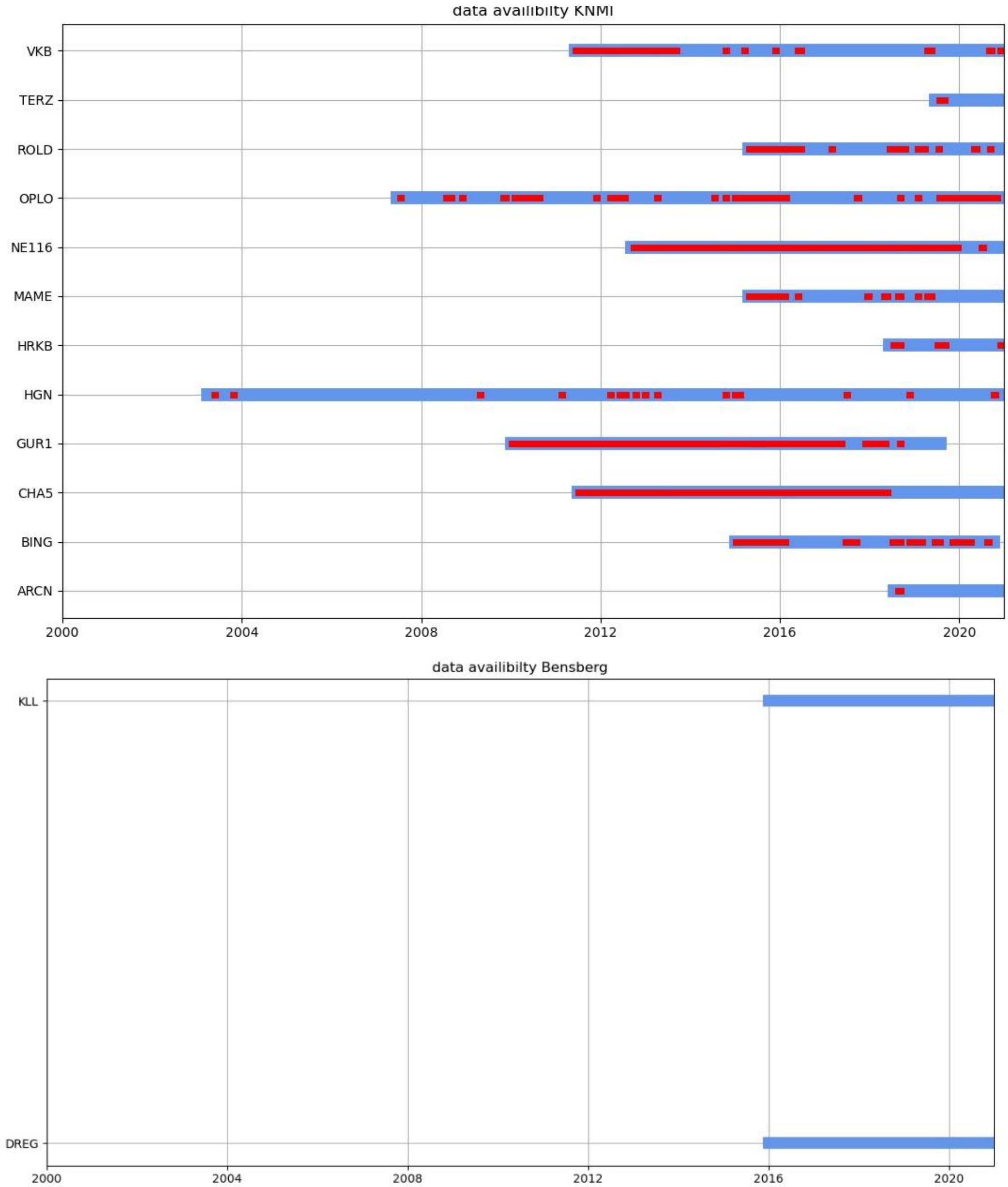

Figure 14: Data availability as a function of time for stations operated by the KNMI (top) and by Bensberg (bottom).

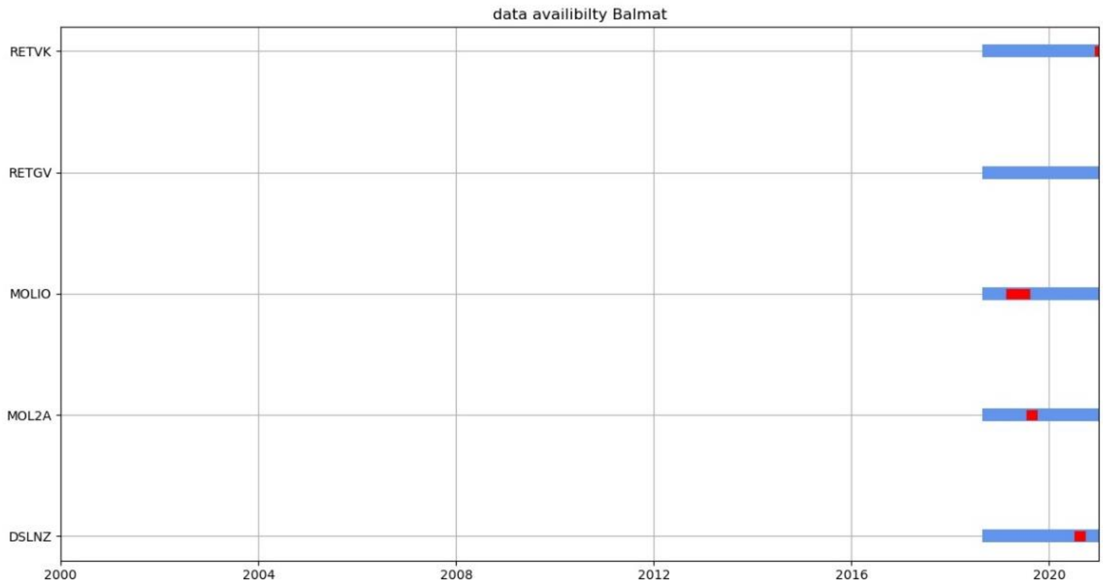

Figure 15: Data availability as a function of time for stations operated by VITO.

1.3.3 STA/LTA Detector

1.3.3.1 Subnetwork 1

Subnetwork 1 covers the northeastern part of Flanders, including the Balmatt geothermal site, and consists of 15 stations (Table 4). The STA/LTA detector was operated on data recordings from the time between November 2008 and end of 2020. No processing was performed for data recorded prior to November 2008, when continuous data was available from less than 3 stations only. Data from subnetwork 1 was used to fine-tune the detector settings for subsequent processing. To benchmark different detector settings, a baseline was determined using n_c=3 and ε=3.2. All other parameters were chosen according to Table 3. A total number of approx. 54,000 triggers resulted, which were visually inspected and interpreted by a seismologist. From this, we identified

- 59 earthquakes classified as “induced” based on their location near the Balmatt site,
- 262 natural earthquakes,
- and approx. 54,217 false triggers / quarry blasts.

Based on these results, the event detector was further optimized for data processing of subnetworks 2-4. According to our scope, we have excluded quarry blasts from the catalogue.

Table 4: Seismological stations belonging to subnetwork 1.

Station code	Operator	Longitude [°]	Latitude [°]
DSLNZ	VITO	5.1282	51.2264
MOL2A	VITO	5.1987	51.2484
MOLIO	VITO	5.1591	51.1978
RETGV	VITO	5.1286	51.2632
RETVK	VITO	5.0759	51.262
BOST	ROB	2.9387	51.2382
DSLB	ROB	5.065	51.232
DSLS	ROB	5.065	51.232
MOLS	ROB	5.085	51.2131
MOLT	ROB	5.0862	51.2135
OPT	ROB	5.636	51.1115
OPTB	ROB	5.636	51.1115
CHA5	KNMI	4.9212	51.5043
GUR1	KNMI	5.7846	51.1687
NE116	KNMI	4.9209	51.5042

1.3.3.2 Subnetwork 2

Subnetwork 2 covers the eastern part of Flanders and the Dutch/German border regions. It consists of 16 stations (Table 5). The STA/LTA detector was operated on data recordings from the time between July 2008 and end of 2020. No processing was performed for data recorded prior to July 2008, when continuous data was available from less than 3 stations only. Parameter settings were chosen according to Table 3 with ε=2.9 and n_c=3 for the time periods when data from only 3 stations was available and n_c=4 when data from 4 or more stations was available. A total number of 2,470 triggers resulted, which were visually inspected and interpreted by a seismologist. From this, we identified

- 318 natural earthquakes,
- and 2,152 false triggers/quarry blasts.

According to our scope, we have excluded quarry blasts from the catalogue.

Table 5: Seismological stations belonging to subnetwork 2.

Station Code	Operator	Longitude [°]	Latitude [°]
MOL2A	VITO	5.1987	51.2484
MOLIO	VITO	5.1591	51.1978
BEBN	ROB	5.6778	50.797
OPT	ROB	5.636	51.1115
OPTB	ROB	5.636	51.1115
0171	KNMI	5.8691	51.0354
ARCN	KNMI	6.1924	51.5101
BING	KNMI	5.9268	50.9708
GUR1	KNMI	5.7846	51.1687
HGN	KNMI	5.9317	50.764
HRKB	KNMI	6.1678	51.1879
MAME	KNMI	5.9727	50.8
OPLO	KNMI	5.8121	51.5888
ROLD	KNMI	6.0847	50.8694
TERZ	KNMI	5.9061	50.7568
VKB	KNMI	5.7847	50.8669

1.3.3.3 Subnetwork 3

Subnet 3 covers the southeastern part of Flanders and parts of Wallonia. It consists of 20 stations (Table 6). The STA/LTA detector was operated on data recordings from the time between March 2005 and end of 2020. No processing was performed for data recorded prior to March 2005, when continuous data was available from less than 3 stations only. Parameter settings were chosen according to Table 3 with ε=2.9 and n_c=3 for the time periods when data from only 3 stations was available. The latter parameter was increased to n_c=4 (or n_c=5 or n_c=6) for those periods were data from 4+ (or 8+ or 11+) stations was available.

A total number of approx. 23,000 triggers resulted, which were visually inspected and interpreted by a seismologist. From this, we identified

- 1 earthquake classified as “induced” based on its temporal correlation and its location near the Balmatt site,
- 857 natural earthquakes,
- and 22,120 false triggers / quarry blasts.

According to our scope, we have excluded quarry blasts from the catalogue.

Table 6: Seismological stations belonging to subnetwork 3.

Station Code	Operator	Longitude [°]	Latitude [°]
BEBN	ROB	5.6778	50.797
CLA	ROB	5.302	50.419
GES	ROB	5.087	50.385
KLB	ROB	6.109	50.1
LCH	ROB	5.5988	50.6395
MEM	ROB	6.0096	50.6087
MEMS	ROB	6.0096	50.6087
MRG	ROB	6.0741 / 6.0747	50.5112 / 50.5114
RCHB	ROB	5.2268	50.1552
STI	ROB	5.5639	50.583
TNL	ROB	6.1295	50.5862
0171	KNMI	5.8691	51.0354
BING	KNMI	5.9268	50.9708
HGN	KNMI	5.9317	50.764
MAME	KNMI	5.9727	50.8
ROLD	KNMI	6.0847	50.8694
TERZ	KNMI	5.9061	50.7568
VKB	KNMI	5.7847	50.8669
DREG	Bensberg	6.233	50.663
KLL	Bensberg	6.3113	50.6467

1.3.3.4 Subnetwork 4

Subnet 4 covers the southern part of Flanders and parts of Wallonia. It consists of 11 stations (Table 7). The STA/LTA detector was operated on data recordings from the time between July 2008 and end of 2020. No processing was performed for data recorded prior to July 2008, when continuous data was available from less than 3 stations only. Parameter settings were chosen according to Table 3 with ε=2.9 and n_c=3 for the time periods when data from only 3 stations was available and n_c=4 when data from 4 or more stations was available.

A total number of approx. 14,500 triggers resulted, which were visually inspected and interpreted by a seismologist. From this, we identified

- 290 natural earthquakes,
- and 14,274 false triggers / quarry blasts.

According to our scope, we have excluded quarry blasts from the catalogue.

Table 7: Seismological stations belonging to subnetwork 4.

Station Code	Operator	Longitude [°]	Latitude [°]
BOST	ROB	2.9387	51.2382
BOU	ROB	3.945	50.389
BRQ	ROB	4.1413	50.4825
LES	ROB	3.843	50.7114
MRD	ROB	4.7681	50.3023
RQR	ROB	4.2246	50.6062
SKQ	ROB	4.0797	50.6486
SNF	ROB	4.2823	50.5077
TGA	ROB	4.5223	50.6046
UCC	ROB	4.3604	50.7972
UCCS	ROB	4.3605	50.7973

1.3.4 Earthquake Processing

For all earthquake detections which cannot be associated with the Flanders Catalogue or Extended Catalogue within the tolerance boundaries defined in section 1.2.2, hypocenters were determined using NonLinLoc (Lomax et al., 2000, 2009) and the seismic velocity model described in Figure 16. Earthquake magnitude was determined using the formula by Dost et al. (2004).

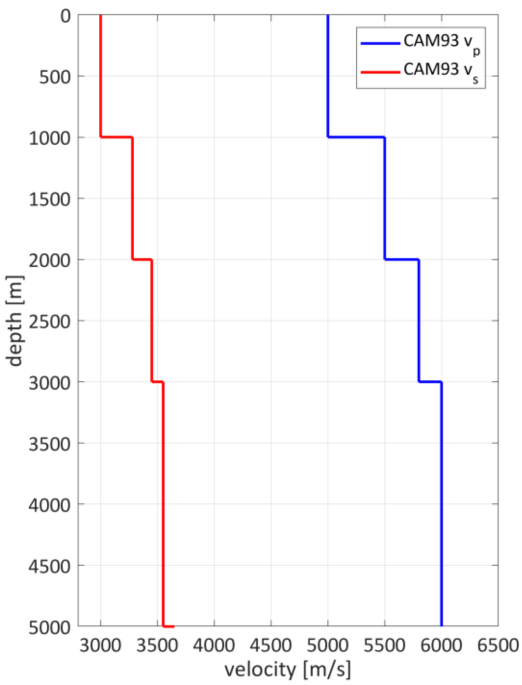

Figure 16: Seismic wave velocity model after Verbeeck (2019). This is the same velocity model used by the ROB for routine processing.

1.3.5 Lower Detection Threshold

For assessing to what extend the detection sensitivity improved in the current study compared to the routine processing of the ROB, numerical simulations of the lower detection threshold were performed. These simulations are based on forward modelling of ground vibrations and require assumptions regarding the seismic background noise level at the monitoring stations. To ensure that our simulations adequately reflect actual detection capabilities of the ROB network, we have "calibrated" our model against the detection capabilities (as of 2019) published by the ROB. Subsequently, we have used the calibrated parameter settings for modelling the detection capabilities of our subnetwork configurations (as of 2019).

In subsequent sections we compare the simulated detection capabilities of the subnets to the detection capabilities of the ROB network. It should be noted that less of an improvement in the detection capabilities can be expected for the cases in which ROB includes stations from neighboring countries for processing. At least for the more recent earthquakes, data from neighboring countries is routinely included by the ROB.

1.3.5.1 Calibration

No specific ground motion attenuation model exists for Flanders. We have chosen the formula of Dost et al. (2004) for relating magnitude to ground motions.

Within a sensitivity analysis we tried to match the published detection threshold of the ROB network (Van Camp et al., 2020). We have chosen the same parameter settings as Van Camp et al. (2020) and varied the (homogeneous) background noise level. A good match is obtained for a configuration, where the detection limit for earthquake signals is PGV = 0.009 mm/s (Figure 17).

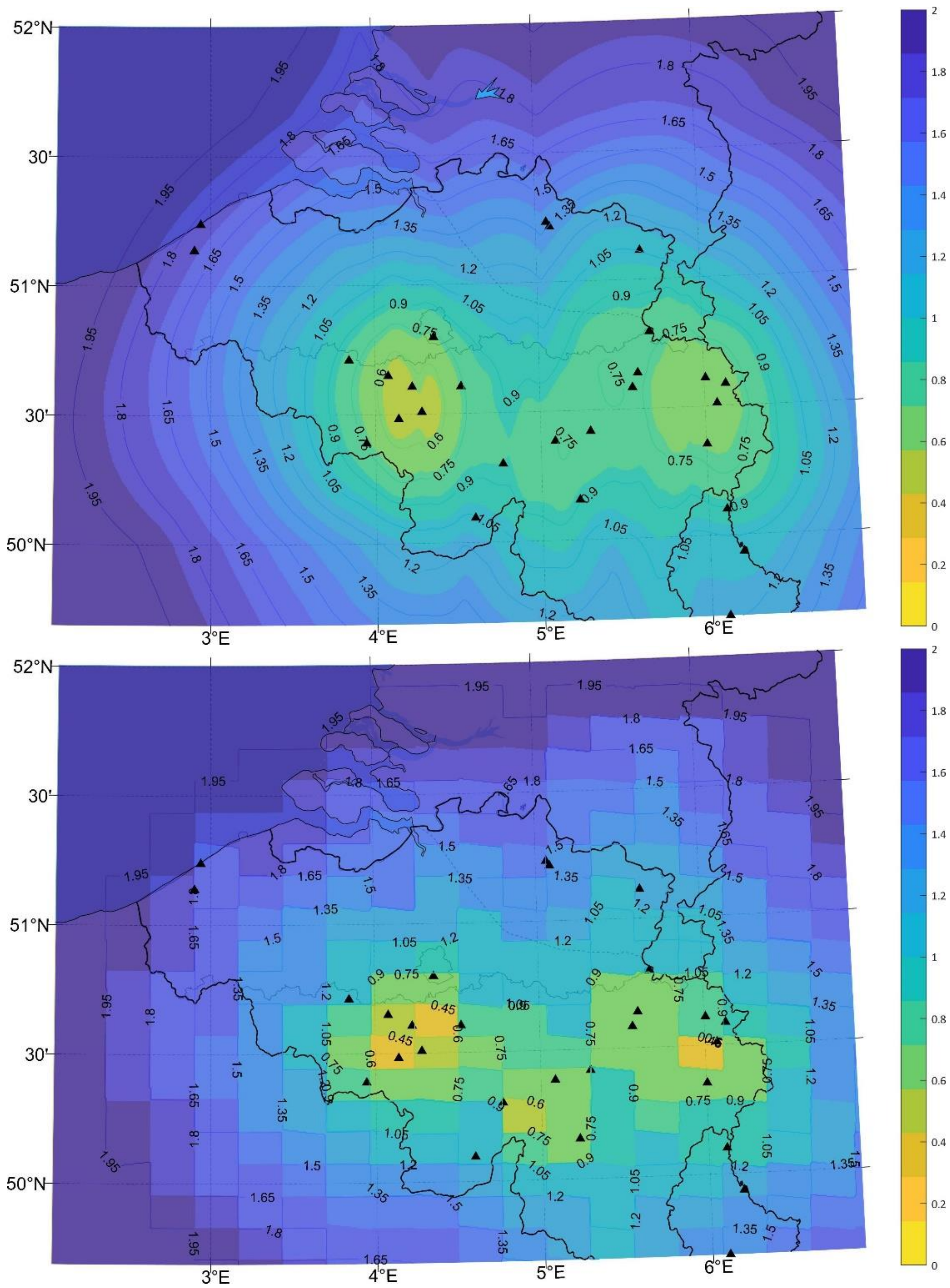

Figure 17: Top: Simulated lower magnitude detection threshold of the ROB network for an earthquake occurring at 10 km depth. Typical noise conditions during daytime are assumed, which were "calibrated" using Figure 20 of Van Camp et al. (2020). The diagram is based on the ROB station network as of 2019 and earthquakes need to be measured by at least four stations (n_c=4). Bottom: Simulation data provided by the ROB. Note the lower resolution level in the lower plot. When accounting for data resolution, differences between the two plots are typically less than 0.2 magnitude units (M_L).

1.3.5.2 Subnetwork 1

Figure 18 shows the (simulated) improvement of the detection capabilities compared to the scenario, where the ROB network would be the only one used. Results indicate that detection capabilities locally increased by up to approx. 1 magnitude unit (M_L) with the subnet-based approach. The region of improved detection capabilities covers large parts of the Campine Basin.

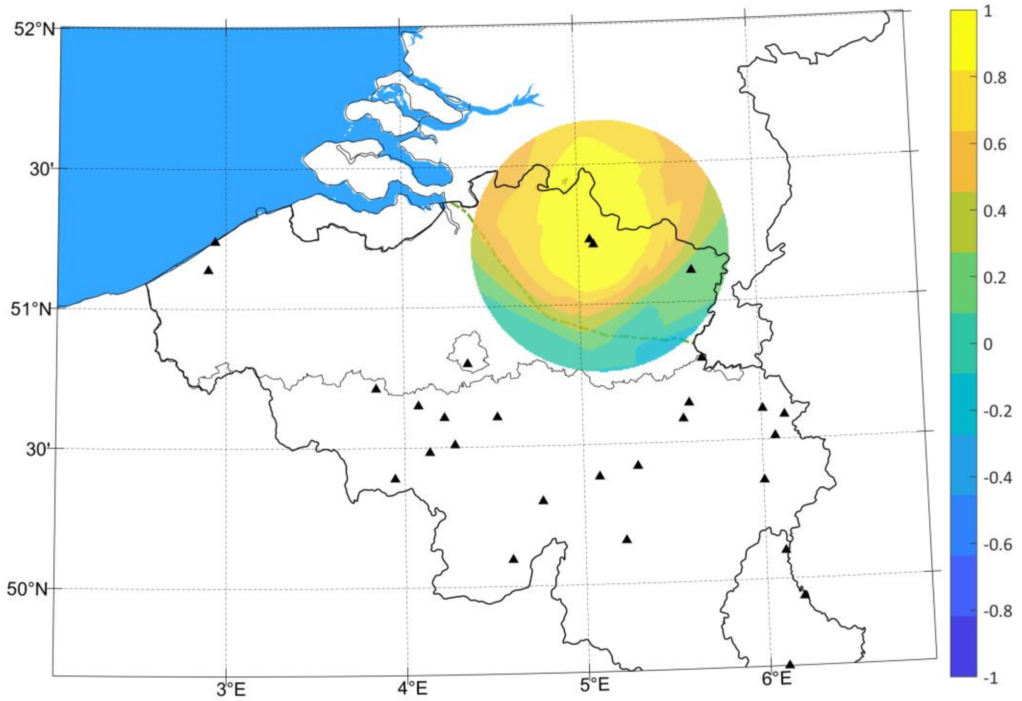

Figure 18: Improvement of the detection capabilities in M_L units according to the colormap. The improvement is calculated as the difference between the lower detection limit simulated for the ROB network (i.e., Figure 16, top) and for processing with subnet 1 (configuration as of 2019). The earthquake depth is assumed at 10 km. Green dash-dotted line indicates the western boundary of the “geological” Campine Basin after Vandenberghe et al. (2014).

1.3.5.3 Subnetwork 2

Figure 19 shows the (simulated) improvement of the detection capabilities compared to the scenario, where the ROB network would be the only one used. Results indicate that detection capabilities locally increased by up to approx. 0.8 magnitude units (M_L) with the subnet-based approach. Detection capabilities improved primarily in the Eastern part of Flanders and the border regions.

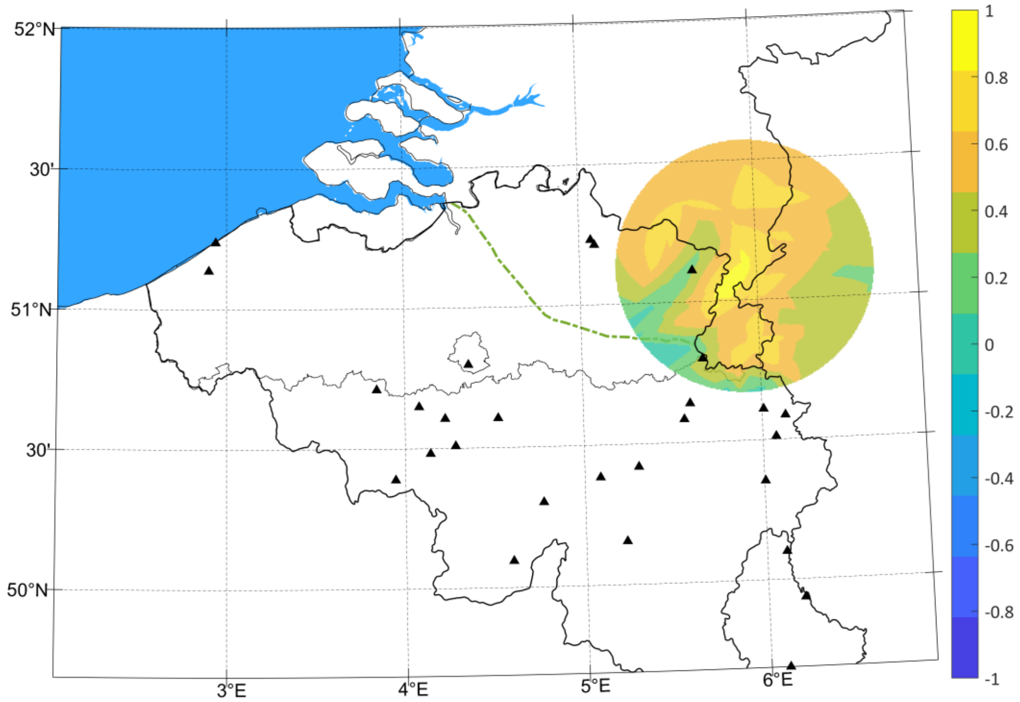

Figure 19: Improvement of the detection capabilities in M_L units according to the colormap. The improvement is calculated as the difference between the lower detection limit simulated for the ROB network (i.e., Figure 16, top) and for processing with subnet 2 (configuration as of 2019). The earthquake depth is assumed at 10 km. Green dash-dotted line indicates the western boundary of the "geological" Campine Basin after Vandenberghe et al. (2014).

1.3.5.4 Subnetwork 3

Figure 20 shows the (simulated) improvement of the detection capabilities compared to the scenario, where the ROB network would be the only one used. Results indicate only minor improvement of the detection capabilities, primarily outside Flanders. Within the eastern part of Flanders, the detection capabilities decreased. It should be noted, however, that the associated regions are covered by subnetwork 2, exhibiting improved detection capabilities (Figure 19).

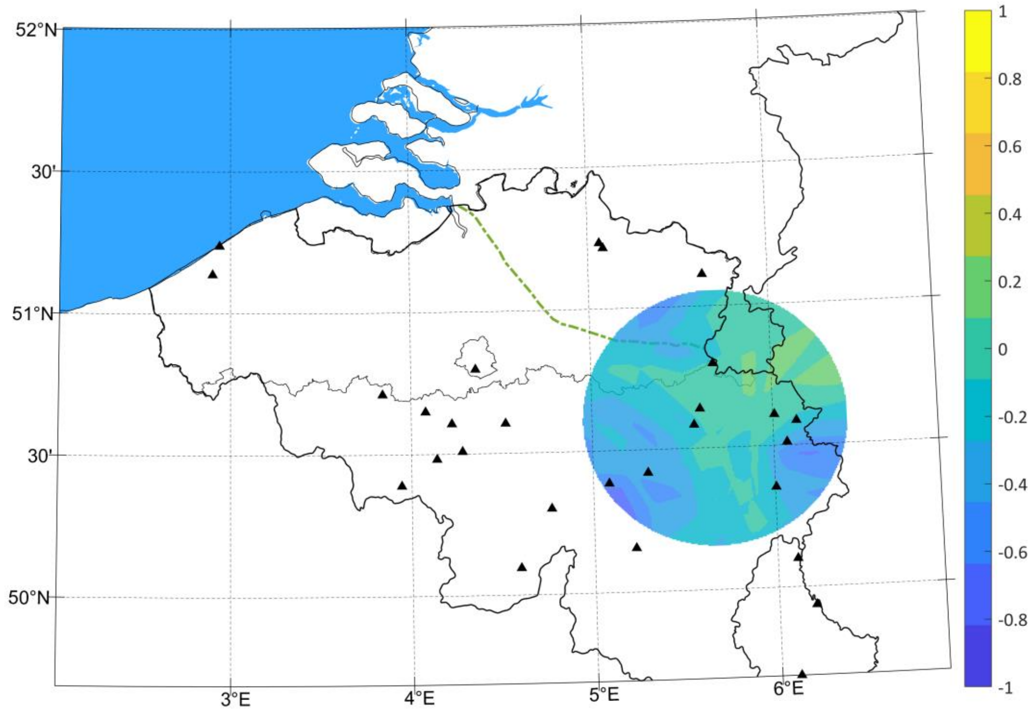

Figure 20: Improvement of the detection capabilities in M_L units according to the colormap. The improvement is calculated as the difference between the lower detection limit simulated for the ROB network (i.e., Figure 16, top) and for processing with subnet 3 (configuration as of 2019). The earthquake depth is assumed at 10 km. Green dash-dotted line indicates the western boundary of the "geological" Campine Basin after Vandenberghe et al. (2014).

1.3.5.5 Subnetwork 4

Figure 21 shows the (simulated) improvement of the detection capabilities compared to the scenario, where the ROB network would be the only one used. Results indicate that detection capabilities in the southern part of Flanders locally increased by 0.1-0.2 magnitude units (M_L) with the subnet-based approach.

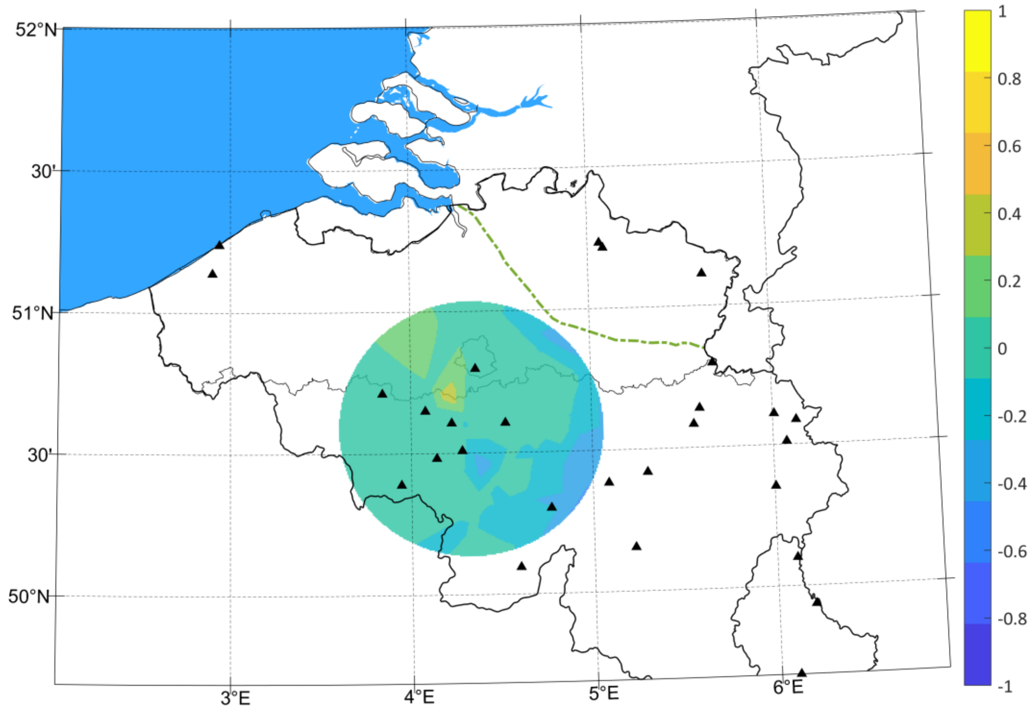

Figure 21: Improvement of the detection capabilities in M_L units according to the colormap. The improvement is calculated as the difference between the lower detection limit simulated the ROB network (i.e., Figure 16, top) and for processing with subnet 4 (configuration as of 2019). The earthquake depth is assumed at 10 km. Green dash-dotted line indicates the western boundary of the "geological" Campine Basin after Vandenberghe et al. (2014).

1.3.6 Summary of Results

The subnet-based approach yields almost 95,000 event triggers for the time for which continuous data recordings exist. All triggered events were visually inspected, and false triggers were removed. The remaining seismic events were compared to the Flanders Catalogue and the Extended Catalogue.

For the time over which the detectors were operated we find that:

- All but one earthquake (M_L=-0.4) from the Flanders Catalogue were detected with our subnet approach. It is unclear to us how this earthquake was detected by the ROB, given that its magnitude is well below their lower detection threshold. Inspection of waveforms for this event indicates that earthquake signals are visible at 2 stations only.
- Within Flanders, no additional earthquakes were detected.
- Many events were detected which exhibit the typical waveforms of blasts from different quarries previously identified by the ROB. These events were removed from the detection list.
- For about 3 dozen detected events the waveform signatures appeared to be different from the known quarry blasts. These events were initially classified as potential earthquakes. Based on their epicenter locations (Figure 22), however, it appears likely that many of these detections also originate from quarry blasts. These events were also removed from the detection list. The remaining 9 detections were integrated into the Extended Catalogue.

- Numerical simulations indicate that the subnet-based approach improved the detection capabilities by up to 0.5-1 magnitude units (M_L) over large parts of the Campine Basin.
- The total numbers of earthquakes listed in the final catalogues are provided in Table 8. These numbers include the template detections described in the subsequent chapter.

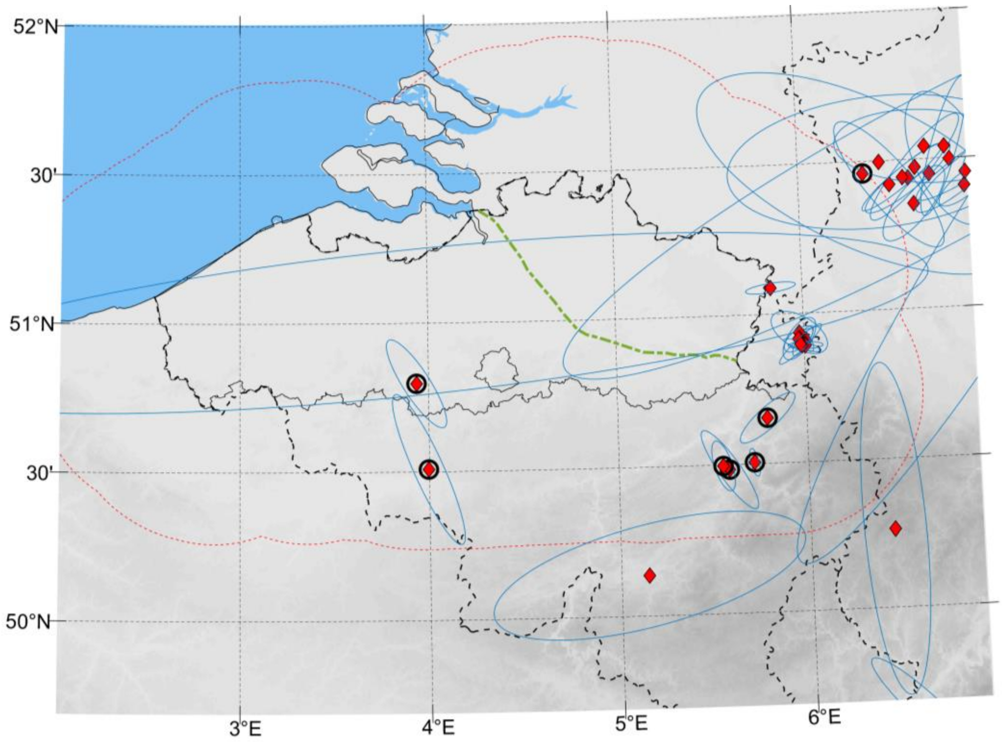

Figure 22: Epicenter locations (red diamonds) and confidence estimates of selected seismic events detected by subnet processing. These events are not listed by the regional earthquake agencies (section 1.2.1). Based on seismograms the events were considered earthquake candidates. Many candidates are located close to known regions with mining activity. These events were classified as quarry blasts (marked by black open circles). Dotted red line indicates boundaries for the Extended Catalogue. Earthquakes with epicenters outside these boundaries were not further analyzed/classified.

Table 8: Number of earthquakes listed in the final Flanders Catalogue and the Extended Catalogue. Note: The numbers of earthquakes also include template detections (chapter 1.4).

Catalogue	Flanders	Extended
Number of natural earthquakes	66	2,920
Number of induced earthquakes	608	628

1.4 TEMPLATE MATCHING

The template matching technique (e.g., Schmittbuhl et al., 2021) aims at detecting small magnitude earthquakes that are not detected by classical detection algorithms such as STA/LTA (section 1.3.3). In this approach, the seismogram from a reference earthquake ("template") is compared to time continuous recordings of the ground motion at the same station. Signal similarity is determined in terms of a correlation coefficient calculated on a sliding time window (e.g., Baisch et al., 2008) and a detection is declared if the signal correlation exceeds a pre-defined threshold value.

In the same way, a multi-station detector can be designed, requiring coincident similarity detections at different recording stations. This can provide an efficient measure to reduce the number of false detections while maintaining a high level of sensitivity. As a downside, however, the multi station criteria make the detector less sensitive to earthquakes occurring not in the immediate vicinity of the template earthquake. Furthermore, the multi-station approach requires that (good) quality data from several stations is available. For the current data set, this is frequently not the case, and we thus considered the single-channel template detector to be more suitable.

1.4.1 Induced Seismicity at Balmatt

At the Balmatt geothermal site, local monitoring stations were deployed only after geothermal activities had already started (e.g., INERIS, 2020). Consequently, the early phase of subsurface activities at the geothermal site were solely monitored by seismological stations operated by the ROB.

To cover the entire time window of geothermal operations, different templates recorded by different stations were defined and each template was used in a single-station template detector. The stations were chosen based on proximity to the geothermal site, data availability and signal quality.

The most important station is MOLT operated by the ROB. This station is located at approx. 2.1 km distance to the geothermal site and provided time-continuous data for the entire time window of interest. Additional templates were defined for stations DSLB, MOL2A, and DSLNZ. Station DSLB exhibits large data gaps in the time window of interest (Figure 13) and stations MOL2A, and DSLNZ were deployed only after subsurface activities had already started (Figure 15).
Table 9 lists the template earthquakes used for the analysis. Vertical channels were used as templates and each template has a length of 2.5 s. Templates and continuous data were bandpass filtered between 2 Hz and 20 Hz using a 2nd order Butterworth filter. A detection is declared if the cross-correlation coefficient exceeds 0.5.

Template triggering was performed for the time window 14. September 2015, prior to drilling, until January 2021. Figure 23 shows template detections as a function of time. The detections were found only after drilling has started, indicating that the detector is sensitive to the signals of induced earthquakes and that it has a very low false-detection rate at station MOLT, which is the only station providing data prior to drilling.

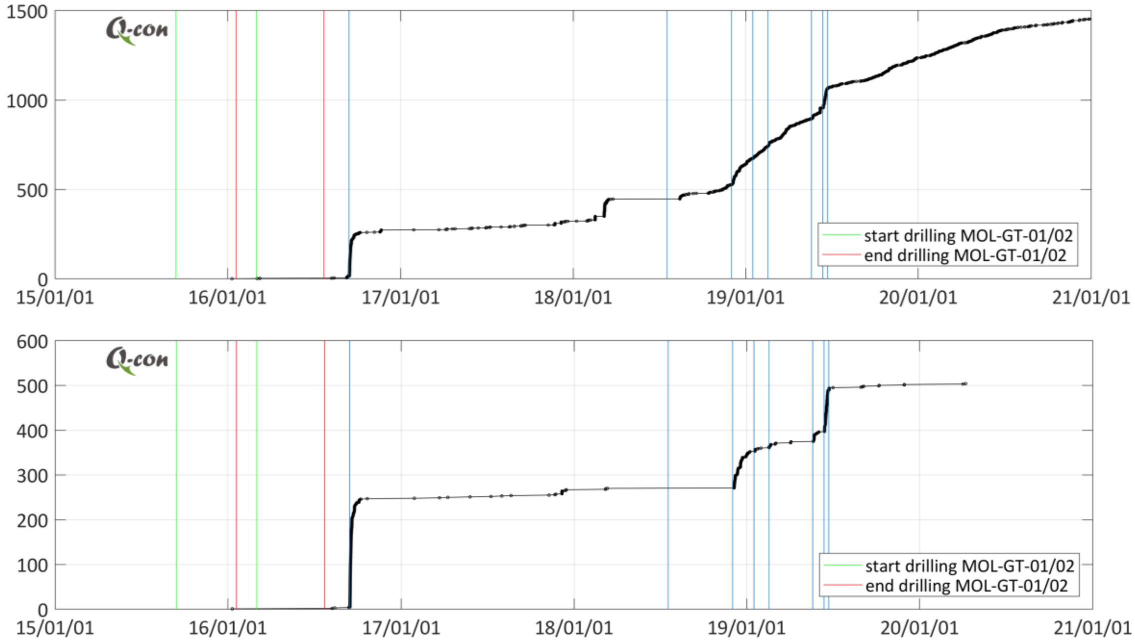

Figure 23: Cumulative number of template detections as a function of time (top) and template detections exhibiting clear waveforms (bottom). Green and red vertical lines indicate drilling periods according to the legend. Blue vertical lines denote hydraulic operations at the Balmatt wellbores.

In total, 1492 seismic events were detected of which 507 exhibit clear waveforms and were confirmed by visual inspection as induced earthquakes (see waveform examples in Figure 24). Interestingly, the first event was detected on January 10th, 2016 (04:41:29 UTC) during drilling of the first geothermal well (Figure 23). This indicates that the local (undisturbed) stress conditions at reservoir level promote seismic failure already by minor stress perturbations.

The last template detection exhibiting clear waveforms was found on April 4th, 2020, indicating that seismic activity at a small magnitude level was an ongoing process for many months after subsurface activities were terminated.

From the set of detections with clear waveforms, 365 detections could not be associated with induced events listed in the VITO catalogue. These template detections were included into the Flanders catalogue, while assigning them the hypocenter location of the strongest event and a generic (large) location error of 2.5 km (1 σ) into all three directions.

It should be noted that not all the known earthquakes at Balmatt (section 1.2.3) were detected by the template trigger. Missing an earthquake can result if the template-stations have no or only noisy data at the time of the earthquake. Additionally, the waveforms of an earthquake may be different to those of the templates due to differences in source location and source mechanisms (Baisch et al., 2008). As a possible strategy for maximizing template detections, 'missed earthquakes' could be systematically implemented as additional templates. This, however, is beyond the scope of the current study.

Table 9: Templates used for detecting Balmatt events.

Earthquake Time	Detector Station
15-Sep-2016 09:50:18	DSLB
16-Jun-2019 03:26:58	MOL2A
16-Jun-2019 03:26:58	DSLNZ
17-Jun-2019 10:17:02	MOLT

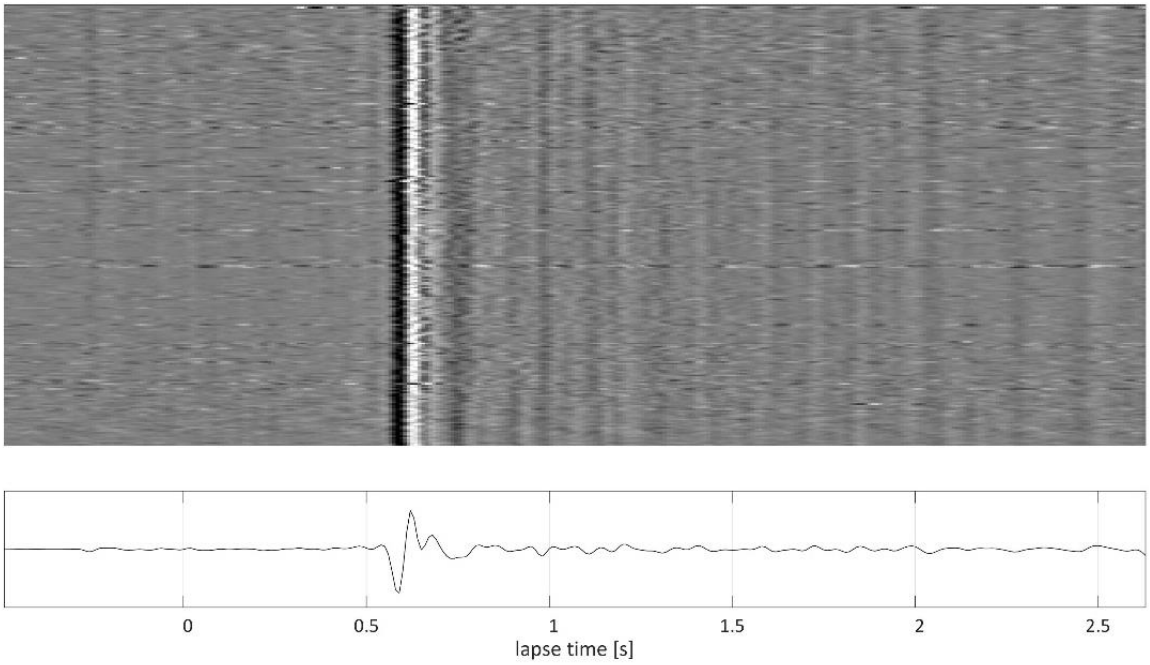

Figure 24: Waveform example of 262 template detections which are not listed in the ROB or VITO catalogues. Waveforms are recorded at station DSLB (horizontal) and are aligned relative to their P onsets. Seismograms are displayed as a 3D surface where peaks are light and troughs are dark. Stacked waveforms are shown in the bottom trace.

1.4.2 Testing Template Design for Natural Earthquakes

For designing a template trigger, *ad hoc* parameter choices must be made. Optimum parameter settings are data-specific and critically depend on earthquake-station distance. In the current study we aim to design a template trigger for local and regional earthquakes occurring at distances up to approx. 100 km.

We used the earthquake sequence at Balmatt (compare previous section) for testing the performance of our template trigger at distant stations. For this, we have selected five monitoring stations located at an epicentral distance between 75 km and 105 km (Figure 25). At each station we used the recordings of the strongest earthquake from the Balmatt sequence for defining a template with the parameters listed in Table 10.

In the time between 13.06.2019 and 24.06.2019, the template detector triggered 7 Balmatt earthquakes in the magnitude range M_L=0.8 to M_L=1.8. Signals of the smaller magnitude earthquakes are significantly attenuated at these distances and the template detector successfully detected earthquake signals with very low SNR (Figure 26).

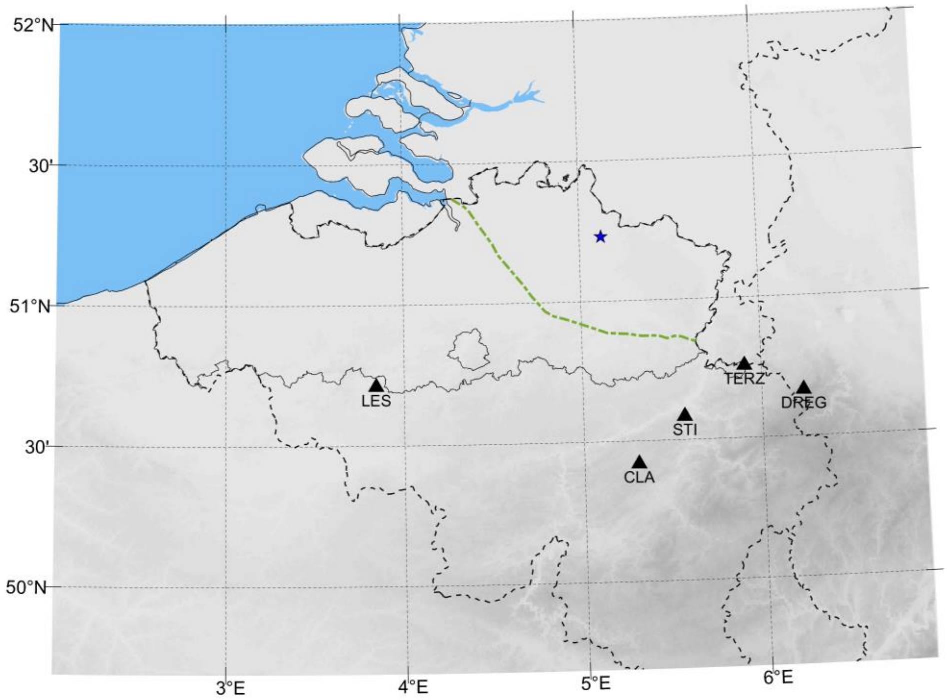

Figure 25: Location of seismological stations used for testing the template trigger design. Test signals are the earthquakes induced at the geothermal site Balmatt (star). Hypocentral distance ranges between 75 km (station TERZ) and 105 km (station LES).

Table 10: Parameter settings for template detector.

Parameter	Settings
band pass filter	2 Hz to 20 Hz, 4th order Butterworth
template channel	vertical
template window length	25 s – 30 s
correlation coefficient threshold	0.5

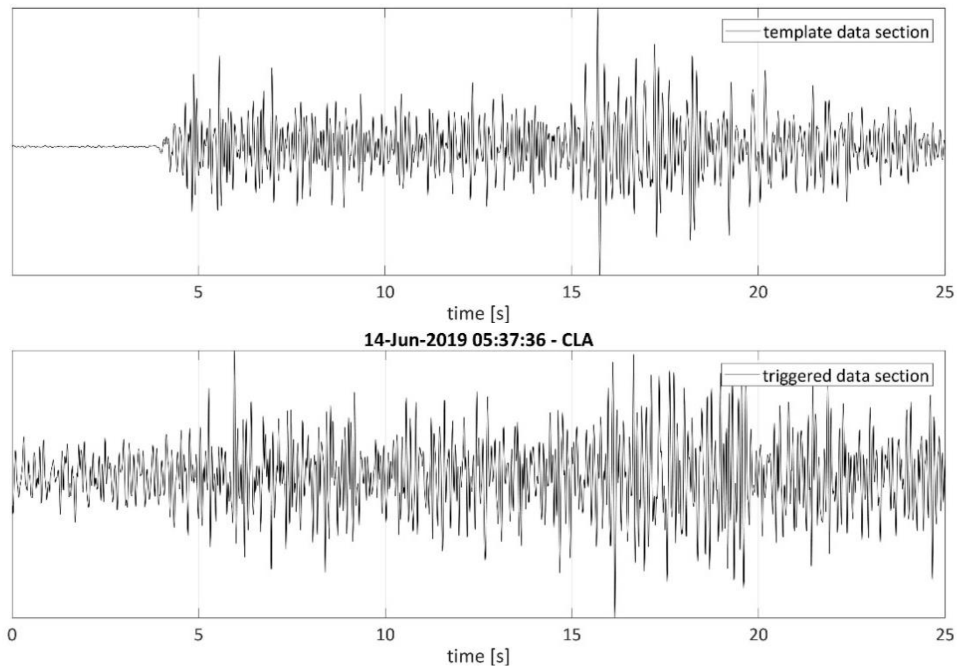

Figure 26: Top: Waveform example of a template used at station CLA (vertical) to detect Balmatt events at regional distances. Bottom: Template detection with low SNR for an event occurring on 14-Jun-2019 05:37:36 UTC.

1.4.3 Template Triggering Flanders, 2019

Using the parameters listed in Table 10, templates of natural earthquakes were defined for the different regions in Flanders where earthquakes have occurred. Waveform data exhibiting clear seismograms exist for 7 different regions (Figure 27). Several templates were defined using triggered seismogram data since the template earthquakes have occurred before continuous data was routinely archived. Triggered waveform data was provided by the ROB (T. Lecocq, 22.07.2021).

In all 7 regions, template-triggering was performed in the time window January 1st, 2019 to December 31st, 2019. Compared to the Extended Catalogue (section 1.2.4), no additional earthquakes were detected.

Due to time constraints, template triggering could only be tested on a limited time window. Based on findings from the previous section, we see a potential for triggering additional earthquakes when applying template triggering to the entire time window for which continuous waveform data exists (roughly 2008-2021). This, however, is beyond the scope of our study. Given the comparatively low detection threshold of the subnet-based approach (section 1.3.5), we expect, however, to detect only a small number (if any) of additional earthquakes.

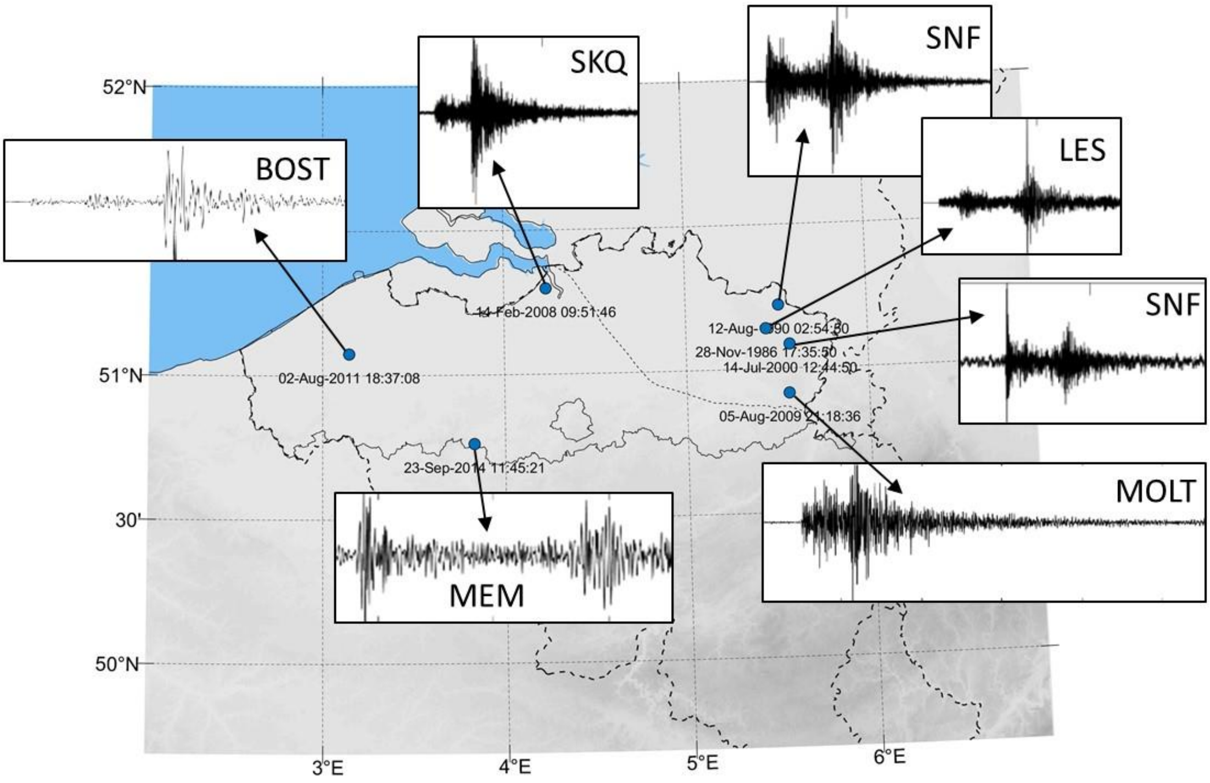

Figure 27: Template waveforms (insets) defined for 7 regions with earthquake activity within Flanders.

1.5 FAULT MECHANISMS

Fault mechanisms of induced earthquakes at Balmatt were analyzed in previous studies (DMT, 2019b; INERIS, 2019, 2020). Our study focusses on the fault mechanisms of natural earthquakes occurring within Flanders.

We pre-selected a set of 30 natural earthquakes in the magnitude range $0.7 \leq M_L < 3.1$ for analyzing fault mechanisms. Besides choosing earthquakes with the best data quality, we aimed to determine fault plane solutions for all regions within Flanders and the immediate border region where earthquake activity occurs. Figure 28 shows those five regions, for which earthquakes were pre-selected. We also inspected the data situation for the isolated earthquakes scattered over Flanders (compare Figure 8) but did not find further candidates for which the determination of fault mechanisms appears feasible.

In a first step, we determined P-wave polarities and S/P amplitude ratios at all recording stations. Due to a low SNR, 10 earthquakes had to be excluded from subsequent analysis. For the remaining 20 earthquakes, FPS were determined using a 3D grid search algorithm (Snoke, 1984) to match the observed P-polarity pattern. The search increment for strike, dip, and rake was set to 10°. Additionally, a unique FPS was determined by additionally matching the observed S/P amplitude ratios. In our analysis we used the layered seismic velocity model depicted in Figure 16. From sensitivity tests we note, however, that our results are not critically depending on details of the layered velocity model.

Figure 29 shows the resulting fault mechanisms when requiring that all P-wave polarity readings are matched. This criterion can be fulfilled only for 17 earthquakes. Of these, 10 fault mechanisms are only loosely constrained (i.e., exhibiting a large variety of gray lines in Figure 29). The remaining 7 FPS show a considerable variety in their mechanisms and even neighboring earthquakes may exhibit a fundamentally different fault plane solution.

To further investigate whether the observed variety of fault mechanisms reflects actual subsurface processes rather than unconstrained data, we have repeated the analysis while allowing for a single polarity misreading, i.e., we assume that one of the polarity readings is wrong. Given the low SNR of most data, we consider this to be a realistic assumption. Figure 30 shows the resulting mechanisms. The polarity pattern can be matched for the same 17 earthquakes. For the remaining three earthquakes, a solution is only obtained when allowing for more than one polarity misreading.

From Figure 30 we note that FPS are generally not well constrained. This is mainly due to a poor station coverage and unclear phase assignments due to low SNR.

Few information on fault mechanisms of earthquakes in Flanders is published in the scientific literature. Camelbeeck (1990) shows fault plane solutions for earthquakes in Belgium (Figure 31). Of these, a single earthquake is located in Flanders (Bilzen earthquake, 16.7.1985, M_L=3.0). The mechanism of this earthquakes indicates normal faulting on a steepling dipping plane. Although waveform data for the Bilzen earthquake is not available for this study, we note that a more recent earthquake (Zutendaal, 05.08.2009, ML=2.7) occurred in close vicinity to the Bilzen earthquake.

The fault mechanism of the Zutendaal earthquake is depicted in more detail in Figure 32. The mechanism is better constrained compared to most other earthquakes studied here. The range of possible solutions, however, is still large and includes normal faulting as well as oblique strike slip. Despite these uncertainties, we note, that the polarity pattern (and the best matching solution) is consistent with the solution of Camelbeeck (1990).

Additional fault plane solutions for earthquakes in the Lower Rhine Graben and in the border zone of Belgium are provided by Vanneste et al. (2013). Besides for the Bilzen earthquake, fault mechanisms are shown for two earthquakes (Stramproy, 05.06.1980; Maaseik, 22.05.1982) near the Dutch-Belgian border. Both earthquakes exhibit a normal faulting mechanism.

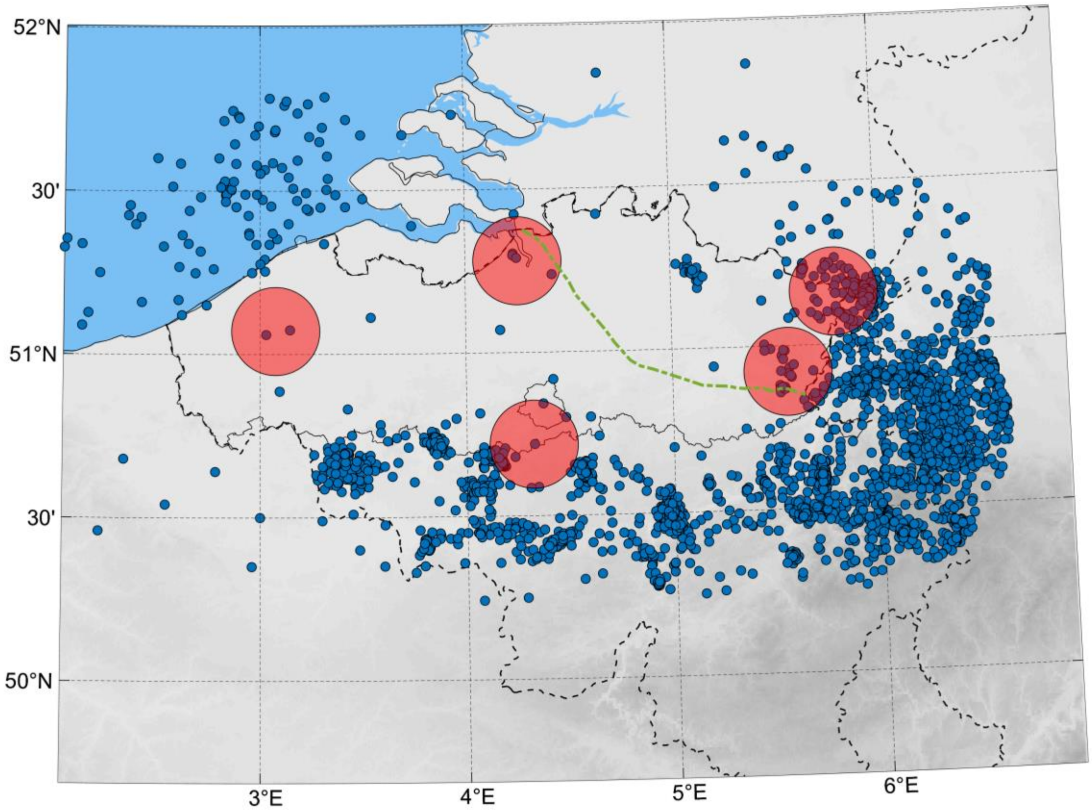

Figure 28: Regions of seismic activity (red shaped circles) within Flanders selected for fault plane mechanism analysis.

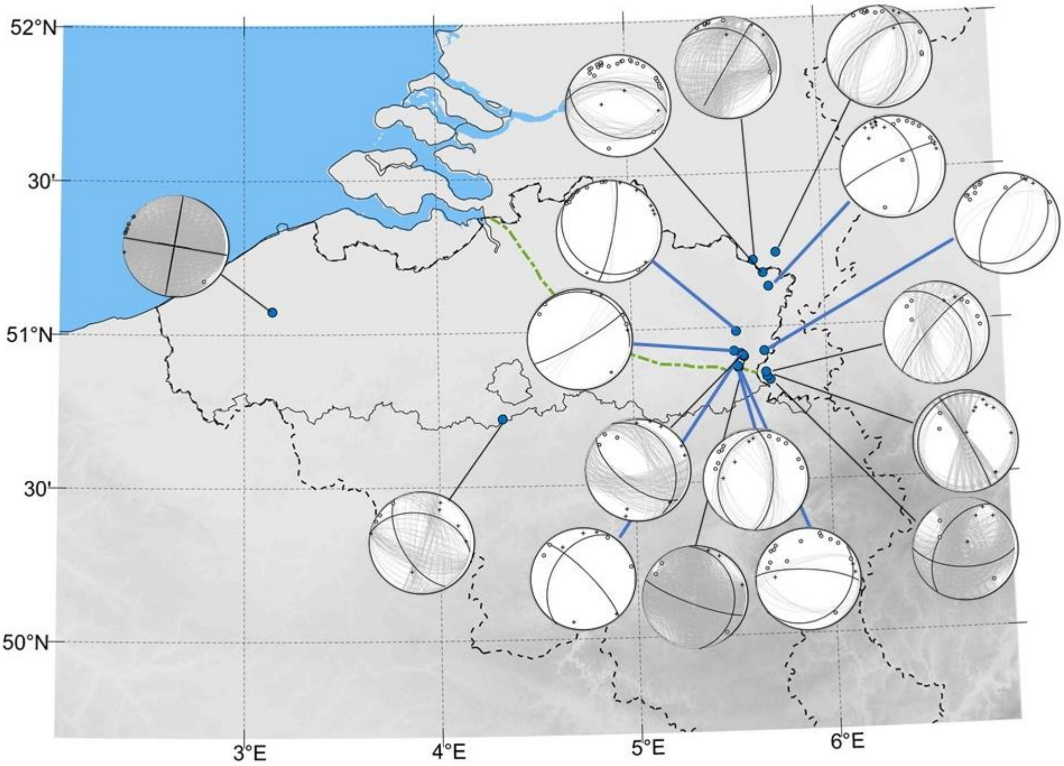

Figure 29: Fault plane solutions for 17 earthquakes within Flanders. Gray lines indicate fault plane solutions which are consistent with the observed P-wave polarities (plusses indicate compression). A best matching fault plane solution (black line) is determined by additionally matching observed S/P amplitude ratios. Only those solutions are shown, where P-wave polarities are exactly matched at all recording stations. Only the 7 solutions marked by blue lines are reasonably well constrained. See text for details.

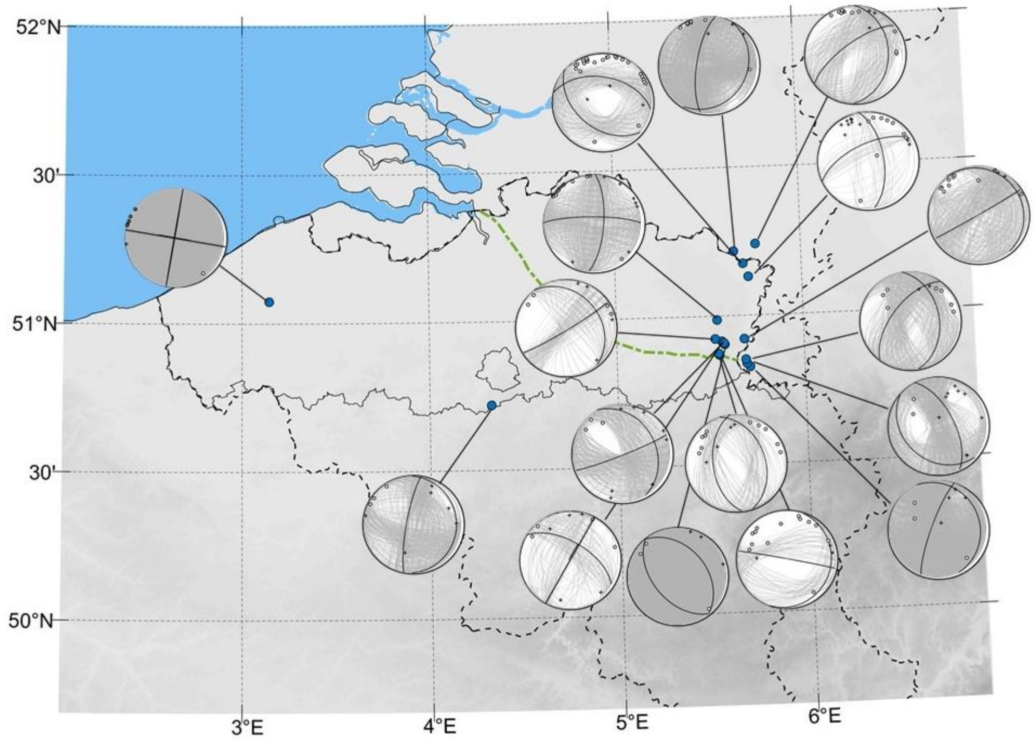

Figure 30: Fault plane solutions for 17 earthquakes within Flanders. Gray lines indicate fault plane solutions which are consistent with the observed P-wave polarities (plusses indicate compression) when allowing for a single polarity misreading. A best matching fault plane solution (black line) is determined by additionally matching observed S/P amplitude ratios. See text for details.

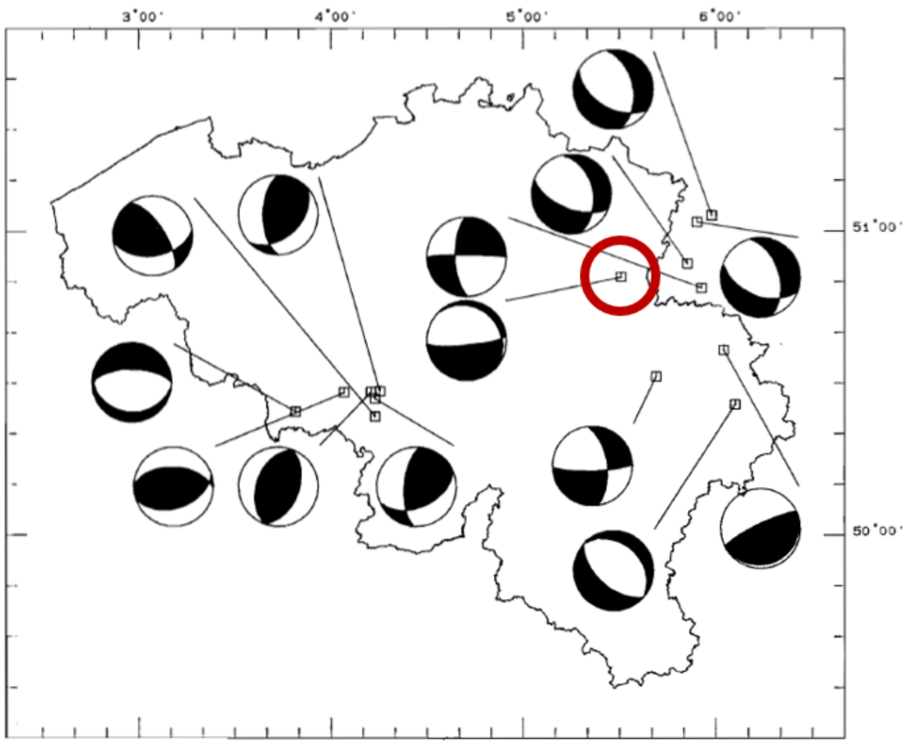

Figure 31: Fault mechanism after Camelbeeck (1990, Fig.14). The Bilzen earthquake (16.7.1985, M_L=3.0) is marked by a red circle.

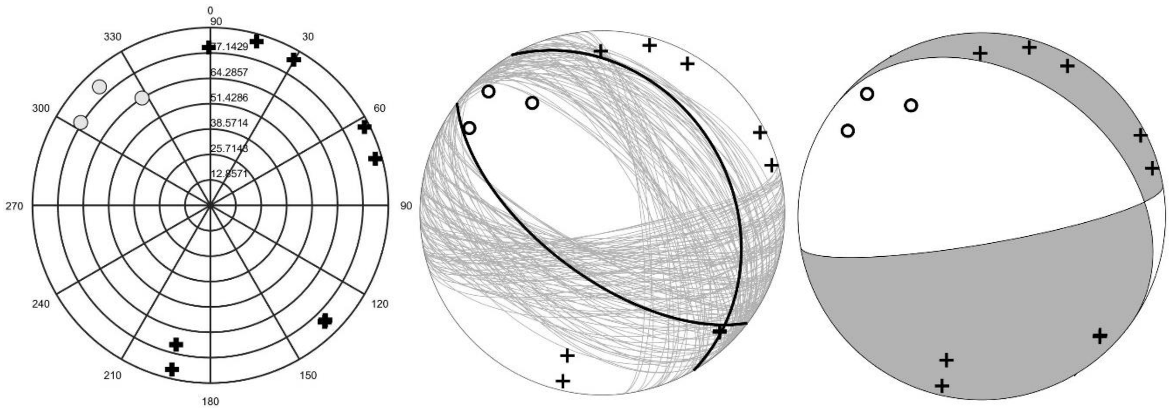

Figure 32: Fault mechanism analysis of the Zutendaal earthquake (05.08.2009 21:18:36 UTC, M_L=2.7). Left: P-wave polarity readings projected on the lower hemisphere with plusses and circles indicating compression and dilation, respectively. Middle: Possible FP solutions taking into account P-wave polarities (gray lines) and best matching solution when additionally accounting for the S/P amplitude ratios (black line). Right: Fault plane solution corresponding to Camelbeeck (1990) for the Bilzen earthquake. Note that P-wave polarities observed for the Zutendaal earthquake (crosses and circles) are consistent with the fault plane solution of Camelbeeck (1990).

1.6 ROLE OF FAULTS

It is well understood that earthquakes occur on faults. A key question in this study is whether earthquake can be associated with known (mapped) faults and whether the associated faults exhibit specific characteristics making them seismogenic. Understanding the seismogenic behavior of faults can significantly improve future assessments of natural and induced earthquake hazards.

The basis of this investigation is the fault model G3Dv3 for the Campine Basin (https://www.dov.vlaanderen.be/page/g3dv3-downloadpagina, accessed April 9th, 2021). In a first step, earthquake locations are compared to mapped faults while considering location uncertainty. By this, faults which could have hosted an earthquake are identified. In the second step, the stress state on fault patches is modelled and those fault patches possibly associated with earthquakes are interpreted in terms of their slip tendency.

1.6.1 Associating Earthquakes with Faults

Two general limitations need to be accounted for when attempting to associate earthquakes with mapped faults. Firstly, the location of an earthquake can be subject to considerable uncertainty and the earthquake depth is frequently only poorly constrained (except for the induced seismicity at Balmatt). Secondly, many faults of the G3Dv3 model are mapped only at a shallower depth level compared to earthquake locations (Figure 33). It is not clear whether faults truly terminate at the shallower depth levels, or whether the lower fault boundaries merely reflect the resolution limit. Deckers et al. (2019) note that the model generally covers faults down to the lower Carboniferous and is incomplete below. Due to these limitations, earthquakes can usually not unambiguously be associated with a particular fault.

We have experimented with different strategies for associating earthquakes with faults. For example, we have extrapolated faults downwards and moved hypocenter locations (within confidence limits) towards faults. Given the large uncertainty of the hypocentral depth and the uncertainty of fault dip, however, we prefer to base the association on lateral coordinates only. In our preferred approach, we compare epicenter locations and uncertainty to the surface projection of the mapped faults (Figure 34). By this we identify all (patches of) faults falling into the epicenter location error ellipse. It is important to notice that an earthquake can be associated with multiple faults.

We have restricted our analysis to the 66 natural earthquakes of the Flanders catalogue. By this we have excluded the earthquakes induced at the Balmatt geothermal site, which are not associated with faults of the G3Dv3 model. Balmatt events detected by template matching, however, were intentionally assigned large location errors (section 1.4.1), which could lead to false fault associations.

Two of the natural earthquakes exhibit lateral location errors > 20 km (2 σ) and could be associated with many faults. These earthquakes were excluded from the analysis. Furthermore, generic location errors of 5 km (in each principal direction) were assigned to those 29 earthquakes, for which confidence limits are not stated in the Flanders Catalogue. In subsequent plots, a reference depth of 10 km is assigned to those 23 earthquakes, for which the hypocentral depth is unknown. This, however, has no impact on the fault associations.

From the 66 natural earthquakes, 41 earthquakes can be associated with at least one fault (Figure 35). In total, 78 out of 175 mapped faults could have hosted an earthquake.

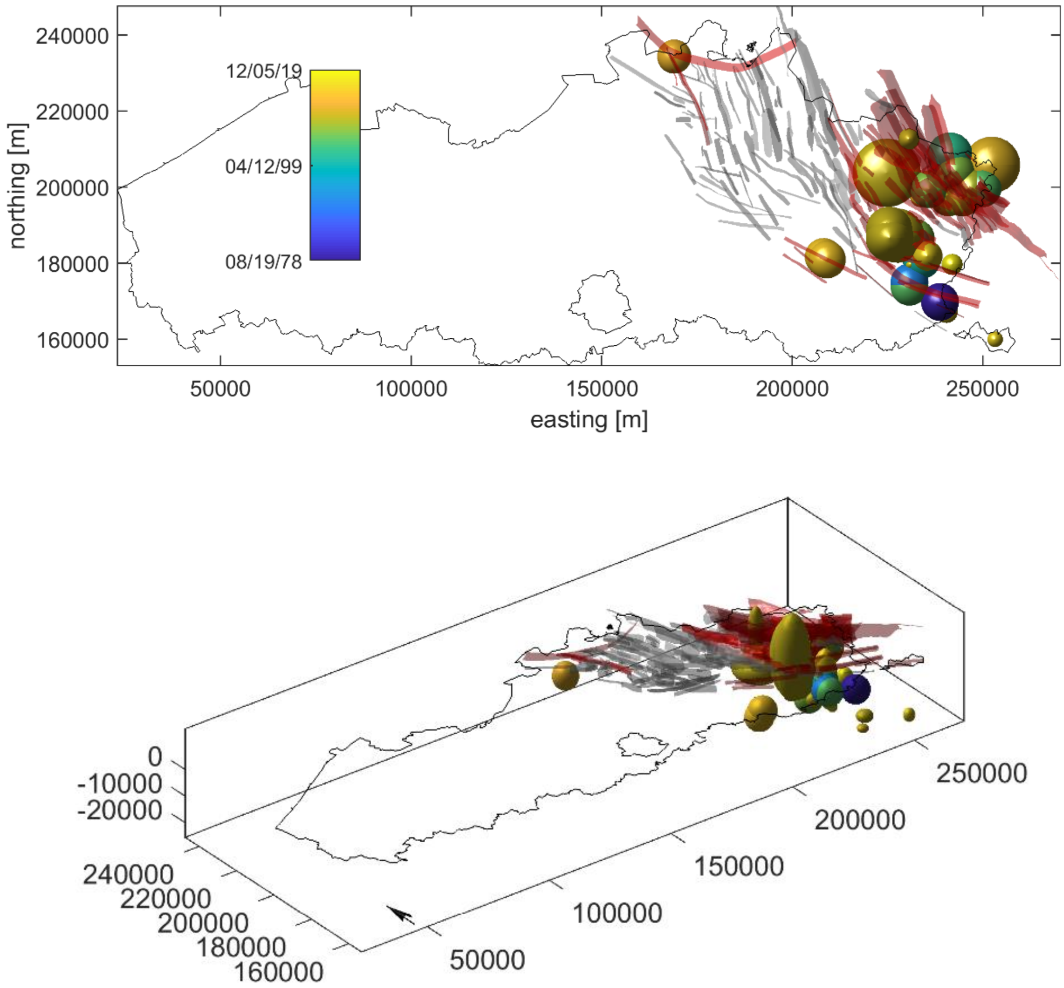

Figure 33: Hypocenter locations of natural earthquakes in Flanders in map view (top) and perspective view (bottom). Earthquakes are shown as ellipsoids scaled to their 2σ location errors. Colour-encoding denotes occurrence times according to the colormap embedded into to the upper plot. Red shaded fault traces denote faults associated with at least one earthquake. Faults that are not associated with earthquakes are shown in gray.

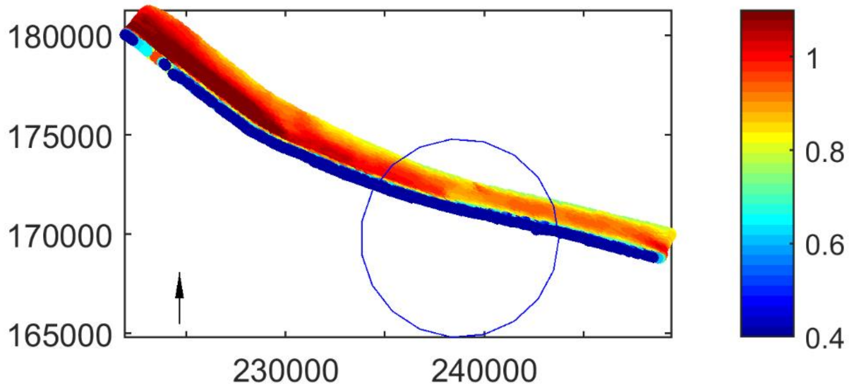

Figure 34: Example illustrating the approach of associating an earthquake to a fault. The lateral 2σ location error of an earthquake is shown by a blue circle. The colored trajectory indicates the surface projection of a nearby fault trace (color encoding denotes slip tendency as referred to in section 1.6.3). The blue circle intersects only this fault, and the earthquake can be unambiguously associated with this fault.

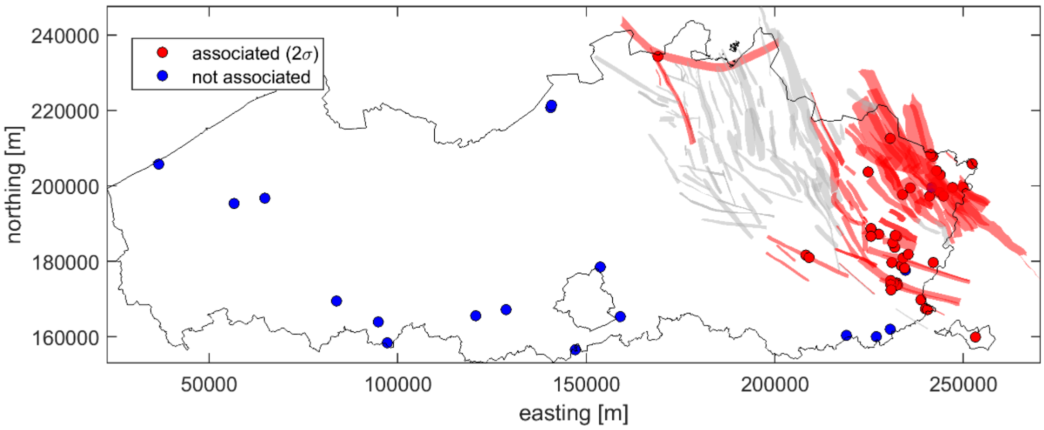

Figure 35: Epicenter locations of natural earthquakes in Flanders. Earthquakes are shown as blue dots if their epicenter location cannot be shifted within 2σ-uncertainty onto the surface projection of a fault (gray and red shaded traces). Otherwise, earthquakes are shown as red dots. Red shaded fault traces denote faults associated with at least one earthquake. Faults that are not associated with earthquakes are shown in gray.

1.6.2 Selected Case Studies

1.6.2.1 Rauw Fault

The 55 km long Rauw fault in the border region of The Netherlands and Flanders is an approximately NNW-SSE striking normal fault elongating from the northern part of the Campine Basin to the southern part of North Brabant. Due to its proximity to the planned surface storage site for nuclear waste in Dessel as well as to regions of geothermal exploration, the stability of the Rauw fault is of particular interest (Figure 36). Based on geological and geophysical investigations and the lack of seismicity, the Rauw fault has been interpreted as being episodically active with a "dormant" status at present (Verbeeck et al., 2017). In a seismic hazard assessment for the Dessel site, the Rauw fault was identified *as the most important fault for the site in terms of closeness and indications of (early) Quaternary activity* (Verbeeck, 2019). From its geometrical extension, the Rauw fault can host a magnitude M7 earthquake, for which the return period is estimated in the order of several hundred thousand to a million years (Table 28 in Verbeeck, 2019).

While the catalogue of the ROB does not include earthquakes that can be associated with the Rauw fault (making Verbeeck, 2019, conclude that there is no instrumental seismicity associated with the fault), an earthquake located by the KNMI (28.11.1932 03:59:22, M3.5) correlates with the trajectory of the Rauw fault in The Netherlands. The same earthquake is located by the ROB approx. 50 km further to the North.

Although not explicitly stated in the earthquake catalogues, we assume that the earthquake location is subject to large uncertainty given the sparse coverage of seismological stations operated at that time. Therefore, we feel that it is not possible to unambiguously identify the fault on which the earthquake has occurred. We nevertheless note that the Rauw fault is oriented favorably for slip (Figure 40) and should be considered as being potentially active.

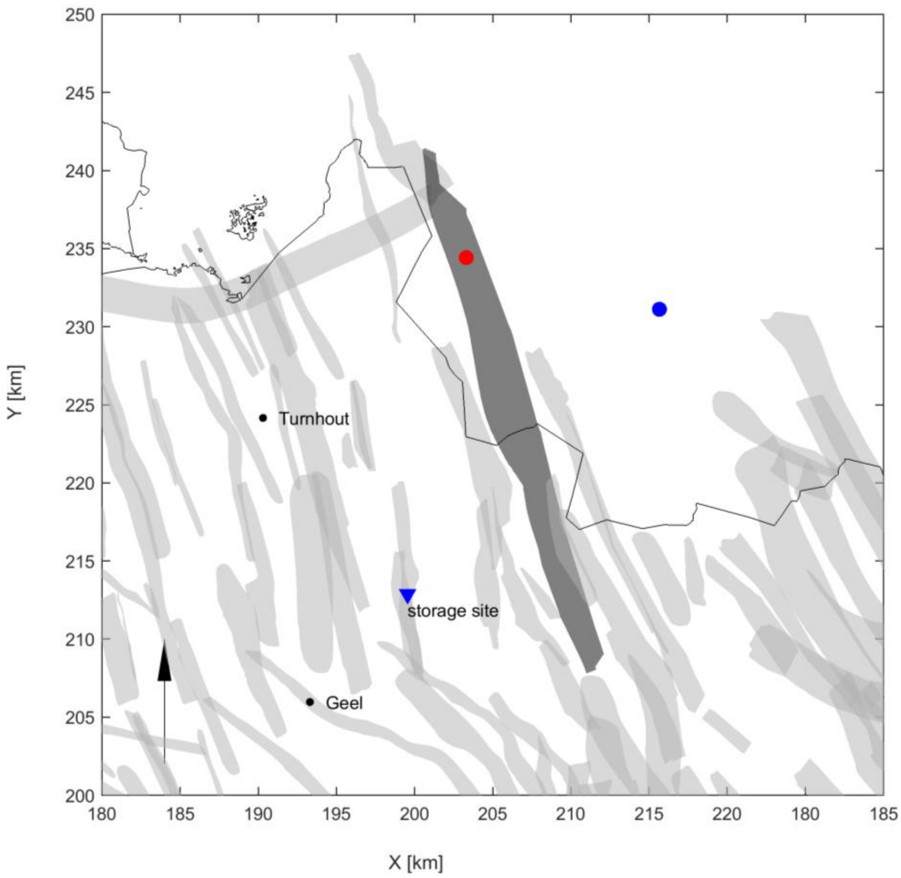

Figure 36: Local faults in the region of the surface storage site for nuclear waste at Dessel (blue triangle). Location of the Rauw fault is shown in dark gray. The location of the M3.5 earthquake (KNMI catalogue) is indicated by a red dot. Blue dot indicates the location of a very recent earthquake (M2.6, 15.11.2021 02:47; data source: https://cdn.knmi.nl/) which is not included in the extended catalogue.

1.6.2.2 Earthquake near Loenhout

The Fluxys Loenhout underground gas storage (UGS) project started operations in 1985 (Amantini et al., 2009). The project is in the western part of the Campine Basin and utilizes karstified limestones of Dinantian age for gas storage at approx. 1 km depth.

Based on the regional fault model G3Dv3, the reservoir is surrounded and partially crossed by several faults, which intersect the Carboniferous and probably older formations. These faults are oriented favorably for slip as indicated by their slip tendency (Figure 40).

On 1st of August 2001 01:08:06, an M1.8 earthquake occurred only a few kilometers to the northwest of the gas storage project site. Epicenter locations determined by the ROB and the KNMI roughly coincide. Location errors, however, are not stated in the catalogues.

Assuming a generic location error of +/-2.5 km in lateral directions (expert judgement), the earthquake can be associated with three mapped faults: the NW-SE striking western part of the Hoogstraten Fault at the northwestern border of the reservoir as well as the faults F_105 and F_211, which are running west of the reservoir (see Figure 37). Furthermore, it cannot be excluded that the earthquake occurred on an unmapped fault. The data situation does not allow discriminating between a natural earthquake and an earthquake that might have been induced by gas storage operations.

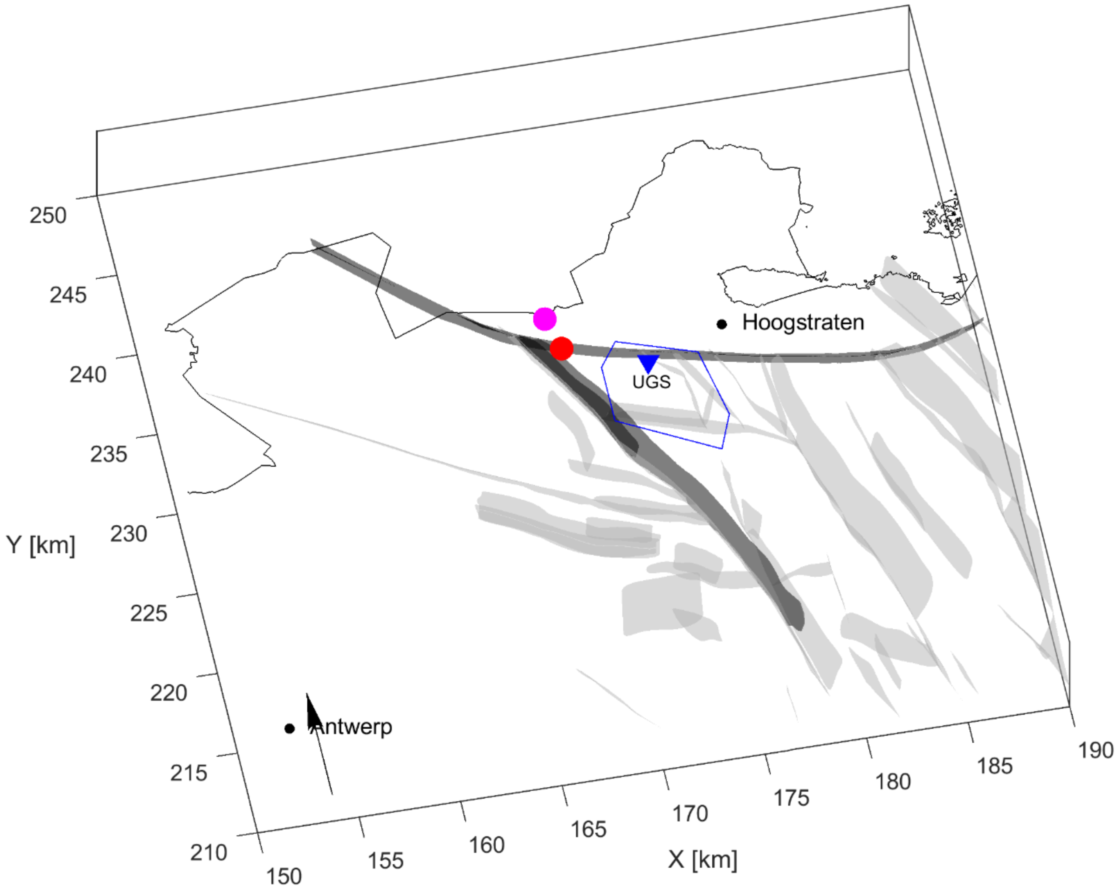

Figure 37: Local faults in the region of the Loenhout UGS near Hoogstraten (blue triangle). Location of the Hoogstraten Fault, Fault F_105 and Fault F_211 are shown in dark gray. The location of the M1.8 earthquake determined by ROB and KNMI is indicated by a magenta and red circle, respectively. Contour of exploitation permit is shown by a blue polygon.

1.6.3 Slip Tendency Analysis

The tendency for failure of a fault segment can be described by its 'slip tendency' (ST), defined as (e.g., Worum et al., 2004)

Equation 1: $$ST = \frac{\tau}{\sigma_n - P_{fl}}$$

with τ and σ_n denoting shear and normal stresses on the fault segment and P_{fl} the fluid pressure within the fault. Mechanical failure occurs if the slip tendency exceeds the coefficient of friction of the fault. Cohesion between failure planes is not considered in this definition.

The slip tendency is sensitive to absolute stress magnitudes and the orientation of the principal stress directions. Knowledge of subsurface stresses and fault strength is limited for Flanders. Therefore, ST values should be considered as a qualitative indicator for fault stability only.

Figure 38 shows the stress field assumed for the slip tendency analysis. The stress model is derived from natural earthquake observations in the Northern Rhine area. Little information exists about subsurface stresses in Flanders. Measurements in the Peer borehole indicate an NW-SE orientation of the maximum horizontal stress (pers. comm. H. Ferket, VPO, 25.10.2021), which is in agreement with the stress model by Hinzen (2003). Additional data was not available for the current study. Therefore we have chosen the Hinzen (2003) stress model, but acknowledge that subsurface stresses in the Campine Basin may deviate from this model. For the mapped faults in Flanders, most ST values are at the upper end of the typical range (Figure 39), indicating that many faults are oriented favorably for slip.

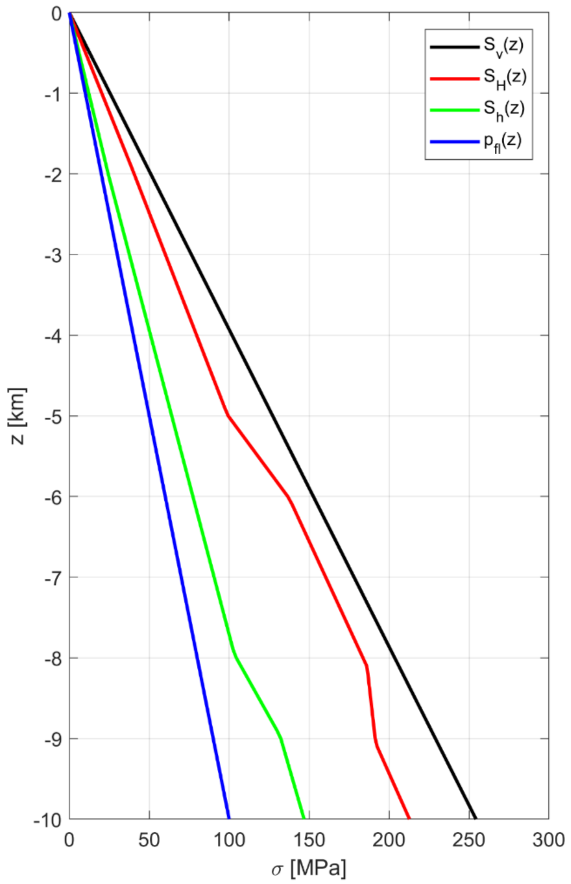

Figure 38: Stress gradients determined by Hinzen (2003). In this stress model, a normal faulting regime prevails in the upper 12 km and the maximum horizontal stress is oriented NW-SE with a strike of 162°.

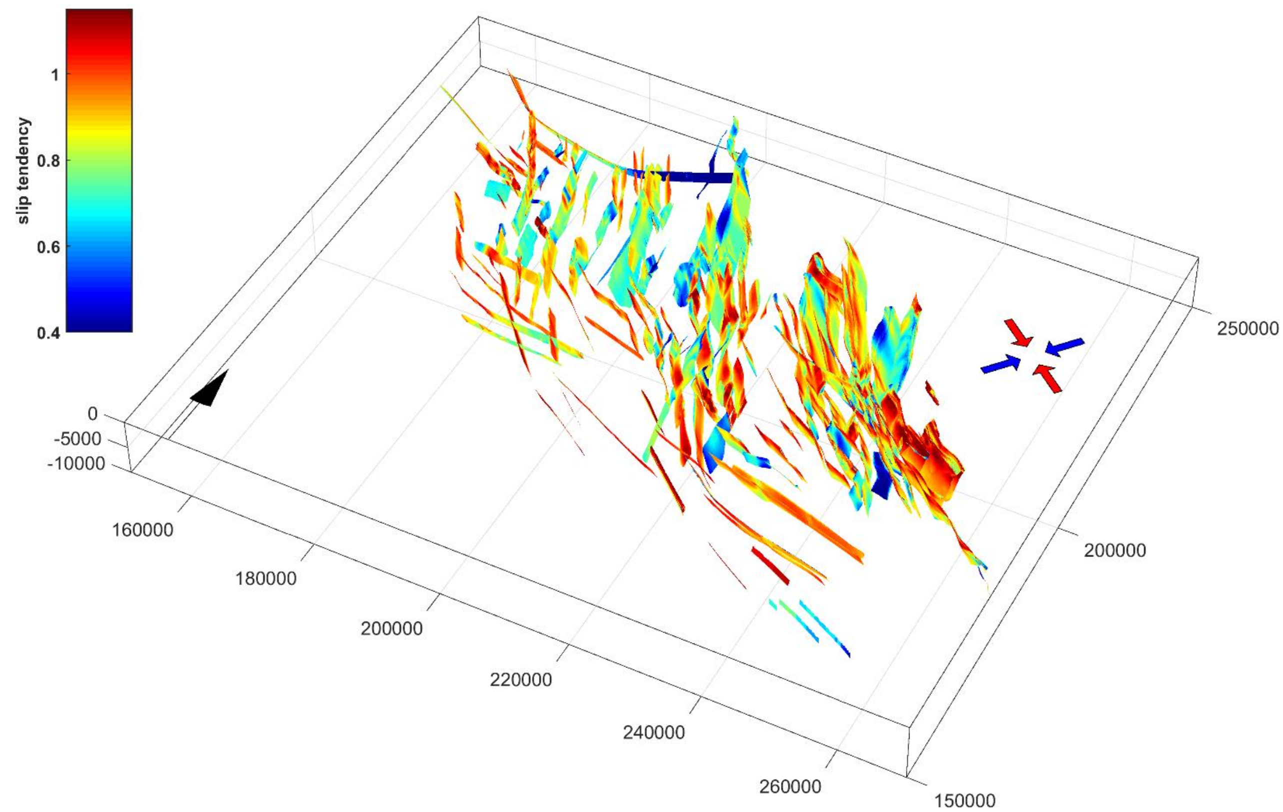

Figure 39: Modelled slip tendency for all fault patches according to the colormap. Black arrow denotes northern direction. Red and blue arrows denote the orientation of the maximum and minimum horizontal stresses, respectively.

1.6.4 Interpretation

Figure 40 shows the maximum ST value of the fault segments that can be associated with an earthquake. Most earthquakes can be associated with a fault patch exhibiting ST > 1, implying that the earthquakes could have occurred on the most critically stressed patches of the fault model. This becomes most evident in Figure 41, where maximum and mean ST-levels of associated fault patches are compared to the overall ST level. All but 6 earthquakes occurred in regions with elevated slip tendencies, where ST values are higher than the average. Considering the large uncertainty in fault mapping and the generic assumption of location errors, the remaining 6 earthquakes might be associated with (unmapped) fault patches with higher ST values. Two earthquakes can solely be associated with fault patches exhibiting ST > 1.

These results indicate that the slip tendency could indeed be a useful parameter for assessing the seismicity potential of a fault. At first glance, this may appear to conflict with the large number of fault segments exhibiting ST>1 which are not (yet) associated with earthquakes. The absence of earthquakes over the last century, however, does not necessarily indicate fault stability. It primarily reflects a small tectonic deformation rate, as e.g., found by Vanneste et al. (2013) for the Roer Valley Rift system.

Observations at Balmatt indicate a near-critical state of stress of the local faults (at the level of Dinantian). Interestingly, the seismogenic faults at Beerse and Balmatt are not mapped in the G3Dv3 model. This implies that damage-relevant earthquakes could also occur on smaller faults, which are not resolved in the fault model.

To further investigate which of the fault patches may have hosted the earthquakes, we have visually compared fault plane solutions to the orientation of associated fault segments. Most fault plane solutions are effectively unconstrained (Figure 30) and we focused on those 7 solutions with a small number of possible orientations only (Figure 29). We acknowledge, however, that the small number of possible orientations may not adequately capture the uncertainty of the fault plane solutions (compare chapter 1.5). All these 8 earthquakes are located at the eastern boundary of Flanders.

We find constellations where an FPS agrees well with the orientation of associated faults. These FPS, however, do not allow discriminating between possible candidates as all neighboring faults exhibit similar orientations. Other FPS do not agree with any associated fault (patch) orientation. We speculate that at least some of the FPS may not adequately reflect the actual fault orientation.

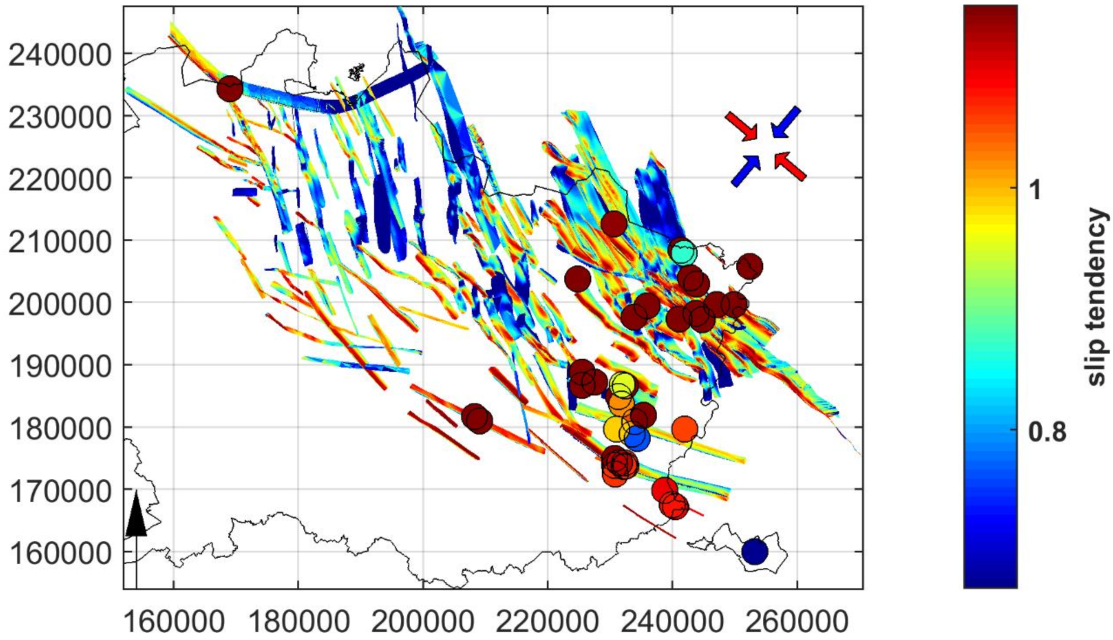

Figure 40: Modelled slip tendency for all fault patches according to the colormap. Black arrow denotes northern direction. Red and blue arrows denote the orientation of the maximum and minimum horizontal stresses, respectively. Colored dots denote epicenters of earthquakes associated with faults. Color encoding of the dots indicates the maximum ST value of the fault segments that can be associated with an earthquake. The colormap is saturated at the lower end at ST=0.6.

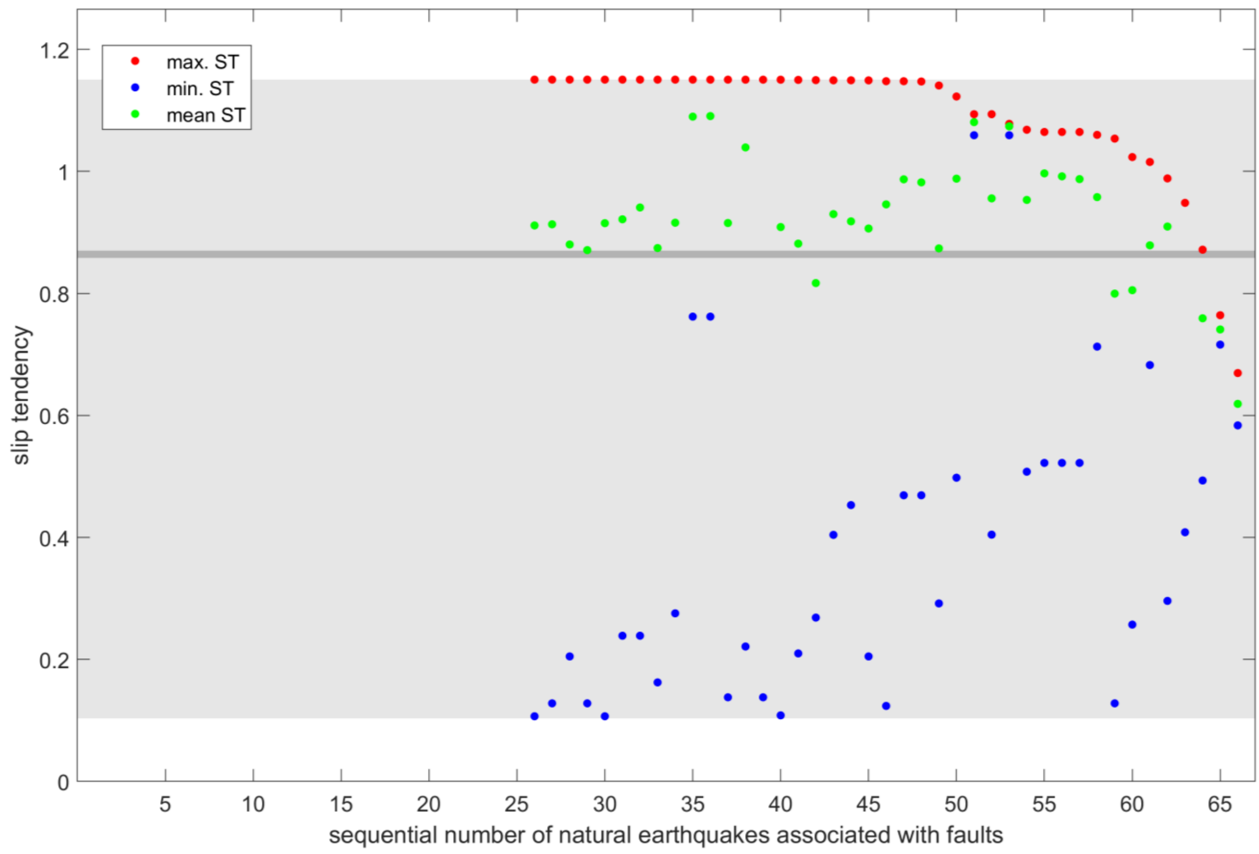

Figure 41: Maximum (red), minimum (blue), and mean (green) slip tendency (ST) of the fault patches associated with the 41 natural earthquakes. Gray shading denotes the range of ST values for the entire fault model. The thick gray line indicates the mean ST of the entire fault model. Note: (i) Most earthquakes can be associated with fault patches with very high ST values. (ii) The majority of earthquakes occurred in regions with elevated ST values (i.e., higher than average).

1.7 RECOMMENDATIONS

Based on the findings in this study we make the following recommendations:

- The routine processing of the ROB is considered state-of-the-art, and no changes are recommended. Analyses performed in this study do not indicate that (detectable) earthquakes were missed during routine processing of the ROB.
- The template triggering approach tested here could be extended to the entire period for which time-continuous waveform data exists. Given the comparatively low detection threshold of the subnet-based approach (section 1.3.5), however, we see only a small potential for detecting additional earthquakes.
- We recommend the Flanders Catalogue and the Extended Catalogue to be used as reference catalogues when addressing seismic hazard aspects in Flanders. These catalogues should be updated when new earthquakes are detected. Updates should follow the rules defined in section 1.2.2. We recommend that VPO should be responsible for supervising the updating process. We note that updates of natural earthquakes in the Flanders Catalogue are automatically provided by the most recent earthquake catalogue of the ROB. If an induced earthquake catalogue recorded by a local (industry) monitoring network becomes available,

such as for Balmatt, then this catalogue should be considered in terms of a separate data source, provided suitability of the catalogue is approved by the ROB.

- We recommend the ROB as the authoritative institution for earthquake activity in Flanders. I.e., the reference for timing, magnitude, and location of earthquakes in Flanders is provided by the ROB. This recommendation is motivated by political aspects rather than by scientific considerations. It forces a unique reference for each earthquake, avoiding confusion possibly caused by competing interpretations of the same earthquake.
- The slip tendencies (section 1.6.3) can be a useful proxy for assessing the seismicity potential of a fault. Damage-relevant earthquakes, however, could occur on smaller faults, which are not resolved in the fault model.

2 PART II: REVIEW OF INDUCED SEISMIC RISK STUDIES FOR THE BALMATT GEOTHERMAL PROJECT

2.1 INTRODUCTION

2.1.1 Context

To date, only few geotechnical installations exist in Flanders. These are in the Campine Basin and include a facility for underground gas storage, which has been operated for many decades, and two geothermal projects being under construction or in a testing phase, respectively. After hydraulic tests at the geothermal site at Balmatt caused felt seismicity, an induced seismicity risk assessment was performed by INERIS.

2.1.2 Scope of this Review

To gain more insight into the risk profile and consequences of deep geothermal exploitation, two evaluations of induced seismicity at the geothermal site of Balmatt conducted by INERIS should be reviewed ('second opinion'). The local seismic monitoring network and the traffic light system in place should be assessed with respect to adequacy. In this context, the status of both, network and traffic light system, at the time of evaluation and as of 2021, should be considered.

2.1.3 Terminology

In the scientific literature, different terminologies were proposed for characterizing the size (magnitude) of an earthquake. Below the level of human perceptibility, small earthquakes are frequently referred to as "micro-earthquakes" or "nano-earthquakes" (e.g., Bohnhoff et al., 2009). We note several shortcomings when using these terminologies:

- (i) In the scientific literature, there is no generally accepted definition of these terminologies and the associated magnitude ranges.
- (ii) The magnitude of an earthquake is subject to measurement uncertainty. The same earthquake may fall into two different classification categories when accounting for its magnitude uncertainty.
- (iii) In public perception, earthquake strength is frequently equated with damage potential. For example, "micro-earthquakes" are not suspected to cause damage. This perception is not necessarily correct. Even small magnitude earthquakes ($M<3$) can cause damage to buildings if occurring at a shallow depth.

Throughout this report, we therefore use the term "earthquake" without further distinguishing between earthquakes of different sizes. We also employ the term "earthquake" for seismic events of very small magnitude (including negative magnitudes), which can only be measured with very sensitive instruments. These earthquakes may be referred to as "micro-" or "nano-earthquakes" elsewhere.

2.1.4 Studies on Balmatt Seismicity

The following documents on the seismicity at Balmatt were provided for the current study:

- Seismic Monitoring Mol, (DMT, 2019a).
- Seismic Monitoring Mol, Evaluation of Source Mechanisms (DMT, 2019b).
- Seismic hazard and risk analysis at Balmatt Part1: Source mechanism analysis (INERIS, 2019).
- Seismic hazard and risk analysis at Balmatt Part2: Characterization of the triggering mechanism, hazard and risk assessment (INERIS, 2020).

The current review is restricted to the two studies by INERIS (INERIS, 2019, 2020). These, however, are interconnected with the studies by DMT. Therefore, the current report starts with a summary of the DMT studies.

2.2 STUDIES BY DMT

2.2.1 Seismic Monitoring Mol

The study DMT (2019a) provides a high-level description of the seismic monitoring of geothermal activities at Balmatt. It does neither provide details on the recording instruments nor on the data processing but focusses on results:

Between October 2018 and August 2019, a total number of 265 earthquakes in the magnitude range M_L=-1.0 to M_L=2.2 were detected by a local 7-station network consisting of instruments deployed in 3 shallow (30 m) and 4 deep (220 m – 600 m) boreholes. The magnitude-frequency distribution indicates b≈1 and a magnitude of completeness Mc~-0.5 (M_L). The strongest earthquake occurred 2.5 days after hydraulic injection tests were terminated and the well was shut-in.

Earthquakes cluster around the lower section of the geothermal injection well in which hydraulic tests were operated in the same period. The macroscopic outline of the distribution of epicenters forms a structure striking NNW. The spatial extension of the structure grows with time.

Source parameter estimates of the largest earthquake indicate 13 MPa stress drop, 40 m source radius, and 1.4 cm displacement. A maximum ground vibration PGV=1.01 mm/s was measured at 600 m depth and 3 km epicentral distance. Significantly larger PGV are expected on the surface.

Similar fault plane solutions were obtained for the strongest events. These are not well constrained by P-polarities due to insufficient coverage of the focal sphere. When combining P-polarities and S-wave angles, an optimum solution of 350/50/210 (strike/dip/rake) is found.

Event pairs/groups with high waveform similarity are interpreted as indicator for close-by rupture and similar mechanisms.

2.2.2 Seismic Monitoring Mol, Evaluation of Source Mechanisms

The study DMT (2019b) complements their previous study (section 2.2.1) providing a more detailed analysis of hypocenters and fault plane solutions:

For determining hypocenters, two alternative models of the seismic wave velocities were tested: In the first model, a station-dependent (average) interval velocity is assumed for P- and S-waves. The interval velocities were determined by assuming that the first earthquake occurred at the flow exit.

The second velocity model includes a 1-D layered velocity structure derived from well logs. The velocity structure was modified during the study by adding an additional near-surface layer with very low S-wave velocity.

While hypocenter locations cluster around the injection well when assuming the first velocity model (reflecting the assumption used for building the velocity model), a systematic shift by ~300 m to the West results when assuming the layered velocity model. In this case, the seismically active structure is not intersected by the injection well.

Fault plane solutions are sensitive to the underlying velocity model. For the layered velocity model, the fault plane solution determined by DMT (2019b) is approximately consistent with the solution obtained by INERIS (2019).

The study concludes that, based on available data, it is not possible to distinguish between the two competing velocity models.

2.3 INERIS STUDY PART I

2.3.1 Study Summary

The study “Seismic hazard and risk analysis at Balmatt - Part1: Source mechanism analysis” (INERIS, 2019) aims at investigating the source mechanisms of the 10 strongest earthquakes associated with geothermal activities at Balmatt and at discussing implications for the traffic light system.

The study builds on seismicity data acquired by DMT (compare chapter 2.2), namely seismogram recordings of ten M_L>1 earthquakes and catalogue data for 216 smaller magnitude earthquakes (including occurrence time, hypocenter location, magnitude).

2.3.1.1 Seismic Velocity Model

In a first step, waveform modelling is used for matching kinematic features of observed with synthetic seismograms to constrain the seismic wave velocity model. Synthetic seismograms were calculated for an explosive point source in a cylindrical symmetric 1D elastic medium, where the far field can be described by Green’s tensors.

The velocity model was built based on stratigraphic profiles, VSP data, and logging data from the geothermal wells. These data indicate an extremely high V_p/V_s ratio with V_s around 500-600 m/s and V_p close to 2,000 m/s in the uppermost 600 meters. Multiple reflections interpreted in observed seismograms are consistent with a strong velocity contrast at 600 m depth.

Waveform matching was performed for the earthquake exhibiting the best observation data (January 18th, 2019; M_{Lcorr} 1.8) and the earthquake hypocenter was taken from the DMT catalogue (i.e. based on velocity model 1 in section 2.2.2 where seismicity is centered around the injection well).

A good match between observed and modelled phase onsets, including reflected phases, is obtained with a five-layer velocity model. Sensitivity tests indicate that the extremely high V_p/V_s ratio of the velocity model is actually required for matching S-wave arrivals and multiple reflections observed at the near surface stations.

2.3.1.2 Source Mechanisms

In a second step, a similar approach of waveform matching is used for determining source mechanisms. Using the Green's tensors determined in the previous step, synthetic seismograms were calculated for a double-couple point source in a cylindrical symmetric 1D elastic medium. Matching of synthetic and observed waveforms was performed by systematically varying strike, dip, rake, and moment (magnitude). The analysis was applied to 5 earthquake groups, where each group contains earthquakes with similar waveforms.

Resulting best-matching fault plane solutions are similar for all 5 groups indicating strike slip faulting either striking N-S to NNE-SSW or WSW-ENE to WNW-ESE (auxiliary plane). It is noted that both orientations do not align with the mapped fault traces striking NNW-SSE.

Sensitivity tests indicate that the best-matching solution represents a global minimum in the parameter space. The variability of the best solution is estimated as

- (N-S plane) strike: 170 – 200°, dip: 65 - 90°, rake: 120 - 150°
- (E-W plane) strike: 260 – 300 °, dip: 30- 90; rake: 0 – 30°.

The solution is found to be insensitive to shifts of epicenter and source depth in the order of 500 m.

2.3.1.3 Ground Vibrations

Using synthetic waveforms modelled in the previous section, peak ground vibrations (PGV) were determined for the strongest M_{Lcorr} 2.2 earthquake and converted into seismic intensities using an empirical relationship from California. At the Earth's surface, a maximum value of PGV=1.8 mm/s is obtained corresponding to intensity III-IV (MMI).

Intensity II is obtained for the M_{Lcorr} 1.8 earthquake, indicating that the event could have been felt.

2.3.1.4 Traffic Light System

The traffic light system (TLS) at Balmatt is based on three criteria: (i) local magnitude M_{Lcorr}, (ii) event location in EW direction, and maximum recorded ground vibrations (peak ground acceleration PGA or peak ground velocity PGV). The reliability of these criteria is discussed in the INERIS study:

- Moment magnitude determined by waveform matching (section 2.3.1.2) is found to agree within 0.1-0.2 magnitude units to M_{Lcorr}. From this it is concluded that M_{Lcorr} is a suitable parameter adequately capturing the physical dimensions of the source size.
- Several suggestions are being made for modifying the event location criterion. These include clear (quantitative) threshold values for the distance between earthquakes and mapped faults as well as a minimum earthquake magnitude to avoid false alerts due to noisy data. Furthermore, it is recommended to invoke earthquake location uncertainty into the evaluation of the TLS thresholds. Sensitivity tests are recommended to explore error contributions by station coverage, phase association, and the assumed velocity model.

- It is noted that ground vibrations (PGA/PGV) are measured in boreholes thus underestimating vibrations on the Earth's surface. Based on waveform modelling a global factor of 2 is suggested to correct for PGV measured in 30-600 m deep boreholes, i.e., measured PGV should be multiplied by a factor of 2 prior to evaluating TLS criteria.

2.3.2 Review Comments

The interpretation of earthquakes at Balmatt is limited by several factors:

- uncertainty of the seismic wave velocities,
- insufficient coverage of the focal sphere due to the small number of recording instruments,
- vibration signals are measured in boreholes only, implying that near surface signal amplification is unknown.

To address these limitations, INERIS has chosen an approach based on full waveform modelling. We consider this to be a reasonable strategy. The strategy differs from previous analysis performed by DMT, thus having the potential to interpret the data from a different view angle.

2.3.2.1 Seismic Velocity Model

A good match between observed and simulated seismograms is obtained using a 5-layer model derived from logging data. It is, however, not possible to completely explore the model parameter space. Clearly, observation data can be matched even better by increasing the number of free parameters in a more complex seismic wave velocity model. Therefore, the good waveform match does not necessarily confirm the general accuracy of the seismic wave velocity model.

The velocity model was built from observation data (VSP and wellbore logs), which in principle adds confidence to the model. Limitations of this approach, however, should be kept in mind. Extrapolating the small-scale velocity measurements conducted near-wellbore in possibly disturbed conditions can lead to significant errors (e.g. Box & Lowrey, 2003).

Using the INERIS velocity model for locating Balmatt seismicity results in a cloud of hypocenters that is offset by several hundred meters from the injection well. While this is a possible scenario, it requires a rather complex geomechanical setting, which we aim to avoid following Occam's razor.

DMT has chosen a different approach, forcing the first detected earthquake to the injection point. The same approach has been applied in various geothermal reservoirs. In one case, the accuracy of the resulting velocity model and associated hypocenter distribution was confirmed by drilling into the seismogenic structure (Baisch, Weidler, Vörös, Wyborn, et al., 2006). While this does not prove general applicability of the approach, it nevertheless qualifies the approach as a possible alternative.

Therefore, we consider the INERIS velocity model as one of several competing hypotheses, the DMT velocity model being an alternative.

The most efficient way for improving our knowledge on subsurface velocities would be to calibrate the interval velocity between the injection point and the recording instruments by check shots.

2.3.2.2 Source Mechanisms

Due to the small number of recording stations, fault plane solutions are not constrained by P-wave polarities (DMT, 2019a). DMT has included observed S-wave angles for constraining fault plane solutions. This approach is more prone to error compared to using P-wave polarity information only.

The alternative approach followed by INERIS is based on full waveform matching, which we consider to be a good strategy.

Results indicate that the ten largest magnitude events exhibit very similar fault mechanisms. This is a typical observation made in various enhanced geothermal reservoirs (e.g., Albaric et al., 2014; Baisch et al., 2015; Deichmann et al., 2014), indicating that seismicity has occurred on different patches of the same, larger scale (planar) fault (Koch et al., 2021).

Best matching fault mechanisms, however, are NNE-SSW trending, in contrast to the NNW-SSE trends of locally mapped faults. Based on a sensitivity analysis, INERIS does not completely rule out NNW-SSE trending fault mechanisms, although observation data appears to be less consistent with this mechanism.

The latter conclusion appears reasonable to us, in particular when accounting for additional sources of error not considered in the INERIS sensitivity analysis. These include model assumptions of a pure double-couple point source and of a homogeneous 1-D seismic wave velocity structure. The impact of these factors is difficult to quantify.

We note that the macroscopic trend of the seismicity (DMT, 2019a) is oriented NNW-SSE, which is in better agreement with the trend of mapped faults. In some other geothermal reservoir, where source mechanisms are better constrained, agreement is found between fault mechanisms and the fault trajectory outlined by the hypocenter distribution (Baisch et al., 2015; Deichmann et al., 2014).

2.3.2.3 Ground Vibrations

Simulated ground vibrations for M_{Lcorr}=2.2 are approximately consistent with measurements and reported intensities.
We emphasize, however, the uncertainty associated with comparing to PGV measurements at depth and the uncertainty associated with converting earthquake magnitude between different scales (see also comments in following section).

2.3.2.4 Traffic Light System

INERIS finds a 1:1 agreement between moment magnitude M_w and corrected local magnitude M_{Lcorr} (being defined as the local magnitude M_L corrected by -0.5 magnitude units).

Theoretical considerations, however, indicate that local and moment magnitude should scale $M_w \sim 2/3\ M_L$ (Deichmann, 2017; Munafò et al., 2016). This could indicate that the 1:1 scaling found by INERIS only holds for earthquake around magnitude 2. Alternatively, we may speculate that the waveform matching procedure (section 2.3.1.2) is most sensitive to the maximum amplitude, which also is the basis of the M_L scale. In this case, we would expect deviations between M_w and M_{Lcorr} if M_w was determined e.g., from observed seismogram spectra (Brune, 1970). Indeed, subsequent analysis by INERIS indicates $M_w \sim 2/3\ M_L$ when M_w is determined from observed seismogram spectra (section 2.4.2.2).

From a practical point of view, however, we agree that using the M_{Lcorr} scale also for modelling and seismic hazard assessment is the most suitable approach. Re-calibration of the magnitude scale (and its conversion to M_w), however, might be necessary when more observation data becomes available. We note that the specific situation at Balmatt, where PGV is not measured at the surface and where local magnitudes are determined from near-event receivers, inevitably leads to uncertainties in magnitude (e.g. Butcher et al., 2017; Kao et al., 2018).

We consider the recommendations by INERIS regarding the location criteria in the TLS as being reasonable. What is lacking at this stage are clear definitions of the modified TLS parameters and their threshold values.

Finally, INERIS suggests doubling measured PGV values to account for near surface amplification effects. A global correction factor of 2 derived from numerical simulations, however, appears small to us. Near surface signal amplification models derived from induced seismicity observations elsewhere indicate that amplification factors can become significantly larger (e.g., Poggi et al., 2011).

As an alternative strategy we recommend operating additional recording instruments at the Earth's surface for future monitoring of Balmatt seismicity.

2.4 INERIS STUDY PART II

2.4.1 Study Summary

The study "Seismic hazard and risk analysis at Balmatt Part2: Characterization of the triggering mechanism, hazard and risk assessment." (INERIS, 2020) aims at assessing seismic hazard and risk and implications for further research.

The study builds on seismicity data acquired by DMT (compare chapter 2.5) and ROB, namely seismogram recordings of all 267 detected earthquakes. Additionally, hydraulic data associated with the tests in the geothermal wells, well-logging and VSP data, as well as the digital fault model were used in the study.

2.4.1.1 Hypocenter Locations

Two competing velocity models are discussed. The '3D-velocity model' is based on associating early seismicity with the flow exit, while the '1-D velocity model' is based on logging and VSP data (compare section 2.3.1.1).

Using the 3-D model, seismicity is approximately centered at the injection point. When using the 1-D model, hypocenters are offset by ~400 m to the West from the injector.

Extensive tests were performed to investigate which of the two models is more consistent with observations:

- For the ten largest events, the rms-misfit is by a factor of 4 larger in the 3-D model. In a probabilistic approach with varying velocity models (Contrucci et al., 2010), hypocenter locations at the flow exit are rejected at high probability.
- The relative changes of seismic velocities in the 3-D model are not consistent with well logging data. Although validity of the 3-D model cannot be ruled out, velocity variations in the 3-D model are considered unlikely based on geological interpretations.
- P-wave polarization angles of induced earthquakes (at station DSLNZ) are found to be more consistent with hypocenter locations West of the injection point (i.e., 1-D velocity model).

Uncertainty exists regarding the sensor orientation, which was re-estimated using VSP surface signals.

Furthermore, INERIS questions the justification for associating early seismicity with the flow exit (namely a sharp increase of production temperature) by noting that subsequent seismicity is not correlated with similar signals in production data. They conclude that *"correlation between exploitation data and seismic event occurrence is not a direct indicator for source location at the injection well"*.

Based on these results, INERIS suggests using the 1D velocity model for locating future seismicity and to account for a location error in the order of around 500 m, being related to picking uncertainties and uncertainty in the velocity model.

Locating the whole data set with the 1-D velocity model results in a spatial hypocenter distribution dominated by two distinct clusters (their Figure 7), rather than by a fault-like structure resulting from the 3-D velocity model. INERIS suggests that the fault-like structure may be a result of location uncertainty.

Based on a cluster analysis events were grouped into 7 families with similar waveforms. Subsequently, hypoDD was used for determining relative hypocenter locations, which exhibit similar location errors as absolute hypocenter locations.

Assessment of network performance yields magnitude of completeness Mc>0 indicating lower sensitivity compared to similar local networks.

2.4.1.2 Source Parameters

Source parameters of 57 events were determined from source spectra using Madariaga's model. The resulting moment magnitudes are consistent with the local magnitude scale.

Source spectra exhibit very similar corner frequencies, despite varying moments over 2 orders of magnitude.

2.4.1.3 Triggering Process

Indications are found that seismicity occurrence is dominated by direct pressure effects. These include an increase of seismic moment with maximum injection pressure, an apparent upper limit of seismic moment as a function of the total injected volume, and an apparent lower limit of seismic moment as a function of the mean flowrate (Figure 11g). Furthermore, indications for a Kaiser effect are found.

Nevertheless, the following observations are interpreted as indications for non-linear hydromechanical coupling processes:

- No seismicity is observed at the injection well.
- Multiplets are interpreted as repeating earthquakes, the occurrence of which contradicts the Kaiser effect.
- Seismicity rate is not linearly related to pressure/flow but occurs episodically.
- Post-injection seismicity occurred more than a month after hydraulic operations were terminated.

Distance-time curves ('r-t curves') of the seismicity occurrence are interpreted as indicator for fluid flow occurring along preferential flow zones of fractures of higher permeability compared to the surrounding intact rock mass. Furthermore, it is speculated that an efficient hydraulic connection between the injection point and the region of seismic activity exists, possibly caused by hydraulic fracturing during previous injections. Such connection is required to explain the seismicity response to injection pressure.

Conceptually, seismicity is interpreted to occur on pre-existing, critically stressed structure (fractures/faults) oriented either N-S or E-W. Relative hypocenter locations may favor E-W oriented fractures, but no rigorous assessment could be made due to a lack of data quality.

The temporal evolution of seismic activity is consistent with Omori's law and INERIS concludes that *[… static stress transfer plays a significant role in the triggering of Balmatt seismicity and might represent the fundamental mechanism explaining seismic activities recorded long time after shut-in period*…].

A rate-state type model is suggested to explain seismicity occurrence, where repeating earthquakes are interpreted to reflect slip of asperities on an otherwise creeping fault. It is concluded that a "*significant number of seismic events do not represent pore pressure increase in seismic structures (weakening part of faults) as predicted by the direct pressure model (Mohr-Coulomb)*".

2.4.1.4 Seismic Hazard and Risk Assessment

The seismic hazard assessment rests on two elements:

- a site-specific ground motion prediction equation (GMPE) for relating earthquake magnitude to ground vibrations is developed,
- a range for the maximum earthquake magnitude is estimated using different approaches based on (i) McGarr's (2014) model, (ii) maximum available fault area, and (iii) the magnitude frequency distribution of seismicity already induced at Balmatt.

The GMPE (their equation 1) was developed using recordings from borehole instruments deployed at 30 m depth. It is noted that vibrations at the surface may be underestimated by measurements at depth. Waveform modelling is used for extrapolating the GMPE to larger magnitudes. An additional low velocity layer for the first 30 m was introduced to account for near-surface amplification.

Several fault models were considered for estimating a maximum earthquake magnitude based on spatial fault extension. Estimates range from M_{max}=3-4 (strike-slip scenario based on the observed seismic cloud) to M_{max}=4-5 (normal-faulting scenario, considered unlikely) up to M_{max}>5 (normal faulting on boundary fault, considered a worst-case scenario).

An alternative approach following McGarr (2014) yields M_{max}=3-4 for the last production phase in 2019. It is noted, however, that McGarr's (2014) model is not generally valid.

The magnitude-frequency distribution of seismicity occurring during previous production tests indicates a <1% chance for inducing an M_w=2 earthquake during a 10 day production period. Limitations of the analysis in terms of the small sample size and the non-stationary process driving induced seismicity are noted.

Predicted ground vibrations for maximum magnitude earthquakes are related to seismic (MMI) intensities using an empirical relationship determined for natural seismicity in California. The seismic intensity scale is used for comparing predicted intensities to threshold values regarding perceptibility, Eurocode 8 building standards, and standards for the Nuclear Research Centre.

2.4.1.5 Conclusions and Recommendations

It is concluded that

- […M_{max} ranges most likely between 3 and 4 meanwhile hazard scenarios with M_{max} larger 4 and 5 cannot be excluded…]
- […light damage at private houses with Eurocode 8 standards (zone 3 Belgium) is likely for Mmax around 4…]
- […damage on the building of the nearby SCK-CEN Nuclear Research Centre is expected for M_{max} close to 5…]
- […for future short-term circulation tests (weeks to months) …] […a probability of exceedance for perceptible earthquakes by local population..] is [… < 1 %...].

It is furthermore noted that observed seismicity cannot be explained by […*using linear hydromechanics models based on homogeneous fluid pressure diffusion models and Mohr-Coulomb failure criteria…].* Besides non-linear fluid flow and static stress transfer, aseismic slip is suggested to play a key role for the earthquake processes at Balmatt.

It is recommended to improve the seismic network and to lower the magnitude threshold of the TLS to M_L=1.8.

2.4.2 Review Comments

2.4.2.1 Hypocenter Locations

The chosen approach appears sound and we agree with the overall conclusion that location uncertainty in the order of 500 m needs to be expected, reflecting picking errors and uncertainties of the seismic velocity model.

Although the 1-D model velocity model appears to be better supported by observation data, we emphasize the uncertainty associated with the 1-D velocity model.

As a result of the 1-D velocity model, hypocenters are significantly offset from the injector. Although this scenario cannot be excluded, it nevertheless appears unlikely as it is difficult to explain geomechanically: Even a high-permeable 2-D structure cannot explain the direct seismicity response to pressure, because pressure signals at 400 m distance will be massively delayed and attenuated. Therefore, a connection from the well to the region of seismic activity had to be through a channel of small diameter (and little storage) to maintain the pressure signal.

Therefore, we consider the 1-D velocity model as one of several competing hypotheses, the 3-D velocity model being an alternative.

The most efficient way for improving our knowledge on subsurface velocities would be to calibrate the interval velocity between the injection point and the recording instruments by check shots.

<u>Technical Comments</u>

- It is not clear to us if polarization information was used in the sensitivity analysis as described in Contrucci et al. (2010). Parameter details were not provided, in particular not regarding Monte Carlo sampling of velocity models. Consequently, we cannot judge how the parameter space has been sampled. We note, however, that simultaneous determination of hypocenter and velocity model is a challenging task using real data. Confidence estimates are meaningful only within the subspace of tested model parameters. Therefore, we are not convinced that hypocenter locations near the flow exit can be excluded at such a high probability level as indicated in the study.
- Furthermore, the impact of the station network geometry has been studied by re-locating hypocenters using different subsets of station combinations. An example is shown, where East-West scattering of the resulting solutions is in the order of 750 m (their Figure 2b). Despite the large scatter, INERIS concludes that no significant 3D effects (in which case the solution would depend on the station configuration) are present. This conclusion appears questionable to us. We are also concerned that the inversion problem is not sufficiently (over-) determined when using 4 P-picks only.
- INERIS notes that the second event with similar waveforms to the 'calibration event' is not associated with an abrupt change of the return temperature as observed at the time of the first event. INERIS concludes that *"correlation between exploitation data and seismic event occurrence is not a direct indicator for source location at the injection well"*. We share this conclusion in particular since it is difficult to imagine a geomechanical process where a small earthquake produces a strong and sharp signal in the production temperature as shown in their Figure 4a. We emphasize, however, that another argument for associating early seismicity with the flow exit is the magnitude of Coulombstress changes, which are largest at the injector.
- INERIS states (their section 4.3) that *[…errors in relative hypocenter locations are significant and are probably in the same order as for absolute locations…*]. On the other hand, we note that their Figure 16 shows inter-event separation frequently in the order of 10 m or even less indicating much higher precision.

2.4.2.2 Source parameters

The M_w/M_L scaling factor of ~2/3 (their figure 10, top left) is in agreement with theoretical models (Deichmann, 2017; Munafò et al., 2016) indicating internal consistency between the magnitude scales. The 1:1 scaling between moment and local magnitude found in the previous INERIS study (section 2.3.2.4) should be discarded.

Similar source radii are obtained independent of seismic moment, which INERIS explains with a conceptual model dominated by aseismic slip. We emphasize, however, the general trade-off between corner frequency (hence source radii) and attenuation correction (Sonley & Abercrombie, 2006). In principle, the observation of approximately constant source radii could also be an indicator that attenuation is not sufficiently compensated and that the spectral fit is dominated by fitting the low-pass signature of signal attenuation.

2.4.2.3 Triggering Process

INERIS motivates their proposed aseismic slip model by several observations. We feel that these observations could be explained equally well by alternative concepts:

- The lack of seismicity near the injection well could simply result from the uncertainty of seismic wave velocities. INERIS acknowledges a general >500 m uncertainty for absolute event locations (their section 7.2), which could explain the apparent lack of seismicity near the injector.
- The occurrence of multiplets does not necessarily contradict the Kaiser effect. Closely spaced earthquakes (even with overlapping source area) could as well reflect progressive rupture, where co-seismic stress load from previous event(s) plays an important role for triggering a subsequent event, e.g. Baisch (2020).
- Episodic occurrence of seismicity could reflect different levels of stress criticality on a larger scale fault, in combination with co-seismic stress transfer as discussed for other geothermal reservoirs, e.g. Baisch (2020).
- Similarly, post-injection seismicity is a typical phenomenon in geothermal reservoirs, which can be explained by hydraulic pressure diffusion in combination with co-seismic stress transfer (Baisch et al., 2010; Baisch, Weidler, Vörös, & Jung, 2006; Hsieh & Bredehoeft, 1981).

In the triggering model proposed by INERIS, seismic deformation can be viewed as a secondary phenomenon resulting from the primary process of aseismic deformation. Conceptually, the deformation energy associated with aseismic deformation must be much larger than the seismic deformation energy. Processes that could drive such large-scale deformations are completely unclear to us, in particular if fluid injection occurred below the fracture opening pressure, which we consider a likely scenario.

2.4.2.4 Seismic Hazard and Risk Assessment

Although INERIS states that their hazard assessment is subject to considerable uncertainty, we are concerned that the figures provided by INERIS may lead to underestimating the induced seismicity risk of future operations.

Our concerns are related to two aspects. We suspect that

- the actual damage threshold may be well below the M4 damage threshold estimated by INERIS,
- the actual probability for the occurrence of a felt event during future geothermal operations (testing) could be much larger than indicated by INERIS.

In the following we explain our concerns in more detail.

<u>Damage Threshold</u>

The INERIS GMPE predicts much larger PGV for M>2.2 earthquakes, e.g. compared to the GMPE by Douglas et al. (2013) in combination with near-surface amplification after Poggi et al. (2011). The latter GMPE is calibrated by (global) induced seismicity observations in the magnitude range M_w=1 to M_w=5.

At the same time, consequences for a given level of ground vibrations might be systematically underestimated by INERIS. The chosen approach of evaluating consequences based on IMMS intensities appears not suitable to us, since the intensity scale is not well calibrated for small (cosmetic) damage. In our view, comparisons to engineering standards, e.g. SBR (2010) or DIN4150-3 (Deutsches Institut für Normung e.V., 1999b), are more suitable for assessing consequences.

While observed ground vibrations and consequences at the M2 level are reasonably well predicted by the INERIS approach, the INERIS GMPE predicts PGV=21.9 mm/s at the epicenter of an M_w=3 earthquake at reservoir depth. Engineering standards consider damage to ordinary buildings possible already at a much lower vibration level (e.g., at 5 mm/s according to the two engineering standards mentioned above). Experience with (shallow) induced earthquakes also indicates a lower damage threshold, e.g. damage compensation for a dozen M2.6-M3.6 in the Groningen gas field amounts to several 100 Mio Euro (van der Voort & Vanclay, 2015), and ~7 Mio Euro were compensated for an M_w=3.2 earthquake caused by geothermal activities underneath the city of Basle (Baisch et al., 2009).

Given measured PGV for the M_{Lcor}=2.2 earthquake, we expect the damage threshold (according to engineering standards) for reservoir seismicity at Balmatt around M_{Lcor}=2.7.

Probability for Felt Earthquake

Reservoir seismicity is a non-stationary process. Subsurface stress changes may accumulate and the seismicity response to a certain type of subsurface operation may change considerably over time, e.g. as observed in producing gas fields (Bourne et al., 2014).

In light of the small data set, the assumption of a stationary process, implicitly made by INERIS, appears questionable to us. Furthermore, we notice that felt seismicity has already occurred, which somewhat contradicts the < 1% probability estimate obtained from the same data set.

2.4.2.5 Recommendations

We agree with the INERIS recommendations that more studies are required, seismic monitoring needs to be improved, and that TLS thresholds should be lowered.

Additionally, we recommend that

- several (additional) surface seismometers (alternative vibration monitors) should be operated during future geothermal activities for measuring ground vibrations directly at the Earth's surface,
- it should be attempted to better calibrate the seismic wave velocities, e.g., by a check-shot at reservoir level.

2.5 CONCLUSIONS

The processes leading to induced seismicity at Balmatt are not fully understood yet, which is mostly due to insufficient observation data. While the studies by INERIS consider aseismic deformations to play a key role, we favor a more common explanation, where seismicity is controlled by fluid pressure increase in combination with co-seismic stress redistribution.

We consider the data analyses performed by INERIS for determining earthquake locations and mechanisms to be state-of-the art. We are, however, concerned that the INERIS prediction of ground vibrations and associated consequences are insufficiently calibrated, finally leading to underestimating risk.

The traffic light system (TLS) operated during previous geothermal operations reflects *ad hoc* threshold choices rather than a strict design criterion of a certain consequence that should be avoided (compare e.g. Schultz et al., 2020; Verdon & Bommer, 2020). We see several issues associated with the TLS operated initially:

- The red-light threshold on magnitude at M_L=2.5 is well in the range of human perceptibility. It has not been investigated to what extent this threshold value could prevent damage to buildings when accounting for magnitude jumps (Verdon & Bommer, 2020) and/or trailing effects (Baisch et al., 2019).
- The TLS was operated using downhole measurements only, which may not adequately represent ground vibrations at the surface.
- The TLS criterion on seismicity migrating 'out-of-zone' includes qualitative aspects (e.g., 'Eventlocaties bewegen naar het oosten'), which are not meaningful e.g., considering location uncertainty.

Following recommendations made in the INERIS studies, the TLS was modified (Figure 42). The TLS includes threshold values on activity rate and earthquake location. Both parameters include subjective components (e.g., start of binning interval for determining activity rate), which may lead to uncertainties in the TLS evaluation. As these parameters are solely used for defining the TLS state orange, associated uncertainties maybe acceptable. The stop-light threshold is based on earthquake magnitude and/or peak ground vibration/acceleration. Given the subjective nature of the magnitude scale, we consider the threshold value on peak ground vibration (PGV) to be most relevant. The PGV=1 mm/s threshold is by a factor of ~3 larger than the level at which human perceptibility may start (Deutsches Institut für Normung e.V., 1999b, p. 41; Groos et al., 2013), implying that operations will be stopped only after a felt earthquake has occurred. This implies that the TLS may not prevent the occurrence of an earthquake with vibrations causing (slight) damage to buildings when accounting for magnitude jumps (Verdon & Bommer, 2020) and/or trailing effects (Baisch et al., 2019). Depending on the legal situation, societal acceptance, and the financial body of the operator we recommend to further reduce the stop-light threshold.

During this study, we were informed that several dozen additional (surface) seismometers were deployed by ROB and VITO for monitoring future geothermal activities at Balmatt. Based on the large number of additional surface stations, we feel confident that the recommendations we have made in this study regarding monitoring network extension are fulfilled.

Risk category	Input monitoring	Action(s)
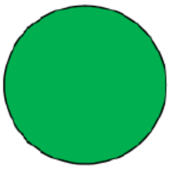	Magnitude $M_{lcorr} \leq 1.2$; *AND* Seismicity ratio (events $M_{lcorr}>0.5$) 0 or 1 per hour; *AND* Distance (events $M_{lcorr}>1.0$) to modelled Retie fault>400m *AND* PGA $\leq 0.02 m/s^2$ *AND* PGV $\leq 0.4 mm/s$	Keep operational parameters
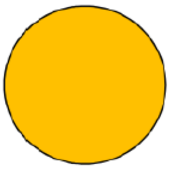	Magnitude $M_{lcorr}>1.2$; *OR* Seismicity ratio (events $M_{lcorr}>0.5$) $\geq$ 2 per hour; *OR* Distance (events $M_{lcorr}>1.0$) to modelled Retie fault $\leq$400m *OR* PGA > $0.02 m/s^2$ *OR* PGV>0.4mm/s	Reduce flow rate of primary loop with 30% (by decreasing frequency of ESP in steps of 0.1Hz/5min) and evaluation of the impact of previous production period on seismic activity by an external party (events M_{lcorr} >0.5) *AND* Report to authorities (see list on sharepoint)
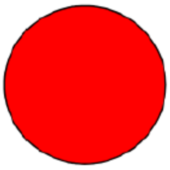	Magnitude $M_{lcorr}>1.8$; *OR* PGA > $0.04 m/s^2$ *OR* PGV > 1.0mm/s	Shut down primary loop (by shutting down ESP) and shut-in injection well. *AND* Report to authorities (see list on sharepoint) *AND* Conduct further seismological analysis by external party on detected event(s) prior to planning start-up

$M_{lcorr} = Ml\ (IAESPEI) - 0.5$

Figure 42: TLS settings valid from April 19th, 2021. Source: VITO (M. Broothaers, 10.05.2021).

3 PART III: POLICY RECOMMENDATIONS FOR INDUCED SEISMICITY RISK MANAGEMENT

3.1 INTRODUCTION

3.1.1 Scope

Based on existing practice in neighboring countries, recommendations shall be given for

- adequate seismic monitoring, and
- policy measures for managing induced seismicity risks associated with deep subsurface operations in Flanders, including geothermal exploitation, underground gas storage (UGS), aquifer-thermal-energy-storage (ATES), coal bed methane (CBM), mining, and carbon capture and storage (CCS).

Recommendations should indicate how risk can already be assessed in the permitting phase of a project prior to drilling. They should include 'measurement plans' to be defined as part of the permitting process. The recommendations should be based on global experience and a conceptual geomechanical understanding of the processes causing seismicity.

3.1.2 Terminology

We adopt the following description by Bohnhoff et al. (2009):

Earthquakes are the vibratory motion of the earth created by the sudden release of energy within the solid rock mass of the planet. Most earthquakes are caused by slip on faults, and as a consequence the term "earthquake" is commonly used to refer to the earthquake source process rather than the seismic waves it causes.

In the scientific literature, different terminologies were proposed for characterizing the size (magnitude) of an earthquake. Below the level of human perceptibility, small earthquakes are frequently referred to as "micro-earthquakes" or "nano-earthquakes" (e.g., Bohnhoff et al., 2009). We note several shortcomings when using these terminologies:

(i) In the scientific literature, there is no generally accepted definition of these terminologies and the associated magnitude ranges.

(ii) The magnitude of an earthquake is subject to measurement uncertainty. The same earthquake may fall into two different classification categories when accounting for its magnitude uncertainty.

(iii) In public perception, earthquake strength is frequently equated with damage potential. For example, "micro-earthquakes" are not suspected to cause damage. This perception is not necessarily correct. Even small magnitude earthquakes ($M<3$) can cause damage to buildings if occurring at a shallow depth.

Throughout this report, we therefore use the term "earthquake" without further distinguishing between earthquakes of different sizes. We also employ the term "earthquake" for seismic events of very small magnitude (including negative magnitudes), which can only be measured with very sensitive instruments. These earthquakes may be referred to as "micro-" or "nano-earthquakes" elsewhere.

It is important to notice that seismometers continuously measure ground vibrations. This ''background noise" originates from different anthropogenic and natural vibration sources, such as e.g. traffic, industry, and wind. Background noise is not associated with earthquakes and the term "earthquake" does not apply.

3.1.3 Abbreviations

ATES	Aquifer Thermal Energy Storage
CBM	Coal Bed Methane
CCS	Carbon Capture and Storage
ΔCS	Coulomb stress changes
DSHA	Deterministic Seismic Hazard Assessment
GMPE	Ground Motion Prediction Equation, empirical relationship for predicting ground motions
HT-ATES	High Temperature Aquifer Thermal Energy Storage
M_L	Local earthquake magnitude (section 3.2.1)
M_w	Moment magnitude (section 3.2.1)
PGA	Peak Ground Acceleration, maximum ground acceleration measured in m/s^2
PGV	Peak Ground Velocity, maximum ground vibrations measured in m/s
PSHA	Probabilistic Seismic Hazard Assessment
ROB	Royal Observatory of Belgium
TLS	Traffic Light System
UGS	Underground Gas Storage

3.2 INDUCED SEISMICITY

This chapter provides a general overview on the processes leading to induced seismicity and on the resulting hazard and risk. Based on global experience, existing hazard classification schemes, risk mitigation measures and risk management guidelines are briefly summarized[1].

3.2.1 Processes Causing Seismicity

The root cause for induced seismicity are stress changes in the subsurface caused by anthropogenic activities. For example, stress changes may bring a pre-existing fracture or fault to failure which may lead to seismicity if the shear stress exceeds the fracture strength or frictional resistance.

Some simple phenomenological approaches exist for shear stresses exceeding the fracture strength of rock:

Let τ and σ_n denote the shear and normal stress resolved on a fracture plane, p_{fl} the in situ fluid pressure, μ the coefficient of friction and c_0 cohesion, then shear slippage occurs on the fracture if (Scholz, 2002):

[1] Several subsections in this chapter closely follow our previous studies, e.g. Baisch et al. (2016) and A'Campo et al. (2020).

Equation 1 $$\tau > \mu\cdot(\sigma_n - P_{fl}) + c_0.$$

Stress perturbations on an idealised, cohesionless fracture can be described by Coulomb stress changes ΔCS, which can be defined as:

Equation 2: $$\Delta CS = \Delta\tau - \mu\cdot(\Delta\sigma_n - \Delta p_{fl}),$$

with $\Delta\tau$, $\Delta\sigma_n$, and Δp_{fl} denoting changes of shear stress, normal stress, and fluid pressure, respectively. Positive ΔCS values increase the tendency to failure of a fracture. The failure process of a fracture can be seismic (associated with earthquakes) or aseismic (not associated with earthquakes), depending on how the instability evolves.

The strength of an induced event is primarily controlled by the dimension of the shearing plane associated with the event:

Equation 3: $$M_0 = G\cdot A\cdot d,$$

where M_0 is the seismic moment, G denotes the shearing modulus, A is the area of the shearing plane, and d is the average slip occurring on the shearing plane. The seismic moment can be determined from seismogram recordings assuming an earthquake model (e.g. Boatwright, 1980; Brune, 1970). Several empirical relationships exist to convert seismic moment to earthquake magnitude M_w. Most common is the definition by Hanks & Kanamori (1979):

Equation 4: $$M_w = 2/3\cdot\log(M_0) - 6.1,$$

for which consistency with simple physical models has been demonstrated (Deichmann, 2006, 2017; Munafò et al., 2016).

Besides the moment magnitude, the Royal Observatory of Belgium (ROB) is using a local magnitude scale M_L as defined in Van Camp et al. (2020).

3.2.2 Earthquake Consequences

For assessing consequences of an earthquake, ground vibrations at the Earth's surface need to be determined. Besides analytical models (e.g. Aki & Richards, 2002), there exist various empirical Ground Motion Prediction Equations (GMPE) relating earthquakes of a certain magnitude and depth to vibrations at the Earth's surface (compare summary of Douglas, 2017). Most published GMPEs were developed from observations of larger magnitude, natural earthquakes occurring at greater depth compared to geotechnical installations. These GMPEs cannot be used for the shallower, induced earthquakes of smaller magnitude. Several GMPEs have been developed specifically for induced seismicity (Atkinson, 2015; Douglas et al., 2013).

Once ground vibrations at the Earth's surface have been assessed, consequences depend on the vulnerability of the exposed objects. Such relations are typically referred to as fragility functions and express the relationship between a level of ground motion intensity and the corresponding probability of exceeding a certain damage grade. For low damage grades, fragility functions are often expressed as a function of peak ground velocity. In general, the vibration level above which damage to a building starts to occur depends on the building construction and cannot be predicted with high accuracy. Engineering standards, for example the Dutch SBR standard (SBR, 2010; updated 2017) and the German DIN4150-3 (Deutsches Institut für Normung e.V., 1999b), provide guidelines of the vibration level above which damage to buildings and other installations tends to occur.

To the authors knowledge, no comparable standard exists in Belgium. Therefore, our considerations are based on the Dutch and German standards.

Both standards list three categories (category 1: industrial buildings; category 2: ordinary buildings; category 3: sensitive buildings). Damage to ordinary masonry buildings according to SBR is unlikely (i.e., < 1% probability) for peak ground velocities (PGV) of < 5 mm/s at 10 Hz. For highly vulnerable buildings damage according to SBR is unlikely (i.e., < 1% probability) at PGV < 3 mm/s at 10 Hz. Threshold values for industrial buildings are higher. DIN4150-3 uses the same threshold values. For higher excitation frequencies, damage thresholds increase according to both standards.

3.2.3 Seismic Hazard and Risk

Following Bommer et al. (2015) we define [*…seismic risk as the likelihood or probability of different levels of undesirable consequences due to the occurrence of earthquakes. Such consequences may include loss of life, injury, damage and collapse of buildings, economic costs, and business interruption, among others. For the specific case of induced seismicity, the consequences could also include annoyance of the affected population, non-structural damage to buildings and reputational damage to the operator of the activity responsible for the earthquakes…]*

In accordance with Bommer et al. (2015) we consider seismic risk to result from the convolution of four factors: (i) seismic hazard, (ii) exposure, (iii) fragility, and (iv) consequences. For induced seismicity, all factors are subject to considerable uncertainty.

The current recommendations aim at preventing induced earthquakes causing vibration levels at which damage may occur. In the proposed strategy, the combined impact of factors (ii), (iii), (iv) is approximated by a single lower-bound vibration threshold value (compare previous section), thereby focusing on seismic hazard. This focus is maintained throughout the subsequent sections.

3.2.4 Hazard/Risk Classification Schemes

Several screening approaches exist in the scientific literature for assessing the potential that subsurface activities may induce seismicity, or that induced seismicity risks may become a concern for a specific project in the future (Baisch et al., 2016; Buijze et al., 2019; Davis & Frohlich, 1993; Muntendam-Bos et al., 2015; van Thienen-Visser et al., 2018; Trutnevyte & Wiemer, 2017).

These screening approaches are typically based on a small set of geological and operational parameters, which are conceptually related to the occurrence of induced seismicity. Some approaches also consider exposed values allowing to visualize risk in terms of a (qualitative) risk-matrix (Baisch et al., 2016). All screening procedures are very simple, focusing at a first order classification of the potential for inducing seismicity. A more detailed seismic hazard/risk assessment may be required if the results of an initial screening indicate that the induced seismicity potential is not low.

Most screening approaches target fluid injection operations, which are relevant e.g., in the context of geothermal exploitation, CCS, fracking, UGS, ATES, and waste-water disposal. Several of these approaches focus on the aspect of critically stressed faults in the subsurface, which could be seismically activated if exposed to hydraulic overpressure. Such faults typically exist in basement (frequently crystalline) rock and the vertical distance to the basement is frequently considered a key parameter for the occurrence of damage relevant seismicity (Hincks et al., 2018; Pawley et al., 2018; Scanlon et al., 2019; Schultz et al., 2016).

In The Netherlands, the risk associated with seismicity induced by gas extraction is addressed using similar classification schemes (Muntendam-Bos et al., 2015; van Thienen-Visser et al., 2018; Van Eijs et al., 2006).

To the best of the author's knowledge, comparable screening approaches have not been applied in the mining industry.

3.2.5 Hazard/Risk Assessment

A seismic hazard or risk assessment is either based on a probabilistic approach, a deterministic approach, or a combination of both. The hazard associated with natural seismicity is typically assessed by a probabilistic seismic hazard analysis, PSHA, e.g. (Cornell, 1968; McGuire, 1995). The fundamental basis for a PSHA is the earthquake model, i.e., a model of the occurrence probability of a certain magnitude event in a given region and a given period of time. For natural seismicity, earthquake models are typically based on the magnitude-frequency distribution of previous seismicity, assuming a stationary earthquake process.

To what extend the occurrence of induced seismicity can be approximated (piecewise) by a stationary process is a strongly debated subject. In practice, such approximations require earthquake data for calibration. Prior to subsurface activities, however, location-specific (induced) earthquake observations do not exist. Furthermore, the seismicity response to subsurface activities strongly depends on site-specific geological and tectonic conditions, as well as on operational parameters. Therefore, induced seismicity observations from other locations may not be transferrable.

In principle, physics-based models could be used to numerically simulate earthquake catalogues as an input to a PSHA (e.g. Baisch et al., 2009; Gischig & Wiemer, 2013; Milner et al., 2021). Seismicity forecasts resulting from these models, however, are strongly depending on *ad hoc* parameter assumptions. Frequently, it is not even possible to predict whether a subsurface operation will produce any measurable seismicity at all (e.g. Schultz, Skoumal, et al., 2020). Within the framework of a PSHA, this implies that hazard probabilities might be largely controlled by expert judgement.

As an alternative, seismic hazard can be assessed deterministically (deterministic seismic hazard assessment, DSHA). This approach focusses on determining a maximum possible magnitude in a worst-case-scenario, without quantifying its occurrence probability (e.g. Wang & Huang, 2014).

Existing guidelines for assessing induced seismicity risks typically have no general preference for either PSHA/PSRA or DSHA (Barth et al., 2015; Ground Water Protection Council and Interstate Oil and Gas Compact Commission, 2015; Majer et al., 2012). Independent of the chosen approach, these guidelines recommend assessing project-specific risks by considering

- the local geology and tectonic situation,
- previous earthquake activity in the project region,
- planned subsurface operations,
- buildings and infrastructure.

Additionally, seismic monitoring in combination with a TLS for risk mitigation is recommended. Several guidelines specifically recommend estimating a maximum earthquake magnitude and associated ground vibrations.

3.2.6 Risk Mitigation Measures

This section provides a general, high-level overview of measures for mitigating the seismic hazard associated with the subsurface technologies listed in section 3.1.1. We distinguish between two different types of mitigations measures. First, seismic hazard can be mitigated by selecting the project location and reservoir target such that stress load on known, potentially seismogenic faults is avoided. This type of hazard mitigation by 'design' can be based on the classification schemes presented in the previous section, aiming to design subsurface operation with low potential for inducing seismicity. It can also invoke a more detailed geomechanical analysis of planned subsurface operations.

The second type of mitigations measures is based on an operational response to the occurrence of induced seismicity. So-called 'traffic-light systems (TLS)' (Bommer et al., 2006) aim to limit the strength of induced seismicity by reducing and ultimately stopping subsurface operations after induced seismicity has exceeded certain threshold values.

The design criterion for many TLS is either to avoid felt seismicity or an earthquake that could cause damage to buildings, e.g. Schultz et al. (2020). Many TLS are based on threshold values for earthquake magnitude, which can be derived using models for earthquake consequences (section 3.2.2). In the following we focus on the most simple (green/red) magnitude-based TLS, where operations are stopped after induced seismicity has exceeded a critical magnitude threshold.

Intuitively, the TLS concept may appear to be a robust mitigation measure, also in situations where subsurface conditions are not well understood. In practice, however, limitations exist which can strongly reduce the efficiency of a TLS:

- The concept of TLS relies on the assumption that larger magnitude earthquakes announce themselves by precursory seismicity. While precursory seismicity is typically observed for seismicity induced by fluid injection, it may be lacking in other technologies, as observed e.g. in the context of gas production (Baisch et al., 2019).
- The precision at which even larger magnitude earthquakes can be prevented by stopping operations is limited by trailing effects, where the largest magnitude earthquake occurs after subsurface activities have already been suspended (Baisch et al., 2019). Trailing effects have been explained by post-injection pressure diffusion (Baisch, Weidler, Vörös, & Jung, 2006; Hsieh & Bredehoeft, 1981) in combination with stress perturbations (Baisch et al., 2010) that may lead to post-operational instabilities (Baisch et al., 2020) similar to after-deformations following tectonic earthquakes.
- A discontinuous increase of the magnitude of induced earthquakes ('magnitude jumps') may result in a scenario where a threshold value is overleaped (Verdon & Bommer, 2020).

The aspect of trailing effects is closely related to the phenomenon of uncontrolled or unarrested rupture (Galis et al., 2017, 2019; Garagash & Germanovich, 2012), where seismicity escalation may be beyond operational control (Bentz et al., 2020). For example, seismicity escalation after suspending subsurface operations was observed in the context of underground gas storage (del Potro & Diez, 2015), geothermal reservoirs (Baisch et al., 2009; The Geological Society of Korea, 2019), mining (Foulger et al., 2018) and fracking operations (De Pater & Baisch, 2011; Verdon & Bommer, 2020).

A common strategy is to anticipate trailing effects in the TLS design by adding an additional safety margin to the magnitude threshold value. For fracking induced seismicity, observations indicate that threshold values need to be up to 2 magnitude units lower than the critical earthquake magnitude that needs to be avoided (Schultz, Beroza, et al., 2020; Verdon & Bommer, 2020). Trailing effects of similar magnitude were also observed in geothermal reservoirs, e.g. 1.4 magnitude units (M_L) after geothermal production at Californië, The Netherlands (Baisch & Vörös, 2019) and the largest trailing effect with approx. 2 magnitude units (M_L) after hydraulic stimulation of a geothermal reservoir at Pohang, Korea (Yeo et al., 2020).

More complex TLS have been implemented, e.g. invoking statistical prediction (Bommer et al., 2006; Király-Proag et al., 2018), and/or additional higher alert levels, during which operational measures are reduced or even counterbalanced (Häring et al., 2008).

Systematic studies on how efficient a TLS has prevented the occurrence of an ‘undesired’ earthquake are still lacking. The limitations discussed above, however, are inherent to the earthquake process and not depending on a particular type of TLS.

3.2.7 Risk Management Guidelines

In the geothermal industry, several recommendations for managing induced seismicity risks were proposed, most of them sharing similar concepts (Baisch et al., 2016; Majer et al., 2012; Wiemer et al., 2017).

For example, Majer et al. (2012) propose a seven step approach, starting with (1) a preliminary screening evaluation (compare section 3.2.3), followed by (2) public outreach, (3) assessment of consequences (compare section 3.2.2), and (4) implementation of seismic monitoring. Steps (5) and (6) aim at assessing seismic hazard and risk. The authors propose to evaluate the natural earthquake hazard at the project location for comparison with the combined natural and induced earthquake hazard. They consider two possible approaches for hazard assessment, deterministic seismic hazard analysis (DSHA) and probabilistic seismic hazard analysis (PSHA). They indicate that PSHA is more suitable for a subsequent risk analysis but acknowledge the general difficulties in defining a (probabilistic) earthquake model. The final step (7) invokes the definition of a TLS as a direct risk mitigation measure, as well as several indirect mitigation measures including increased public outreach, community support, and damage compensation.

Recommendations by other authors follow similar lines, while the incremental assessment of the induced seismicity hazard compared to the natural seismic hazard is specific to Majer et al. (2012).

3.3 RECOMMENDATIONS FOR SEISMIC RISK ASSESSMENT IN FLANDERS

3.3.1 General Considerations

The current recommendations cover a broad range of subsurface technologies, operated at different depth levels from the hundred-meter scale to the scale of several kilometers. Geological conditions and the characteristics of subsurface operations are technology-specific, resulting in large differences of the induced seismicity hazard. For example, technologies operated in weak rocks at shallow depth, like ATES, tend to have a low potential for induced seismicity. Operations at greater depth can be more prone to induced seismicity, as evidenced by the Balmatt geothermal site.

In this chapter, we adopt the perspective of the regulator, seeking a workflow to avoid damaging earthquakes at a high confidence level. We recommend a combination of pre-operational hazard screening (compare section 3.2.3), monitoring (chapter 3.4), and a response protocol (compare section 3.2.6). We note, however, that project developers may want to conduct a more detailed SHA/SRA for economic reasons prior to the beginning of operations.

The key parameters for the induced earthquake potential are technology-dependent and a 'one-size-fits-all' hazard screening approach does not appear feasible in this case. Therefore, customized recommendations are advised for different subsurface technologies. The approach is schematically summarized in Figure 43 and the subsurface technologies are classified in Table 11

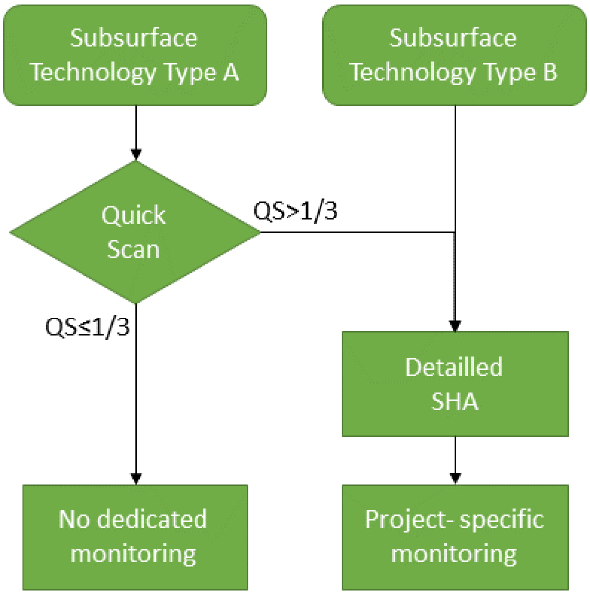

Figure 43: Schematic diagram showing the induced seismicity hazard management for the two different technology types. Type A technologies cover those activities which are associated with induced seismicity only under specific circumstances. A Quick-Scan is used for assessing the induced seismicity potential. In case of a low potential for induced seismicity (QS≤1/3), activities do not require a dedicated seismic monitoring. In case of a larger potential (QS>1/3) and for type B technologies, a more detailed seismic hazard assessment (SHA) is recommended. Risk mitigation measures including a traffic light protocol should be defined as part of the SHA, leading to a project-specific seismic monitoring.

Our recommendations either include a Quick-Scan for seismic hazard screening or a project-specific SHA. For the seismic hazard screening, a common topic is the aspect of critically stressed faults in the subsurface. On these faults, stress conditions might be altered by subsurface operations. Following an existing practice in The Netherlands, the proposed hazard screening suggests for which operations a more detailed SHA (prior to drilling) and intensified seismic monitoring is deemed necessary. General guidelines for a detailed SHA are provided in section 3.2.5.

It is important to notice that the Quick-Scan is a very simple, empirically based approach which is not equivalent to a physics-based analysis of the seismic hazard. The sole purpose of the Quick-Scan is to identify operations with very low induced seismicity potential in the sense that similar operations conducted in the past have not caused seismicity. The Quick-Scan should be handled in a conservative way, i.e., with a tendency to over-estimate the seismicity potential. Quick-Scan results obtained from a Greenfield analysis should be reviewed after in-situ information on subsurface conditions have become available.

In general, we recommend suspending subsurface operations after the occurrence of induced seismicity and (re-)evaluating the induced seismicity risk before resuming operations. This is motivated by our view that even small-magnitude earthquakes alter stress-conditions on faults in the subsurface. Stress contributions from different small earthquakes may accumulate. This accumulation increases the potential for trailing effects and the occurrence of larger magnitude earthquakes (Baisch et al., 2020). If induced seismicity has occurred, we consider it necessary to conduct a detailed SHA for investigating the root cause, identifying mitigation measures, and assessing the mitigated risks before resuming operations.

Although details of the reporting required from the operators need to be specified by the regulator, we nevertheless emphasize that resuming operations after a stoplight earthquake has occurred requires approval by the regulator of the (updated) risk assessment.

For subsurface operations requiring a detailed SHA, we recommend establishing an Expert Panel prior to the beginning of subsurface activities. The Expert Panel should assist the regulator with managing ‘unforeseeable events’ (e.g., stoplight earthquake) and communicating induced seismicity aspects. The Expert Panel should include representatives from the regulator, the ROB, the project developer, and possibly external experts.

The proposed recommendations are evidence-based, relying on previous (global) observations and current interpretations of the potential processes causing induced seismicity. Future observations might bring additional aspects into focus. Adjustments of the proposed workflow may consequently be required. In this respect, the current recommendations are designed to be a living document.

Table 11: Classification of technology types for seismic hazard assessment.

Subsurface Technology	Type	Description
Geothermal	A	section 3.3.3
ATES	no SHA required; no monitoring required	section 3.3.4
HT-ATES	A	section 3.3.4
UGS	B	section 3.3.5
CBM – without fracking	no SHA required; no monitoring required	section 3.3.6
CBM – with fracking	B	section 3.3.6
CCS	B	section 3.3.7
Mining	B	section 3.3.8
Mine water applications – without flooding	no SHA required; no monitoring required	section 3.3.8
Mine water applications – with flooding	B	section 3.3.8

3.3.2 Assessing Consequences of Ground Vibrations

Following section 3.2.2 we recommend peak ground vibration (PGV) as a metric for assessing hazard. According to engineering standards, damage to ordinary buildings is unlikely for PGV < 5 mm/s. For vulnerable buildings, the associated vibration Level is 3 mm/s. Human perceptibility is expected to start at 0.3-0.5 mm/s.

For a first estimate of the earthquake magnitude associated with the PGV threshold values, a global induced seismicity GMPE can be used. Figure 44 shows simulations based on the GMPE by Douglas et al. (2013; model 1). Near-surface amplification factors by Poggi et al. (2011) were used. For soft soil conditions, slight damages to ordinary buildings around the epicenter of a very shallow earthquake (e.g., shallower than 1 km, depending on soil conditions) may occur at a critical magnitude level of M_w ~2.5. We emphasize, however, that these estimates are subject to considerable uncertainty, which is inherent to GMPEs and the empirical nature of the magnitude scales.

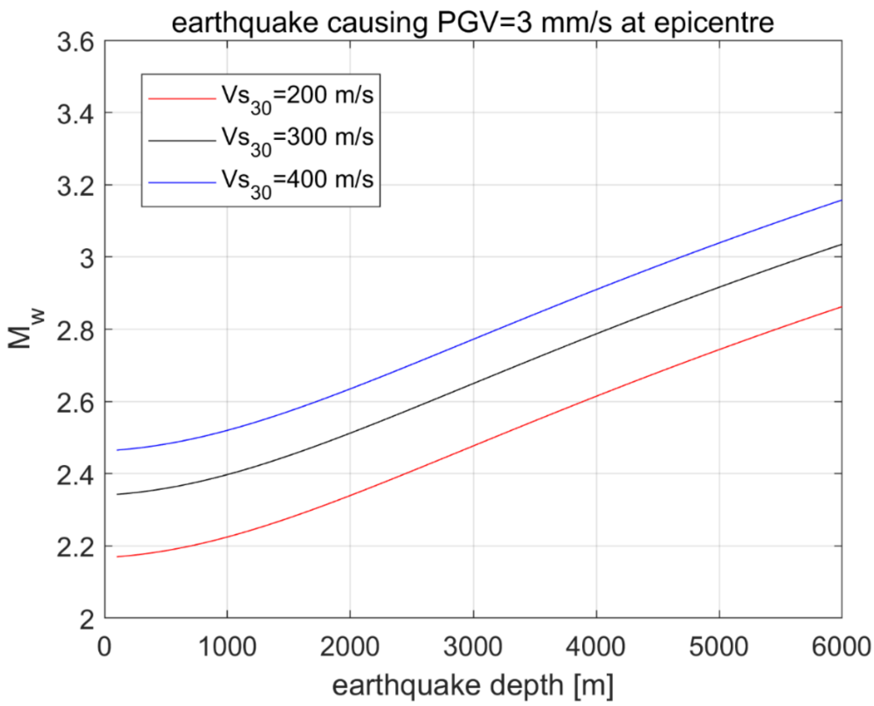

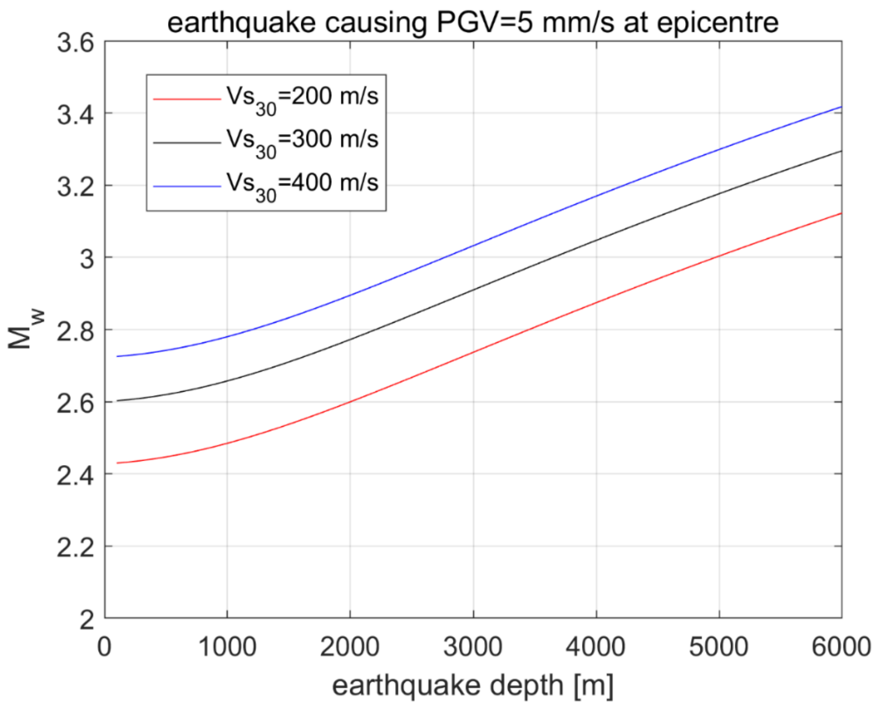

Figure 44: Critical magnitude level M_w at which modelled peak ground vibrations (PGV) exceed the threshold level for sensitive buildings (top) and ordinary buildings (bottom) as a function of earthquake depth. PGV values were calculated based on the GMPE by Douglas et al. (2013) combined with the near-surface amplification factors by Poggi et al. (2011). Different colors indicate the near-surface S-wave velocity (see legend). A dominating signal frequency of 10 Hz was assumed.

3.3.3 Geothermal Exploitation

In The Netherlands, the 'Quick-Scan' approach (Baisch et al., 2016) is currently applied to screen the induced seismicity potential of geothermal projects. Given the proximity to The Netherlands, we recommend using the same approach for screening the induced seismicity potential of geothermal projects in Flanders.

The Quick-Scan is based on a set of key parameters, which are considered relevant for the occurrence of induced seismicity. Most importantly, the occurrence of induced seismicity cannot be described by a single key parameter but requires a combination of several conditions to be fulfilled. Seismic hazard is consequently controlled by specific parameter combinations. Accordingly, the Quick-Scan is conducted using a scoring scheme based on different parameters (Table 11).

Deduced from observations at that time, the original Quick-Scan scheme uses 'distance to basement' as a key parameter. However, subsequent observations in The Netherlands (Californië, Baisch & Vörös, 2019) and Belgium (geothermal sites at Balmatt and Beerse) indicate that the lower Carboniferous responds seismically to geothermal operations. Therefore, we have substituted the parameter 'basement connected' by 'Carboniferous or older formations [hydraulically] connected'.

To apply the Quick-Scan to a geothermal project, scores from each key parameter are added and the total number is divided by the maximum possible number of scores (e.g., 90 if all parameters apply). This yields a normalized score QS in the range between QS=0 and QS=1. The induced seismicity potential is determined from the normalized score.

The Quick-Scan evaluates the overall project risk and does not distinguish between operations such as drilling, hydraulic stimulation, or circulation. Therefore, not all key parameters might be applicable in the planning phase of a geothermal project. Parameters which are not applicable are excluded from the Quick-Scan and the maximum possible number of scores is reduced accordingly. For example, if the Quick-Scan is applied to a geothermal exploration well in which no circulation operations are planned, the parameters 'circulation rate' and 'inter-well pressure communication' need to be excluded. The maximum score is reduced to 70.

The original concept distinguished between three different levels of the induced seismicity potential. Based on more recent experiences, we feel that the more detailed seismic hazard or risk assessments may be dominated by project-specific aspects and would like to avoid setting too narrow boundaries with a pre-defined workflow. Therefore, we propose using only two levels. Geothermal projects are either classified as having a low (QS≤1/3), or non-negligible (QS>1/3) potential for induced seismicity (Figure 45). The proposed hazard screening suggests for which operations a more detailed SHA/SRA (before drilling) and intensified seismic monitoring are deemed necessary.

Table 12: Proposed scoring scheme for the Quick-Scan (Baisch et al. 2016) with added modifications of the first parameter. ‘Carboniferous or older formations connected’ refers to a hydraulic connection between injection well and the Carboniferous or older formations. ‘Inter-well pressure communication’ denotes the hydraulic connection between the injection and production wells. ‘Distance to fault’ quantifies the distance between injection well and the nearest mapped fault. ‘Orientation of fault in current stress field’ describes the orientation of the nearest mapped fault. ‘Net injected volume’ represents the difference between injected and produced fluid volume. Guidelines for assigning Quick-Scan scores are provided in Baisch et al. (2016).

Score	Carboniferous or older formations connected	Inter-well pressure communication	Re-injection pressure [MPa]	Circulation rate [m^3/h]	Epicentral distance to natural earthquakes [km]	Epicentral distance to induced seismicity [km]	Distance to fault [km]	Orientation of fault in current stress field	Net injected volume [1000 m^3]
10	yes	no	> 7	> 360	< 1	< 1	< 0.1	favorable	> 20
7	possible	un-likely	4 - 7	180-360	1 - 5	1 - 5	0.1 - 0.5	shearing possible	5 - 20
3	unlikely	likely	1 - 4	50-180	5 - 10	5 - 10	0.5 – 1.5	shearing unlikely	0.1 - 5
0	no	yes	< 1	< 50	> 10	> 10	> 1.5	locked	< 0.1

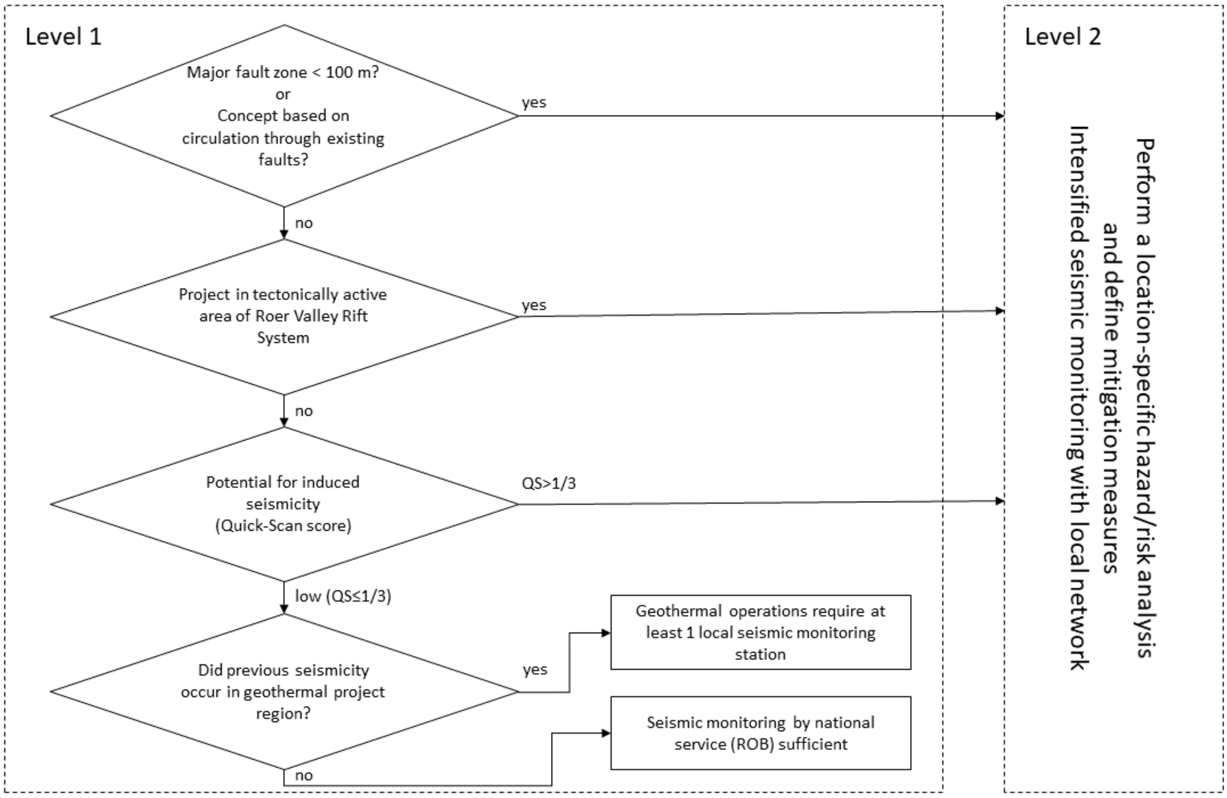

Figure 45: Decision tree for the proposed two-level seismic hazard and risk assessment.

3.3.4 Aquifer Thermal Energy Storage (ATES/HT-ATES)

ATES is an open-loop, bidirectional system, storing and recovering heat using the high permeability of shallow groundwater layers. Most ATES systems are operated at shallow depth ranging from the 10 m level up to a few hundreds of meters. Worldwide, more than 2,800 ATES systems are in operation, mainly in the Netherlands (Schüppler et al., 2019; Stricker et al., 2020). To the authors knowledge, ATES has never been associated with induced seismicity. This is consistent with geomechanical concepts, which state that deformation in weak rocks occurs predominantly aseismic.

For ATES projects we therefore recommend that

- no pre-operational seismic hazard screening needs to be performed,
- no dedicated seismic monitoring needs to be performed.

As a future option, HT-ATES (high-temperature aquifer thermal energy storage) systems are currently being tested, for shifting large amounts of high-temperature excess heat from summer to winter using the deep underground (Stricker et al., 2020).

Little experience exists with HT-ATES and to the authors knowledge, HT-ATES has never been associated with induced seismicity. We note, however, that HT-ATES may impact subsurface stress conditions in a similar fashion as conventional geothermal systems.

If HT-ATES is operated in a doublet system, exchanging fluid between a cold and a hot well (e.g., Schüppler et al., 2019), the geothermal Quick-Scan approach (Table 12) should be used.

If HT-ATES is operated through a single well, we suggest using a modified Quick-Scan approach (Table 13). In this modified approach, the parameters ‘circulation rate’ and ‘inter-well pressure communication’ are excluded and the maximum score possible is reduced to 70.

For both configurations we propose using the decision tree of Figure 45 for evaluating which operations require a more detailed SHA (prior to drilling) and intensified seismic monitoring.

Table 13: Proposed scoring scheme for the Quick-Scan according to Baisch et al. (2016) with several modifications for HT-ATES. ‘Carboniferous or older formations connected’ refers to a hydraulic connection between injection well and the Carboniferous or older formations. ‘Distance to fault’ denotes the distance between injection well and the nearest mapped fault. ‘Orientation of fault in current stress field’ describes the orientation of the nearest mapped fault. ‘Net injected volume’ quantifies the injected fluid volume during injection cycles. Guidelines for assigning Quick-Scan scores are provided in Baisch et al. (2016).

Score	Carboniferous or older formations connected	Re-injection pressure [MPa]	Epicentral distance to natural earth-quakes [km]	Epicentral distance to induced seismicity [km]	Distance to fault [km]	Orientation of fault in current stress field	Net injected volume [1000 m³]
10	yes	> 7	< 1	< 1	< 0.1	favorable	> 20
7	possible	4 - 7	1 - 5	1 - 5	0.1 - 0.5	shearing possible	5 - 20
3	unlikely	1 - 4	5 - 10	5 - 10	0.5 – 1.5	shearing unlikely	0.1 - 5
0	no	< 1	> 10	> 10	> 1.5	locked	< 0.1

3.3.5 Underground Gas Storage (UGS)

At the end of 2019, there were 661 UGS facilities in operation in the world, most of them utilizing depleted hydrocarbon fields (https://www.cedigaz.org/underground-gas-storage-in-the-world-2020-status; last visited 18.8.2021). About half a dozen UGS are operated in depleted gas fields in The Netherlands. Several of the Dutch UGS were associated with induced seismicity at the level $M_L \leq 1.5$ (Vörös & Baisch, 2018). Stronger seismicity up to $M_w=4.3$ has been associated with gas storage offshore Spain (Cesca et al., 2014; Vilarrasa et al., 2021) and up to $M_w=3.6$ at Hutubi, China (Tang et al., 2018). A single UGS is operated in Belgium which might be associated with minor seismicity (compare section 1.6.2.2).

Induced seismicity at low magnitude level has also been observed in shallow salt caverns that are used for storage (e.g. Mercerat et al., 2010). Although damage relevant seismicity caused by storage in salt caverns has not been reported yet, stress changes associated with salt creep and/or cavern collapse can be significant and could cause seismicity on nearby, critically stressed faults. Gas storage in aquifers has also been associated with induced seismicity. For example, (Silverii et al., 2021) relate observed earthquakes up to $M<2.3$ to poro-elastic stress changes caused by gas storage in a carbonate aquifer.

These observations highlight the general potential of the UGS technology for inducing seismicity. We recommend a detailed seismic risk assessment (prior to operations) for all UGS projects in Flanders.

3.3.6 Coal Bed Methane (CBM)

CBM is technically defined as a natural gas that can be recovered from coal seams. Over the last two decades it has become an important energy resource with the largest CBM production sites currently operating in the US, Australia, Canada, and China (Mastalerz, 2014; Mastalerz & Drobniak, 2020). Systematic monitoring of CBM exploitation in Australia yields no indication for induced seismicity (Drummond, 2013, 2016; Glanville et al., 2020). Similarly, no reported showcases of damage relevant seismicity caused by CBM production were found in the literature.

For CBM production we therefore recommend that

- no pre-operational seismic hazard screening needs to be performed,
- no dedicated seismic monitoring needs to be performed.

If fracking technology is used for enhancing CBM production, we recommend performing a detailed assessment of the induced seismicity risk associated with fracking.

3.3.7 Carbon Capture and Storage (CCS)

The CCS technology is still in its infancy with 8 operational, commercial-scale plants. Of these, three are seismogenic with earthquakes $M_w \leq 1.3$ (Foulger et al., 2018). Although CCS has not been associated with damage relevant seismicity, the number of showcases is small and geomechanical considerations do not indicate that a principal limit for the strength of induced seismicity related to CCS exists. Therefore, we generally recommend performing a detailed assessment of the induced seismicity risk for CCS projects in Flanders.

3.3.8 Mining

Foulger et al. (2018) note that mine excavations significantly perturb stresses in surrounding rocks and may reduce some components from values initially of the order of 100 MPa to atmospheric (0.1 MPa). The resulting stress differences can exceed the strength of rocks and cause earthquakes.

Besides failure of rock mass, observations by Alber & Fritschen (2011) demonstrate that mining-related stress perturbations at a much lower level can lead to significant seismicity if tectonic stresses on surrounding faults are already close to critically. Furthermore, allowing mines to flood after mining operations have been terminated can encourage seismicity by decreasing the effective normal stress on faults (Foulger et al., 2018).

Therefore, we generally recommend performing a detailed assessment of the induced seismicity risk for mining activities in Flanders.

Mine water geothermal applications are a possibility for the secondary use of abandoned and flooded mines. To date, only few full-scale projects exist (e.g. Bao et al., 2018; Verhoeven et al., 2014), and to the authors knowledge, none of these has been associated with induced seismicity. Compared to the flooding of a mine, the stress changes associated with geothermal mine water applications are small. Conceptually, induced seismicity is only promoted if geothermal activities cause the water table to exceed the level that has been established after flooding. We recommend performing a detailed assessment of the induced seismicity risk only if mine water applications will likely increase the water in the mine by more than 10 m.

3.4 RECOMMENDATIONS FOR SEISMIC MONITORING IN FLANDERS

3.4.1 General Considerations

Our recommended approach for managing induced seismicity risks rests on the combination of pre-operational hazard screening or hazard/risk assessment, seismic monitoring, and a response protocol. For being able to operate the response protocol, basic requirements for the seismic monitoring are implicitly defined.

We distinguish between two scenarios requiring different levels of seismic monitoring:

- In the Level I scenario, the potential for inducing seismicity is low. The occurrence of induced seismicity is unlikely, and seismic monitoring primarily serves the purpose to mitigate remaining risks by stopping subsurface operations after an earthquake has occurred. As outlined in section 3.4.2, Level I monitoring could be performed over large parts of Flanders with the existing station network operated by the ROB. Extension by a single station might be required to locally improve detection capabilities and the ability for discriminating the cause of an earthquake.
  In our recommendations we tacitly anticipate that an operator could integrate an additional monitoring station into the ROB network, which would then become part of the standard processing for the nation-wide monitoring. We do not expect that the ROB takes over any monitoring responsibilities going beyond their standard mandate.
- In the Level II scenario, there is a fair chance that induced seismicity occurs. Depending on subsurface activities, a project-specific response protocol may require immediate suspension

of operations. In this case, induced seismicity must be monitored in real-time with a dedicated monitoring system of the operator.

For both scenarios our recommendations are focused on the minimum requirements.

For baseline monitoring, we recommend deploying the monitoring station(s) at least 1 month prior to the beginning of subsurface activities.

3.4.2 Level I Monitoring

3.4.2.1 Response Protocol

After a local earthquake has occurred, the Level I response protocol suggests suspending subsurface activities, if the earthquake is most likely associated with the activities. In this case, observations are not in accordance with the initial seismic hazard screening. Hence, a re-assessment of the seismic hazard and risk is required.

In principle, this procedure is independent of the magnitude of the local earthquake. In practice, however, it can be difficult to unequivocally associate earthquakes of small magnitude to a certain subsurface activity. Due to a limited station coverage in combination with a low signal-to-noise ratio, the uncertainty of hypocenter location can be significant, sometimes exceeding the level of 5 km into lateral and/or vertical directions. Furthermore, insufficient knowledge of seismic wave velocities at a specific site introduces additional location uncertainty primarily in the vertical direction. Therefore, especially the depth of an earthquake localization is subject to large errors. This may complicate or even impede the discrimination between e.g., induced seismicity and natural earthquakes typically occurring at a greater depth. In doubt, we recommend to (temporarily) deploy a Level II monitoring network for improving location accuracy.

We propose using ‘avoiding damage relevant earthquakes’ as the design criterium for the response protocol. Here, we equate the terminology ‘damage relevant’ with the vibration level of PGV≥5 mm/s. At this vibration level damage to ordinary buildings cannot be ruled out (section 3.3.2).

We suggest assigning a safety margin of 1 magnitude unit (M_L) to account for trailing effects and magnitude jumps (section 3.2.6). Based on the definition of the local magnitude scale (Richter, 1935), the safety margin corresponds to a factor of 10 in signal amplitude. This implies that operations should be suspended if an earthquake causes vibrations which exceed 0.5 mm/s. Human perceptibility starts at the same level of vibration (Deutsches Institut für Normung e.V., 1999a; Groos et al., 2013). We note that this stoplight threshold of PGV=0.5 mm/s is consistent with the recommendations for TLS design by Schultz et al. (2020).

The stoplight criterion defines the lower magnitude limit above which earthquakes need to be detected by the monitoring system. This magnitude limit depends on the depth of the earthquake and can be estimated e.g., using the approach described in section 3.3.2. For example, simulated ground vibrations for an M_w=1.6 earthquake at 3 km depth, assuming soft soil conditions with V_{s30}=200 m/s, yield PGV=0.5 mm/s in the epicenter. Therefore, the monitoring system should provide at least a lower detection limit of M_w=1.6 in the area where subsurface activities are operated at 3 km depth with soft soil conditions.

3.4.2.2 ROB Monitoring Network

Earthquake activity in Belgium is monitored by the Royal Observatory of Belgium (ROB). The capability for detecting earthquakes with the ROB seismic monitoring network varies over Flanders and has changed over time as new monitoring stations were deployed (Van Camp et al., 2020). Figure 46 shows a simulation of the lower magnitude detection threshold for the ROB seismic network at nighttime. The simulation was set up to mimic the (automatized) routine processing of the ROB station network as of 2019. The magnitude threshold for earthquake detection varies by approximately two magnitude units with the lowest detection capabilities prevailing in western Belgium.

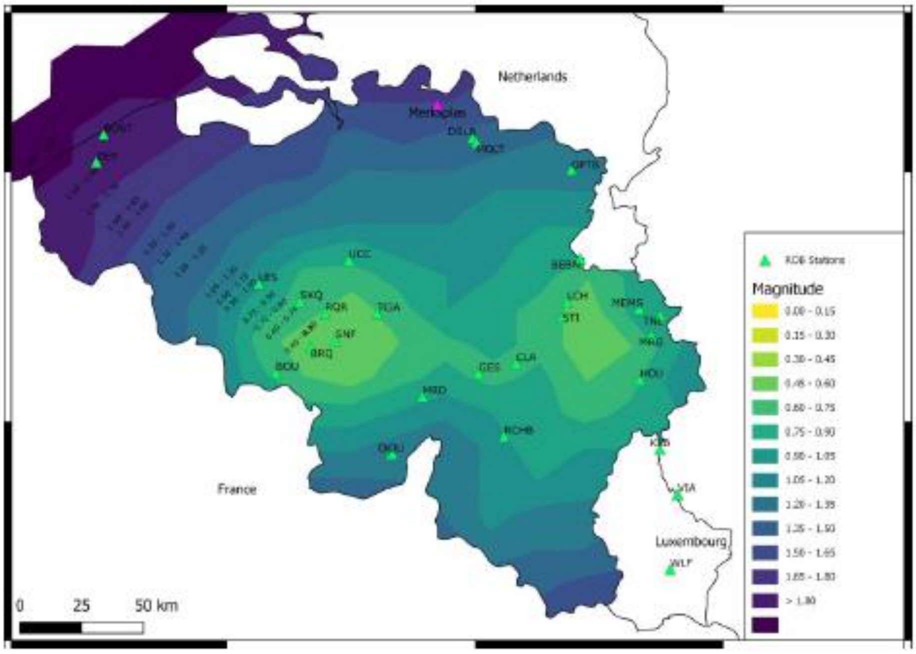

Figure 46: Simulated lower magnitude detection threshold for automatized, routine processing (implying coincident detections at ≥6 stations) according to the colourmap for the ROB seismic station network as of January 2019. Magnitude denotes the local magnitude M_L (email comm. Thomas Lecocq, 02.09.2021). The earthquake is assumed to be located at a depth of 10 km. The locations of the seismic stations are indicated by green triangles. Figure from Van Camp et al. (2020).

3.4.2.3 Detector Station

At those locations with previous seismicity or in areas where the minimum detection level of the ROB network is not sufficient for operating the response protocol (section 3.4.2.1), a local monitoring station ('detector station') needs to be deployed. If subsurface activities in Flanders are expected to scale up, we recommend densifying the backbone seismological network of the ROB. Ideally, the backbone network should cover regions with subsurface activities with a station spacing in the order of 15 km – 30 km.

If a dedicated detector station is used, we recommend deploying the station in the immediate vicinity of the subsurface operations at a location with low seismic background noise. If possible, the ROB should be consulted for finding an optimum location.

We note that earthquakes cannot (accurately) be located using data from a single detector station only. The detector station should complement the seismological network of the ROB to locally improve detection capabilities and to better constrain the depth of those local earthquakes, which are also recorded by stations of the ROB network.

We recommend using instrumentation fulfilling the following specifications:

- Short-period, 3 component seismometer.
- 24bit acquisition system.
- GPS synchronization.
- Time continuous recording with sampling frequency ≥100 Hz.
- Data recordings in standard format compatible with the ROB (e.g., miniSeed).
- Real-time data streaming using the SeedLink protocol.

3.4.3 Level II Monitoring

Requirements for Level II monitoring are strongly depending on the response protocol developed as part of the project-specific SHA/SRA. The following recommendations are generic and closely refer to the minimum requirements defined by Ritter et al. (2012):

- A minimum number of 5 monitoring stations should be operated. An optimized station geometry depends on the number of stations included within the network and can be modelled as part of the network design. The 2σ hypocenter location accuracy for seismicity in or near the geothermal reservoir should be at least +/- 500 m in horizontal and +/- 2,000 m in the vertical direction, respectively
- The locations of the stations should exhibit a comparatively low level of background noise. The detection threshold for reservoir earthquakes should be in the range between M_L=0 and M_L=1.
- To facilitate the detection of secondary seismic waves, 3-component seismometers should be used.
- The eigenfrequency of the seismometers should be ≤1 Hz.
- The instrumental registration should be based upon an absolute time base (GPS synchronization). The sampling frequency should be at least 100 Hz.
- Data should be recorded time continuously with a 24bit acquisition system.
- Real-time data access is required.
- The data should be recorded in standard format compatible with the ROB (e.g., miniSeed).
- Real-time data should be transferred using the SeedLink protocol.

Wherever possible, we recommend operating instruments at the Earth's surface since these provide direct measurements of PGV. Due to the geological conditions in the Campine Basin, however, it may not be possible to fulfill the minimum requirements regarding the background noise level with surface instruments. If all instruments of the monitoring network need to be operated in boreholes, we recommend deploying at least one additional seismometer near the wellhead of one of the borehole stations. This configuration aims at quantifying near-surface signal amplification.

We recommend that raw waveform data is archived by the operator for the entire duration of the seismic monitoring campaign. The data archive should be maintained for a period of at least 5 years following completion of the seismic monitoring. We encourage operators to share their waveform data through ORFEUS (http://orfeus.knmi.nl).

During operation of the seismic monitoring, we recommend the following minimum requirements for reporting to the regulator:

- TLS events should be reported immediately. Reported earthquake parameters should include date, time, magnitude, hypocenter location, confidence limits, maximum measured PGV, and the TLS status.
- Local seismicity should be summarized in annual reports. Earthquake parameters should include date, time, magnitude, hypocenter location, confidence limits, measured PGV. TLS events should be listed separately. These reports should also include a documentation of the state-of-health of the monitoring system and possible downtimes.

REFERENCES

A'Campo, Y. W. L., Baisch, S., Buter, E., Slob, S., Laenen, B., Besseling, F., & Boter, E. L. (2020). *Risk assessment for UDG and EGS and an inventory of preventive and mitigating measures* (Final report project KEM-06 No. 105911/20–005.135) (p. 142). Witteveen&Bos. Retrieved from https://kemprogramma.nl/file/download/57979640/kem-06-report-on-risk-assessment-udg-and-egs-rewrite-1-0.PDF

Aki, K., & Richards, P. (2002). Quantitative Seismology, 2nd Ed.

Albaric, J., Oye, V., Langet, N., Hasting, M., Lecomte, I., Iranpour, K., et al. (2014). Monitoring of induced seismicity during the first geothermal reservoir stimulation at Paralana, Australia. *Analysis of Induced Seismicity in Geothermal Operations*, *52*, 120–131. https://doi.org/10.1016/j.geothermics.2013.10.013

Alber, M., & Fritschen, R. (2011). Rock mechanical analysis of a Ml= 4.0 seismic event induced by mining in the Saar District, Germany: Ml= 4.0 seismic event induced by mining. *Geophysical Journal International*, *186*(1), 359–372. https://doi.org/10.1111/j.1365-246X.2011.05047.x

Amantini, E., Ricaud, Y., & Grégoire, N. (2009). Development of the Performance of the Loenhout UGS (Antwerp - Belgium) - Drilling through a highly karstified and fissured Limestone Reservoir under Gas Storage Operation. In *Conference Proceedings* (p. 9). Buenos Aires, Argentina.

Atkinson, G. M. (2015). Ground-Motion Prediction Equation for Small-to-Moderate Events at Short Hypocentral Distances, with Application to Induced-Seismicity Hazards. *Bulletin of the Seismological Society of America*, *105*(2A), 981–992. https://doi.org/10.1785/0120140142

Baisch, S. (2020). Inferring In Situ Hydraulic Pressure From Induced Seismicity Observations: An Application to the Cooper Basin (Australia) Geothermal Reservoir. *Journal of Geophysical Research: Solid Earth*, *125*(8).

https://doi.org/10.1029/2019JB019070

Baisch, S., & Vörös, R. (2019). *Earthquakes Near the Californie Geothermal Site: August 2015 – November 2018* (Internal report prepared for Californie Lipzig Gielen Geothermie BV No. CLGG005) (p. 50).

Baisch, S., Weidler, R., Vörös, R., & Jung, R. (2006). A Conceptual Model for Post-Injection Seismicity at Soultz-sous-Forêts. *GRC Transactions*, *30*, 601–605.

Baisch, S., Weidler, R., Vörös, R., Wyborn, D., & de Graaf, L. (2006). Induced Seismicity during the Stimulation of a Geothermal HFR Reservoir in the Cooper Basin, Australia. *Bulletin of the Seismological Society of America*, *96*(6), 2242–2256. https://doi.org/10.1785/0120050255

Baisch, S., Ceranna, L., & Harjes, H.-P. (2008). Earthquake Cluster: What Can We Learn from Waveform Similarity? *Bulletin of the Seismological Society of America*, *98*(6), 2806–2814. https://doi.org/10.1785/0120080018

Baisch, S., Carbon, D., Dannwolf, U., Delacou, B., Devaux, M., Dunand, F., et al. (2009). *Deep Heat Mining Basel - Seismic Risk Analysis* (p. 553). SERIANEX study prepared for the Departement für Wirtschaft, Soziales und Umwelt des Kantons Basel-Stadt, Amt für Umwelt und Energie. Retrieved from http://www.wsu.bs.ch/geothermie

Baisch, S., Vörös, R., Rothert, E., Stang, H., Jung, R., & Schellschmidt, R. (2010). A numerical model for fluid injection induced seismicity at Soultz-sous-Forêts. *International Journal of Rock Mechanics and Mining Sciences*, *47*(3), 405–413. https://doi.org/10.1016/j.ijrmms.2009.10.001

Baisch, S., Rothert, E., Stang, H., Vörös, R., Koch, C., & McMahon, A. (2015). Continued Geothermal Reservoir Stimulation Experiments in the Cooper Basin (Australia). *Bulletin of the Seismological Society of America*, *105*(1), 198–209. https://doi.org/10.1785/0120140208

Baisch, S., Koch, C., Stang, H., Pittens, B., Drijver, B., & Buik, N. (2016). *Defining the Framework for Seismic Hazard Assessment in Geothermal Projects V0.1 - Technical Report* (No. 161005) (p. 65).

Baisch, S., Koch, C., & Muntendam-Bos, A. (2019). Traffic Light Systems: To What Extent Can Induced Seismicity Be Controlled? *Seismological Research Letters*, *90*(3), 1145–1154. https://doi.org/10.1785/0220180337

Baisch, S., Vörös, R., Carstens, P., & Wittmann, K. (2020). (When) Do Earthquakes Respect Traffic Lights? Presented at the 82nd EAGE Conference & Exhibition 2020, Amsterdam, The Netherlands.

Bao, T., Liu, Z., Meldrum, J., & Green, C. (2018). Large-Scale Mine Water Geothermal Applications with Abandoned Mines. In D. Zhang & X. Huang (Eds.), *Proceedings of GeoShanghai 2018 International Conference: Tunnelling and Underground Construction* (pp. 685–695). Singapore: Springer Singapore. https://doi.org/10.1007/978-981-13-0017-2_69

Barth, A., Schmidt, B., Joswig, M., Baisch, S., Fritschen, R., Gaucher, E., et al. (2015). Empfehlungen zur Erstellung von Stellungnahmen zur seismischen Gefährdung bei tiefengeothermischen Projekten. *Mitteilungen Der Deutschen Geophysikalischen Gesellschaft*, *1*, 5–7.

Bentz, S., Kwiatek, G., Martínez-Garzón, P., Bohnhoff, M., & Dresen, G. (2020). Seismic Moment Evolution During Hydraulic Stimulations. *Geophysical Research Letters*, *47*(5). https://doi.org/10.1029/2019GL086185

Boatwright, J. (1980). A spectral theory for circular seismic sources; simple estimates of source dimension, dynamic stress drop, and radiated seismic energy. *Bulletin of the Seismological Society of America*, *70*(1), 1–27.

Bohnhoff, M., Dresen, G., Ellsworth, W. L., & Ito, H. (2009). Passive Seismic Monitoring of Natural and Induced Earthquakes: Case Studies, Future Directions and Socio-Economic Relevance. In S. Cloetingh & J. Negendank (Eds.), *New Frontiers in Integrated Solid Earth Sciences* (pp. 261–285). Dordrecht: Springer Netherlands. https://doi.org/10.1007/978-90-481-2737-5_7

Bommer, J. J., Oates, S., Cepeda, J. M., Lindholm, C., Bird, J., Torres, R., et al. (2006). Control of hazard due to seismicity induced by a hot fractured rock geothermal project. *Engineering Geology*, *83*(4), 287–306. https://doi.org/10.1016/j.enggeo.2005.11.002

Bommer, J. J., Crowley, H., & Pinho, R. (2015). A risk-mitigation approach to the management of induced seismicity. *Journal of Seismology*, *19*(2), 623–646. https://doi.org/10.1007/s10950-015-9478-z

Bossu, R., & Mazet-Roux, G. (2012). An operational authoritative location scheme [Application/pdf]. *New Manual of Seismological Observatory Practice 2 (NMSOP2)*, 8. https://doi.org/10.2312/GFZ.NMSOP-2_IS_8.5

Bourne, S. J., Oates, S. J., van Elk, J., & Doornhof, D. (2014). A seismological model for earthquakes induced by fluid extraction from a subsurface reservoir. *Journal of Geophysical Research: Solid Earth*, *119*(12), 8991–9015. https://doi.org/10.1002/2014JB011663

Box, R., & Lowrey, P. (2003). Reconciling sonic logs with check-shot surveys: Stretching synthetic seismograms. *The Leading Edge*, *22*(6), 510–517. https://doi.org/10.1190/1.1587672

Broothaers, M. (2020). *Jaarrapport 2 Opsporingsvergunning aardwarmte Beerse – Janssen Pharmaceutica nv* (p. 51). Mol, Belgium: VITO.

Brune, J. N. (1970). Tectonic stress and the spectra of seismic shear waves from earthquakes. *Journal of Geophysical Research (1896-1977)*, *75*(26), 4997–5009. https://doi.org/10.1029/JB075i026p04997

Buijze, L., van Bijsterveldt, L., Cremer, H., Paap, B., Veldkamp, H., Wassing, B. B. T., et al. (2019). *Review of worldwide geothermal projects: mechanisms and occurrence of induced seismicity* (No. TNO 2019 R100043) (p. 257).

Butcher, A., Luckett, R., Verdon, J. P., Kendall, J. -Michael, Baptie, B., & Wookey, J. (2017). Local Magnitude Discrepancies for Near-Event Receivers: Implications for the U.K. Traffic-Light Scheme. *Bulletin of the Seismological Society of America*, *107*(2), 532–541. https://doi.org/10.1785/0120160225

Camelbeeck, T. (1990). L'Activite Seismique Actuelle (1985-1988) en Belgique.

Comparaison avec les donnees de seismicité historique et instrumentale. Analyse Seismotectonique. *Annales de La Société Géologique de Belgique*, *112*(2), 347–365.

Cesca, S., Grigoli, F., Heimann, S., González, Á., Buforn, E., Maghsoudi, S., et al. (2014). The 2013 September–October seismic sequence offshore Spain: a case of seismicity triggered by gas injection? *Geophysical Journal International*, *198*(2), 941–953. https://doi.org/10.1093/gji/ggu172

Contrucci, I., Klein, E., Bigarré, P., Lizeur, A., Lomax, A., & Bennani, M. (2010). Management of Post-mining Large-scale Ground Failures: Blast Swarms Field Experiment for Calibration of Permanent Microseismic Early-warning Systems. *Pure and Applied Geophysics*, *167*(1–2), 43–62. https://doi.org/10.1007/s00024-009-0005-4

Cornell, C. A. (1968). Engineering seismic risk analysis. *Bulletin of the Seismological Society of America*, *58*(5), 1583–1606.

Davis, S. D., & Frohlich, C. (1993). Did (Or Will) Fluid Injection Cause Earthquakes? - Criteria for a Rational Assessment. *Seismological Research Letters*, *64*(3–4), 207–224. https://doi.org/10.1785/gssrl.64.3-4.207

De Pater, H. J., & Baisch, S. (2011). *Geomechanical Study of Bowland Shale Seismicity - Synthesis Report* (p. 71). Retrieved from https://www.semanticscholar.org/paper/Geomechanical-Study-of-Bowland-Shale-Seismicity-Pater-Baisch

Deckers, J., De Konick, R., Bos, S., Broothaers, M., Dirix, K., Hambsch, L., et al. (2019). *Geologisch (G3Dv3) en hydrogeologisch (H3D) 3D-lagenmodel van Vlaanderen* (No. 2018/RMA/R/1569) (p. 614). Mol, Belgium: VITO.

Deichmann, N. (2006). Local Magnitude, a Moment Revisited. *Bulletin of the Seismological Society of America*, *96*(4A), 1267–1277. https://doi.org/10.1785/0120050115

Deichmann, N. (2017). Theoretical Basis for the Observed Break in ML/Mw Scaling between Small and Large Earthquakes. *Bulletin of the Seismological Society of America*, *107*(2), 505–520. https://doi.org/10.1785/0120160318

Deichmann, N., Kraft, T., & Evans, K. F. (2014). Identification of faults activated during the stimulation of the Basel geothermal project from cluster analysis and focal mechanisms of the larger magnitude events. *Geothermics*, *52*, 84–97. https://doi.org/10.1016/j.geothermics.2014.04.001

Deutsches Institut für Normung e.V. (1999a). DIN 4150-2:1999-06 - Erschütterungen im Bauwesen - Teil 2: Einwirkungen auf Menschen in Gebäuden. Beuth Verlag GmbH. https://doi.org/10.31030/8067954

Deutsches Institut für Normung e.V. (1999b). DIN 4150-3:1999-02 - Erschütterungen im Bauwesen - Teil 3: Einwirkungen auf bauliche Anlagen. Beuth Verlag GmbH. Retrieved from https://www.beuth.de/de/norm/din-4150-3/5146115

DMT. (2019a). *Seismic Monitoring Mol* (Presentation) (p. 14). DMT.

DMT. (2019b). *Seismic Monitoring Mol - Evaluation of source mechanisms* (Presentation) (p. 17). DMT.

Dost, B., van Eck, T., & Haak, H. (2004). Scaling peak ground acceleration and peak ground velocity recorded in The Netherlands. *Bolletino Di Geofisica Teorica Ed Applicata*, *45*(3), 153–168.

Douglas, J. (2017). *Ground motion prediction equations 1964-2016* (p. 576). Glasgow, United Kingdom: Department of Civil and Environmental Engineering - University of Strathclyde. Retrieved from http://www.gmpe.org.uk/

Douglas, J., Edwards, B., Convertito, V., Sharma, N., Tramelli, A., Kraaijpoel, D., et al. (2013). Predicting Ground Motion from Induced Earthquakes in Geothermal Areas. *Bulletin of the Seismological Society of America*, *103*(3), 1875–1897. https://doi.org/10.1785/0120120197

Drummond, B. (2013). *Background Paper on Seismicity* (Prepared for the New South Wales Chief Scientist and Engineer as part of the Review of coal seam gas activities in NSW) (p. 103). Government of New South Wales.

Drummond, B. (2016). *Review of hydrofracturing and induced seismicity* (No. Record 2016/02). Geoscience Australia. Retrieved from http://dx.doi.org/10.11636/Record.2016.002

Foulger, G. R., Wilson, M. P., Gluyas, J. G., Julian, B. R., & Davies, R. J. (2018). Global review of human-induced earthquakes. *Earth-Science Reviews*, *178*, 438–514. https://doi.org/10.1016/j.earscirev.2017.07.008

Galis, M., Ampuero, J. P., Mai, P. M., & Cappa, F. (2017). Induced seismicity provides insight into why earthquake ruptures stop. *Science Advances*, *3*(12), eaap7528. https://doi.org/10.1126/sciadv.aap7528

Galis, M., Ampuero, J.-P., Mai, P. M., & Kristek, J. (2019). Initiation and arrest of earthquake ruptures due to elongated overstressed regions. *Geophysical Journal International*, *217*(3), 1783–1797. https://doi.org/10.1093/gji/ggz086

Garagash, D. I., & Germanovich, L. N. (2012). Nucleation and arrest of dynamic slip on a pressurized fault: Nucleation on pressurized fault. *Journal of Geophysical Research: Solid Earth*, *117*(B10). https://doi.org/10.1029/2012JB009209

Gischig, V. S., & Wiemer, S. (2013). A stochastic model for induced seismicity based on non-linear pressure diffusion and irreversible permeability enhancement. *Geophysical Journal International*, *194*(2), 1229–1249. https://doi.org/10.1093/gji/ggt164

Glanville, H., Allen, T., Stepin, B., & Bugden, C. (2020). *Seismic monitoring of NSW CGS areas: monitoring of seismic activity in the CGS production area of Camden and the seismicity of the region.* Geoscience Australia. https://doi.org/10.11636/Record.2020.020

Groos, J. C., Fritschen, R., & Ritter, J. R. R. (2013). Untersuchung induzierter Erdbeben hinsichtlich ihrer Spürbarkeit und eventueller Schadenswirkung anhand der DIN 4150. *Bauingenieur*, *88*, 11.

Ground Water Protection Council and Interstate Oil and Gas Compact Commission. (2015). *Potential Injection-Induced Seismicity Associated with Oil & Gas Development: A Primer on Technical and Regulatory Considerations Informing Risk Management and Mitigation* (p. 141).

Hanks, T. C., & Kanamori, H. (1979). A moment magnitude scale. *Journal of Geophysical Research*, *84*(B5), 2348–2350. https://doi.org/10.1029/JB084iB05p02348

Häring, M. O., Schanz, U., Ladner, F., & Dyer, B. C. (2008). Characterisation of the Basel 1 enhanced geothermal system. *Geothermics*, *37*(5), 469–495. https://doi.org/10.1016/j.geothermics.2008.06.002

Hincks, T., Aspinall, W., Cooke, R., & Gernon, T. (2018). Oklahoma’s induced seismicity strongly linked to wastewater injection depth. *Science*, *359*(6381), 1251–1255. https://doi.org/10.1126/science.aap7911

Hinzen, K.-G. (2003). Stress field in the Northern Rhine area, Central Europe, from earthquake fault plane solutions. *Tectonophysics*, *377*(3–4), 325–356. https://doi.org/10.1016/j.tecto.2003.10.004

Hsieh, P. A., & Bredehoeft, J. D. (1981). A reservoir analysis of the Denver earthquakes: A case of induced seismicity. *Journal of Geophysical Research: Solid Earth*, *86*(B2), 903–920. https://doi.org/10.1029/JB086iB02p00903

INERIS. (2019). *Seismic hazard and risk analysis at Balmatt - Part1: Source mechanism analysis (Deliverable D1)* (No. Ineris-200066-830488-v1.0) (p. 20). INERIS.

INERIS. (2020). *Seismic hazard and risk analysis at Balmatt - Part2: Characterization of the triggering mechanism, hazard and risk assessment.* (No. Ineris-200066-2045899-v1.0) (p. 168). INERIS.

Kao, H., Visser, R., Smith, B., & Venables, S. (2018). Performance assessment of the induced seismicity traffic light protocol for northeastern British Columbia and western Alberta. *The Leading Edge*, *37*(2), 117–126. https://doi.org/10.1190/tle37020117.1

Király-Proag, E., Gischig, V., Zechar, J. D., & Wiemer, S. (2018). Multicomponent ensemble models to forecast induced seismicity. *Geophysical Journal International*, *212*(1), 476–490. https://doi.org/10.1093/gji/ggx393

Koch, C., Baisch, S., Rothert, E., & Reinecker, J. (2021). Inferring Hydraulic Pressure Changes from Induced Seismicity Observations: Three Showcases from Geothermal Reservoirs. *International Journal of Geophysics*, *2021*, 15.

https://doi.org/10.1155/2021/6647834

Lomax, A., Virieux, J., Volant, P., & Berge-Thierry, C. (2000). Probabilistic Earthquake Location in 3D and Layered Models. In C. H. Thurber & N. Rabinowitz (Eds.), *Advances in Seismic Event Location* (pp. 101–134). Dordrecht: Springer Netherlands. https://doi.org/10.1007/978-94-015-9536-0_5

Lomax, A., Michelini, A., & Curtis, A. (2009). Earthquake Location, Direct, Global-Search Methods. In R. A. Meyers (Ed.), *Encyclopedia of Complexity and Systems Science* (pp. 2449–2473). New York, NY: Springer New York. https://doi.org/10.1007/978-0-387-30440-3_150

Majer, E., Nelson, J., Robertson-Tait, A., Savy, J., & Wong, I. (2012). *Protocol for Addressing Induced Seismicity Associated with Enhanced Geothermal Systems* (No. DOE/EE--0662, 1219482) (p. DOE/EE--0662, 1219482). https://doi.org/10.2172/1219482

Mastalerz, M. (2014). Coal bed methane: reserves, production and future outlook. In T. M. Letcher (Ed.), *Future energy* (Vol. second edition, pp. 145–158). New York: Elsevier.

Mastalerz, M., & Drobniak, A. (2020). Coalbed Methane: Reserves, Production, and Future Outlook. In T. M. Letcher (Ed.), *Future Energy* (Vol. Third edition, pp. 97–109). Elsevier. https://doi.org/10.1016/B978-0-08-102886-5.00005-0

McGarr, A. (2014). Maximum magnitude earthquakes induced by fluid injection: Limits on fluid injection earthquakes. *Journal of Geophysical Research: Solid Earth*, *119*(2), 1008–1019. https://doi.org/10.1002/2013JB010597

McGuire, R. K. (1995). Probabilistic seismic hazard analysis and design earthquakes: Closing the loop. *Bulletin of the Seismological Society of America*, *85*(5), 1275–1284.

Mercerat, E. D., Driad-Lebeau, L., & Bernard, P. (2010). Induced Seismicity Monitoring of an Underground Salt Cavern Prone to Collapse. *Pure and Applied Geophysics*, *167*(1–2), 5–25. https://doi.org/10.1007/s00024-009-0008-1

Milner, K. R., Shaw, B. E., Goulet, C. A., Richards-Dinger, K. B., Callaghan, S., Jordan, T. H., et al. (2021). Toward Physics-Based Nonergodic PSHA: A Prototype Fully Deterministic Seismic Hazard Model for Southern California. *Bulletin of the*

Seismological Society of America. https://doi.org/10.1785/0120200216

Munafò, I., Malagnini, L., & Chiaraluce, L. (2016). On the Relationship between Mw and ML for Small Earthquakes. *Bulletin of the Seismological Society of America*, *106*(5), 2402–2408. https://doi.org/10.1785/0120160130

Muntendam-Bos, A. G., Roest, J. P. A., & de Waal, J. A. (2015). A guideline for assessing seismic risk induced by gas extraction in the Netherlands. *The Leading Edge*, *34*(6), 672–677. https://doi.org/10.1190/tle34060672.1

Pawley, S., Schultz, R., Playter, T., Corlett, H., Shipman, T., Lyster, S., & Hauck, T. (2018). The Geological Susceptibility of Induced Earthquakes in the Duvernay Play. *Geophysical Research Letters*, *45*(4), 1786–1793. https://doi.org/10.1002/2017GL076100

Poggi, V., Edwards, B., & Fah, D. (2011). Derivation of a Reference Shear-Wave Velocity Model from Empirical Site Amplification. *Bulletin of the Seismological Society of America*, *101*(1), 258–274. https://doi.org/10.1785/0120100060

del Potro, R., & Diez, M. (2015). Induced Seismicity in Underground Gas Storage - The Case of Castor, Offshore NE Spain. Presented at the 77th EAGE Conference and Exhibition - Workshops, Madrid, Spain. https://doi.org/10.3997/2214-4609.201413522

Richter, C. F. (1935). An instrumental earthquake magnitude scale*. *Bulletin of the Seismological Society of America*, *25*(1), 1–32.

Ritter, J., Baisch, S., Fritschen, R., Groos, J., Kraft, T., Plenefisch, T., et al. (2012). Empfehlungen zur Überwachung induzierter Seismizität – Positionspapier des FKPE. *Mitteilungen Der Deutschen Geophysikalischen Gesellschaft e.V.*, *2012/3*, 17–31.

SBR. (2010). *Schade aan Gebouwen, Deel A uit de Meet– en beoordelingsrichtijn: Trillingen*.

Scanlon, B. R., Weingarten, M. B., Murray, K. E., & Reedy, R. C. (2019). Managing Basin-Scale Fluid Budgets to Reduce Injection-Induced Seismicity from the Recent U.S. Shale Oil Revolution. *Seismological Research Letters*, *90*(1), 171–182.

https://doi.org/10.1785/0220180223

Schmittbuhl, J., Lambotte, S., Lengliné, O., Grunberg, M., Jund, H., Vergne, J., et al. (2021). Induced and triggered seismicity below the city of Strasbourg, France from November 2019 to January 2021. *Comptes Rendus. Géoscience*, *353*(S1), 1–24. https://doi.org/10.5802/crgeos.71

Scholz, C. H. (2002). *The Mechanics of Earthquakes and Faulting* (2nd ed.). Cambridge: Cambridge University Press. https://doi.org/10.1017/CBO9780511818516

Schultz, R., Corlett, H., Haug, K., Kocon, K., MacCormack, K., Stern, V., & Shipman, T. (2016). Linking fossil reefs with earthquakes: Geologic insight to where induced seismicity occurs in Alberta. *Geophysical Research Letters*, *43*(6), 2534–2542. https://doi.org/10.1002/2015GL067514

Schultz, R., Skoumal, R. J., Brudzinski, M. R., Eaton, D., Baptie, B., & Ellsworth, W. (2020). Hydraulic Fracturing-Induced Seismicity. *Reviews of Geophysics*, *58*(3). https://doi.org/10.1029/2019RG000695

Schultz, R., Beroza, G., Ellsworth, W., & Baker, J. (2020). Risk-Informed Recommendations for Managing Hydraulic Fracturing–Induced Seismicity via Traffic Light Protocols. *Bulletin of the Seismological Society of America*. https://doi.org/10.1785/0120200016

Schüppler, S., Fleuchaus, P., & Blum, P. (2019). Techno-economic and environmental analysis of an Aquifer Thermal Energy Storage (ATES) in Germany. *Geothermal Energy*, *7*(1), 11. https://doi.org/10.1186/s40517-019-0127-6

Silverii, F., Maccaferri, F., Richter, G., Gonzalez Cansado, B., Wang, R., Hainzl, S., & Dahm, T. (2021). Poroelastic model in a vertically sealed gas storage: a case study from cyclic injection/production in a carbonate aquifer. *Geophysical Journal International*, *227*(2), 1322–1338. https://doi.org/10.1093/gji/ggab268

Snoke, J. A. (1984). *FOCMEC: FOCal MEChanism determinations* (p. 21). Blacksburg, VA, USA: Virginia Tech. https://doi.org/10.1016/S0074-6142(03)80291-7

Sonley, E., & Abercrombie, R. E. (2006). Effects of methods of attenuation correction on source parameter determination. In R. Abercrombie, A. McGarr, H. Kanamori, & G.

Di Toro (Eds.), *Geophysical Monograph Series* (Vol. 170, pp. 91–97). Washington, D. C.: American Geophysical Union. https://doi.org/10.1029/170GM11

Stricker, K., Grimmer, J. C., Egert, R., Bremer, J., Korzani, M. G., Schill, E., & Kohl, T. (2020). The Potential of Depleted Oil Reservoirs for High-Temperature Storage Systems. *Energies*, *13*(24), 6510. https://doi.org/10.3390/en13246510

Tang, L., Lu, Z., Zhang, M., Sun, L., & Wen, L. (2018). Seismicity Induced by Simultaneous Abrupt Changes of Injection Rate and Well Pressure in Hutubi Gas Field. *Journal of Geophysical Research: Solid Earth*, *123*(7), 5929–5944. https://doi.org/10.1029/2018JB015863

The Geological Society of Korea. (2019). *Summary Report of the Korean Government Commission on Relations between the 2017 Pohang Earthquake and EGS Project* (p. 205). The Geological Society of Korea.

van Thienen-Visser, K., Roholl, J. A., van Kempen, B. M. M., & Muntendam-Bos, A. G. (2018). Categorizing seismic risk for the onshore gas fields in the Netherlands. *Engineering Geology*, *237*, 198–207. https://doi.org/10.1016/j.enggeo.2018.02.004

Trutnevyte, E., & Wiemer, S. (2017). Tailor-made risk governance for induced seismicity of geothermal energy projects: An application to Switzerland. *Geothermics*, *65*, 295–312. https://doi.org/10.1016/j.geothermics.2016.10.006

Van Camp, M., Van Noten, K., Lecocq, T., & Vanneste, K. (2020). *Monitoring seismicity in the context of activities in the deep subsurface of Flanders* (No. ROB-VPO 2020-01) (p. 88). Brussel: Royal Observatory of Belgium.

Van Eijs, R. M. H. E., Mulders, F. M. M., Nepveu, M., Kenter, C. J., & Scheffers, B. C. (2006). Correlation between hydrocarbon reservoir properties and induced seismicity in the Netherlands. *Engineering Geology*, *84*(3–4), 99–111. https://doi.org/10.1016/j.enggeo.2006.01.002

Vandenberghe, N., Craen, M. D., & Beerten, K. (2014). *Geological framework of the Campine Basin - Geological setting, tectonics, sedimentary sequences* (No. CK•CEN-ER-262 1) (p. 113). Mol, Belgium: SCK•CEN.

Vanneste, K., Camelbeeck, T., & Verbeeck, K. (2013). A Model of Composite Seismic Sources for the Lower Rhine Graben, Northwest Europe. *Bulletin of the Seismological Society of America*, *103*(2A), 984–1007. https://doi.org/10.1785/0120120037

Verbeeck, K. (2019). *Deterministic Seismic Hazard Assessment in the Belgian Campine Basin at the Mol/Dessel site: from seismic source to site effect*. Katholieke Universiteit Leuven, Department of Earth and Environmental Sciences, Division of Geology, Leuven.

Verbeeck, K., Wouters, L., Vanneste, K., Camelbeeck, T., Vandenberghe, D., Beerten, K., et al. (2017). Episodic activity of a dormant fault in tectonically stable Europe: The Rauw fault (NE Belgium). *Tectonophysics*, *699*, 146–163. https://doi.org/10.1016/j.tecto.2017.01.023

Verdon, J. P., & Bommer, J. J. (2020). Green, yellow, red, or out of the blue? An assessment of Traffic Light Schemes to mitigate the impact of hydraulic fracturing-induced seismicity. *Journal of Seismology*. https://doi.org/10.1007/s10950-020-09966-9

Verhoeven, R., Willems, E., Harcouët-Menou, V., De Boever, E., Hiddes, L., Veld, P. O., & Demollin, E. (2014). Minewater 2.0 Project in Heerlen the Netherlands: Transformation of a Geothermal Mine Water Pilot Project into a Full Scale Hybrid Sustainable Energy Infrastructure for Heating and Cooling. *Energy Procedia*, *46*, 58–67. https://doi.org/10.1016/j.egypro.2014.01.158

Vilarrasa, V., De Simone, S., Carrera, J., & Villaseñor, A. (2021). Unraveling the Causes of the Seismicity Induced by Underground Gas Storage at Castor, Spain. *Geophysical Research Letters*, *48*(7). https://doi.org/10.1029/2020GL092038

van der Voort, N., & Vanclay, F. (2015). Social impacts of earthquakes caused by gas extraction in the Province of Groningen, The Netherlands. *Environmental Impact Assessment Review*, *50*, 1–15. https://doi.org/10.1016/j.eiar.2014.08.008

Vörös, R., & Baisch, S. (2018). *Geomechanical Study – Small Gas Fields in the Netherlands* (No. SODM002) (p. 57). Bad Bergzabern: Q-con GmbH.

Wang, J. P., & Huang, D. (2014). Deterministic seismic hazard assessments for Taiwan considering non-controlling seismic sources. *Bulletin of Engineering Geology and the Environment*, *73*(2), 635–641. https://doi.org/10.1007/s10064-013-0491-6

Wiemer, S., Kraft, T., Trutnevyte, E., & Roth, P. (2017). *“Good Practice” Guide for Managing Induced Seismicity in Deep Geothermal Energy Projects in Switzerland* [Application/pdf] (p. 69 p.). ETH Zurich. https://doi.org/10.3929/ETHZ-B-000254161

Worum, G., van Wees, J.-D., Bada, G., van Balen, R. T., Cloetingh, S., & Pagnier, H. (2004). Slip tendency analysis as a tool to constrain fault reactivation: A numerical approach applied to three-dimensional fault models in the Roer Valley rift system (southeast Netherlands). *Journal of Geophysical Research: Solid Earth*, *109*(B2). https://doi.org/10.1029/2003JB002586

Yeo, I. W., Brown, M. R. M., Ge, S., & Lee, K. K. (2020). Causal mechanism of injection-induced earthquakes through the Mw 5.5 Pohang earthquake case study. *Nature Communications*, *11*(1), 2614. https://doi.org/10.1038/s41467-020-16408-0